# Analysis and Optimisation of a Novel Wind Turbine

Xu Zhang

A thesis submitted in partial fulfilment of the requirements of the University of Hertfordshire for the degree of Doctor of Philosophy

The programme of research was carried out in the School of Engineering and Technology, University of Hertfordshire

July 2013

# Abstract

The technologies of urban wind turbines have been rapidly developed in recent years, but urban wind turbines have not found a wide application due to the limitations of their designs. The power output of urban wind turbine is significantly affected by urban terrain, which can cause low speed flow with frequent change of its direction. Thus, there is a need for a new wind turbine to meet the requirements of an urban wind turbine.

In this study, a novel wind turbine for urban areas was designed and developed. The investigations of the novel urban wind turbine were carried out by using computational fluid dynamic (CFD) simulations and wind tunnel tests. The results from the investigation have shown that the novel wind turbine has a great potential to harvest wind energy in urban areas.

A detailed study of effects of each parameter on wind energy concentration of the novel wind turbine was carried out with CFD simulations. According to the simulation results, the shroud structure of the novel wind turbine was modified and the dimensions of the final structure were identified. It was determined that the capability of wind energy concentration of the novel wind turbine shroud has been significantly improved through the structure optimisations.

Furthermore, guide vane and impulse turbine were implemented in the novel wind turbine. The flow characteristics through the guide vane was studied and discussed. It was found that the wind flow characteristics can be properly modified by implementing guide vane and the structure of impulse turbine was suitable to be implemented in the novel wind turbine due to the flow characteristic through the guide vane.

# Acknowledgements

I would like to take this opportunity for respecting my gratitude to my supervisory team: Dr Yongkang Chen, Dr Vitaly Voloshin and Dr Raj Calay who have given me encouragement, academic supervision and patience throughout the duration of the project. I am especially thankful to Dr Yongkang Chen and Dr Vitaly Voloshin for their comments on my thesis. Thanks Pei Ying for his assistance for power coefficient prediction.

I would also like to thank my wife Zhixuan Zheng, who always stand by my side.

The last but not the least thanks go to my father who always encourages and trusts me.

# Contents

# List of Tables

# List of Figures

# Nomenclature

| | |
|---|---|
| $\alpha$ | Angle of attack |
| a | Axial induction factor |
| a’ | Tangential induction factor |
| r | Blade local radius (m) |
| $\Omega$ | Angular velocity (rad/s) |
| c | Airfoil chord length(m) |
| $\rho$ | Air density ($kg/m^3$) |
| U | Air flow velocity (m/s) |
| $\lambda$ | Tip speed ratio |
| $F_D$ | Drag force (N) |
| $F_L$ | Lift force (N) |
| M | Moment (N.m) |
| P | Power output |
| $C_D$ | Drag coefficient |
| $C_L$ | Lift coefficient |
| $C_M$ | Moment coefficient |
| $C_P$ | Power coefficient |
| $P_t$ | Total pressure (Pa) |
| $P_s$ | Static press (Pa) |
| c | Chord of an airfoil (m) |
| n | Number of blades |
| $U_{rel}$ | Relative flow velocity (m/s) |

| | |
|---|---|
| T | Torque to a rotor (N.m) |
| ω | Rotor speed (rad/s) |
| σ | Blade solidity |
| p | Total pressure |
| $p_d$ | Dynamic pressure |
| AoA | Angle of Attack |
| BEM | Blade Element Momentum (Theory) |
| CFD | Computational Fluids Dynamics |
| DNS | Direct numerical simulations |
| DSM | Differential stress models |
| EVM | Eddy-viscosity model |
| HAWT | Horizontal axis wind turbine |
| LES | Large-eddy simulation |
| NLEVM | Non-linear eddy viscosity model |
| RANS | Reynolds-Average Navier-Stokes |
| RSTM | Reynolds-stress transport model |
| SOC | Second-order closure models |
| TSR | Tip speed ratio |
| VAWT | Vertical axis wind turbine |

# Chapter 1 – Introduction

This chapter will introduce the necessity and importance of this research and lay out the aims and objectives of the work. The layout of the remainder of this thesis will be addressed as well.

## 1.1. Necessity of a Wind Turbine in Urban Areas

Due to the global warming and depletion of fossil fuel, the development of renewable and clean energy has become a very important issue for several decades. Wind energy is one of the most popular renewable resources. Having been used for thousand years, wind energy has started to draw more attention due to huge amount of wind energy resources since oil crisis happened in the mid-seventies (Carlin, Laxson, & Muljadi, 2001). In principle, the wind energy resources could meet the world's electricity needs. However, in comparison with the overall demand for energy, the scale of wind power usage is still small. The application of wind energy is limited by the local area suitable for wind power plants, the complex terrain and the turbulent nature of the local wind.

In recent decades, the technologies of wind turbine have been rapidly developed. There are three important factors which have driven the development of modern wind turbines. Firstly, it is caused by strong demand of energy. The fossil fuels have been used for energy generation. However, it has been noticed that the environment is being damaged by using fossil fuels. As the most popular renewable energy, the amount of wind energy resources is huge. In theory, the technical potential of onshore wind energy is from $20{,}000\times10^{9}$ to $50{,}000\times10^{9}$kWh. It is possible for wind energy to meet the current total annual world electricity requirement of about $15{,}000\times10^{9}$kWh by capturing wind energy (Joselin Herbert,

Iniyan, Sreevalsan, & Rajapandian, 2007). Secondly, technological capacity of wind turbines has been increased due to the developments of relevant technologies, which included material, electricity storage and manufacture. Thus, wind energy can be expected to play a significantly important role in the future energy generation. Thirdly, the political issues will push the development and usage of wind turbine. In order to promote the use of wind energy, a series of policies, which include pricing laws, quota requirements, production incentives, tax credits, trading systems, etc. have been developed and implemented (Kissel & Krauter, 2006).

However, the transformation of wind energy to electricity is mainly through large scale wind turbines in the form of wind farms, on-shore and off-shore. Those wind farms take advantages of suitable flow conditions for electricity generation. The capacity of wind energy generation was significantly increased in last decade as shown in Fig.1.1. However, the increase of wind energy generation capacity was mainly through large wind farms, and the locations of these wind farms usually are at countryside and far from residential areas which will increase cost and waste during electricity transition. It has been reported that there is also an abundant resource of wind energy in urban areas, and generating electricity from wind energy in an urban environment becomes attractive. By 2050, the UK aims to achieve an 80% reduction in $CO_2$ from current level (Flavin, 2008) and it is found that approximately 50% of UK energy is used in buildings (Walker, 2011). Thus, utilising the wind energy in urban areas is an efficient way to reduce $CO_2$. Implementation of urban wind turbines means placing a source of supply at a site with strong energy demand, therefore, the cost and waste during such a transit process could be significantly reduced. However, the wind flow conditions in urban areas are complex and structure features of conventional wind turbines are limited to be used in urban areas.

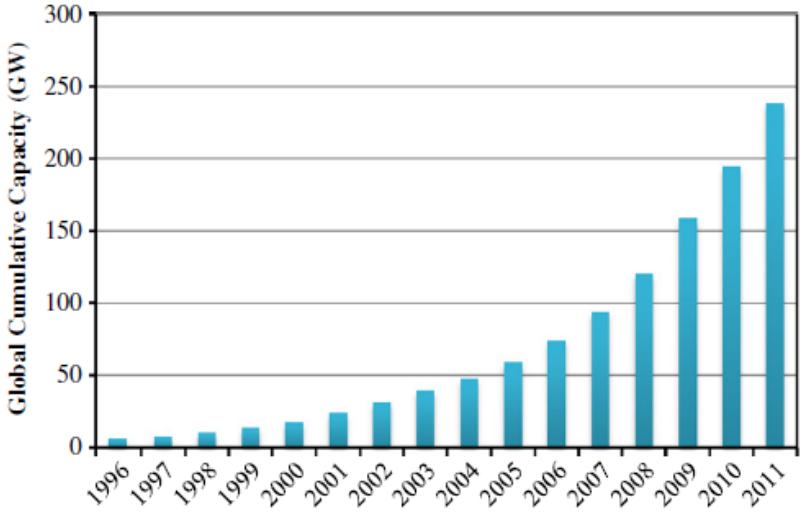


**Fig.1.1. Global wind energy capacity in last 15 years (MR Islam, Mekhilef, & Saidur, 2013)**

The conventional wind turbines can be divided by a working axis into two types, horizontal axis wind turbine (HAWT) and vertical axis wind turbine (VAWT). With their structure features, each type of wind turbine has its own drawbacks when used in urban area. In recent years, many researches about urban wind turbines, based on optimisation of conventional wind turbines, have been carried out. These studies are focused on optimising the conventional wind turbine structures to meet the requirements of urban wind turbines. Some additional structures, such as diffuser, duct, stator vane, were implemented on conventional wind turbines (Abe et al., 2005; Gilbert, Oman, & Foreman, 1978; A. Grant, Johnstone, & Kelly, 2008; K. Pope et al., 2010). The power outputs of these wind turbines can be improved, but the limitations of structure features still reduce the performance of a wind turbine system. The previous researches about urban wind turbines have not filled the gaps utilising wind energy in urban areas. Thus, a novel wind turbine is needed to break out of the limitations of conventional wind turbine structures to achieve optimum utilisation of wind energy in urban areas.

## 1.2. Aim and Objectives of This investigation

A novel shroud wind turbine was designed to meet the requirements of urban environment. Two methods, computational fluid dynamic (CFD) and wind tunnel, were employed to validate the performance of the novel wind turbine. The project aimed to determine and optimise the power output potential of novel wind turbine in order to achieve an improvement in power output.

The study had the following objectives:

- Conduct a literature review of current wind turbine technologies. Find out the technologies which could be used for the novel wind turbine design.
- Study the methodologies used for the development of wind turbines so that the latest technologies could be employed for the optimisation of the novel wind turbine.
- Identify the parameters of original novel wind turbine prototype and carry out aerodynamic analysis of the novel wind turbine prototype and determine the prototype performance.
- Optimise the novel wind turbine structures. The effects of each parameter will be determined. The final model will be created with considering the improvements of each parameter.
- Determine the performance of final model and validate the improvements of the final model.
- Conduct a literature review about selecting blades for the novel shroud wind turbine and determine the power coefficient of the novel wind turbine.
- Discuss the innovations of the novel wind turbine and conclude the improvements of the novel wind turbine compared with existing urban wind turbines.

## 1.3. Thesis Layout

In summary, this thesis addresses the modelling and optimisation of the specific designed novel wind turbine for an urban area by using CFD and wind tunnel tests. The work is divided into nine chapters. A conclusion is carried out to summary the research contribution of this thesis as well as suggestions for further work. The breakdown of each chapter is detailed as follows:

- Chapter 2 comprises a critical literature review of the areas relevant to the study, which includes development of conventional wind turbine, flow feature in urban areas, current urban wind turbine technologies. A discussion was carried out to validate the drawbacks of current urban wind turbines and to find out the importance of developing a novel wind turbine.
- Chapter 3 contains an introduction section of the methodologies for analysing performance of wind turbines.
- Chapter 4 presents the validation of the novel wind turbine. The design concept and prototype parameters of the novel wind turbine were introduced. The performance of the novel wind turbine was determined by CFD modelling and validated by the wind tunnel test.
- Chapter 5 addresses an investigation of the chamber numbers of the novel wind turbine shroud using CFD modelling.
- Chapter 6 details the structure optimisation of a single chamber of the novel wind turbine using CFD modelling.
- Chapter 7 presents the development of the blade for the novel shroud wind turbine and the initial power coefficient of the novel wind turbine was measured.

- Chapter 8 discusses the optimisation and validation of the performance of the novel wind turbine and highlights the improvement of novel shroud wind turbines
- Chapter 9 lists the conclusions and research contributions of this thesis as well as suggestions for the further work.

# Chapter 2 – Development of Urban Wind Turbines

This chapter will introduce and evaluate the existing wind turbines to determine their drawbacks in application for urban areas. The requirements of an urban wind turbine have been discussed.

## 2.1. Conventional Wind Turbine

The usage of wind energy can be traced back to thousands of years ago, which in the form of vertical axis windmills was found at the Persian-Afghan borders around 200 BC (Carlin, et al., 2001). The horizontal axis windmills were used much later (1300-1875 AD) in the Netherlands and the Mediterranean(Fleming & Probert, 1984) . The most important milestone of wind turbine development happened in 1973 after the oil crisis, when USA government started to involve in the wind energy research and development (R&D) (de Carmoy, 1978; Thomas & Robbins, 1980). The modern wind turbine is defined as a machine which converts the energy from the wind into electricity.

In modern wind turbines, the most widely used type of wind turbines is horizontal axis wind turbine. The conversion process of modern wind turbines is based on that the aerodynamic lift force produces a net positive torque on a rotating shaft. The mechanical power can be generated by the torque, and then the mechanical energy is transformed to electricity by a generator. The wind energy can be captured at the locations where wind is blowing. In general, the wind conditions at country or coast are more suitable for electricity generation. That is the reason why modern wind power stations are located far from cities in the form of a wind farm. Due to the remote locations of wind farms, the cost of energy transit can be

increased. Thus, the research interests of wind turbines are moved into wind energy in urban areas.

There is a huge amount of wind resources in urban areas, and the most important reason of implementing urban wind turbines is that capturing wind energy at the location with high energy demands could significantly reduce the cost and waste during electricity transit. Before moving into urban wind turbines, a brief review of conventional wind turbine structures is carried out and the structure features of different types of conventional wind turbine will be introduced and discussed. The drawbacks of implementing conventional wind turbines or small scaled conventional wind turbines have been found out.

### 2.1.1. Lift and Drag Driving Force Wind Turbines

The lift force wind turbines are most widely used as commercial wind turbines due to their higher power coefficient than that of drag force wind turbine. The wind turbines can be divided into two types, drag machines and lift machines, by driving forces. The drag machines use a drag force to generate power, such as windmills used in the Middle East over a thousand years ago(R. Miller, 1988). The lift machines use a lift force to generate power, which are widely used in modern commercial wind turbines. The schematics of drag machine and lift machine are shown as Fig.2.1 and Fig.2.2, respectively. The drag force machines had been used hundreds years before lift force machine, but the usage of drag machine was not as widespread as lift force machine due to its low efficiency. The reason can be explained from the fundamentals, the working principles of these two types of wind turbines. The flow through a drag force wind turbine can be seen in Fig.2.1. In Fig.2.1, $U$ is velocity of the undisturbed air flow; $\Omega$ is angular velocity of wind turbine rotor; $r$ is radius.

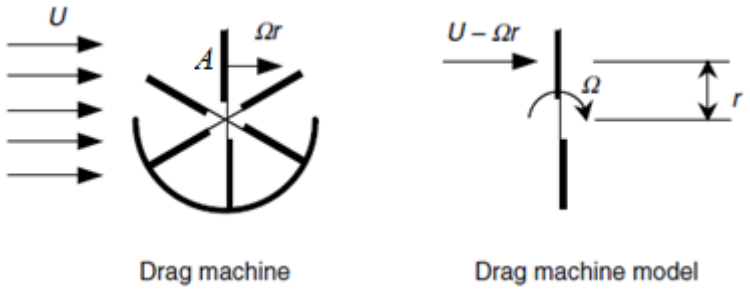


**Fig.2.1. Simple drags machine and model**

The wind turbine driven force, drag force ($F_D$), can be expressed by a function of the relative wind velocity at the rotor surface as below,

$$F_D = C_D[\tfrac{1}{2}\rho(U-\Omega r)^2 A] \qquad (2.1)$$

where A is the drag surface area and $C_D$ is three-dimensional (3D) drag coefficient.

A torque was generated due to the drag force and rotational speed of the rotor, so that the power output of rotor can be expressed as a function of blade radius(r), as follow:

$$P = C_D[\tfrac{1}{2}\rho A(U-\Omega r)^2]\Omega r = (\rho A U^3)[\tfrac{1}{2}C_D\lambda(1-\lambda)^2] \qquad (2.2)$$

where the power coefficient of drag force wind turbine can be expressed by a function of λ, the ratio of the rotating speed to the wind speed.

$$C_P = [\tfrac{1}{2}C_D\lambda(1-\lambda)^2] \qquad (2.3)$$

From equation 2.3, it can be found that the power coefficient of a drag force wind turbine is zero at speed ratios of either zero or one. The peak power coefficient is 0.18, which occurs at the speed ratio of 1/3. It is noticed that this power coefficient is extremely lower than Betz limit of 0.593(Betz, 1926). This is the reason that pure drag force wind turbines are limited to be used in modern wind energy capture(Gasch & Twele, 2007). The rotor surface of drag force wind turbine could never rotate faster than the wind speed. To drag wind turbine, the

wind velocity relative to the power-producing surfaces of machine ($U_{rel}$) is limited to the free stream and can be expressed as,

$$U_{rel} = U(1-\lambda) \qquad (\lambda < 1) \tag{2.4}$$

From Equation 2.4, it can be seen that the velocity relative to the power-producing surfaces of machine ($U_{rel}$) of a drag force wind turbine is always smaller than free stream flow (U). On the contrary, the velocity relative to the power-producing surfaces of machine ($U_{rel}$) of a lift force wind turbine is always higher than free stream flow (U). This is the main reason that lift force wind turbines generally have higher power coefficient than that of drag force wind turbines. The relative wind velocity of a lift wind turbine can be seen in Fig.2.2.

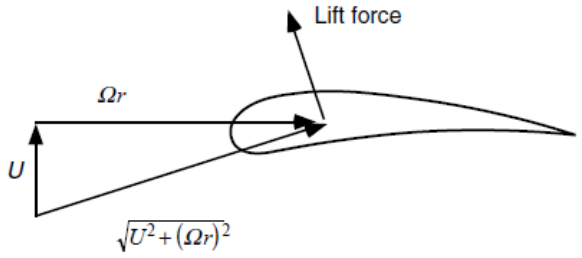


**Fig.2.2. Relative velocity of a lift force wind turbine**

From Fig.2.2, it can be found that the relative wind velocity at the aerofoil of a lift machine can be expressed as,

$$U_{rel} = \sqrt{U^2 + (\Omega r)^2} = U\sqrt{1+\lambda^2} \tag{2.5}$$

From equation 2.5, it can be found that the relative wind velocity which can be achieved with lift machines is much higher than that of drag machine achieved. The driving force is a function of the square of the relative speed, so that the forces generated by lift machines are significantly greater than those achieved by drag machine with the same surface area. The force is an important factor for wind turbines to generate power. However, it should be

pointed out that achievable maximum power coefficients for some drag-based machine, such as the Savonius rotor, are about 0.18 and the tip speed ratios may be greater than 1. It is because the lift forces are generated during the process of the rotor surfaces turning out of the wind when the rotor rotates (Wilson, Lissaman, & Walker, 1976). Due to the low energy efficiency, the drag force wind turbine is not widely used in the modern conventional wind turbines.

### 2.1.2. Horizontal Axis Wind Turbine (HAWT) and Vertical Axis Wind Turbine (VAWT)

The lift driven force wind turbines are widely used in modern commercial wind turbines, because of their potentials to achieve high power coefficient. These lift driven force wind turbines can be divided into two types, horizontal axis wind turbine (HAWT) and vertical axis wind turbine (VAWT), by the direction of their working axes. According to different directions of working axes, each type of wind turbines has its own advantages and disadvantages so that they are implemented for different conditions. The HAWTs have been significantly developed and widely used over last decades and have emerged as the dominant technology in modern wind energy technologies. The reason of a wide usage of HAWTs is that higher energy efficiency can be achieved. However, the higher energy efficiency of HAWTs happened only when the energy quality, which included flow velocity and flow direction, of the wind is high (Ghosh & Prelas, 2011). In complex wind conditions, such as high wind turbulence, wind fluctuations and high directional variability, VAWTs could achieve better performance in operation. In order to increase the usage capability of wind energy, all the aspects, which include sustainable and environmental technologies, should be fully considered and developed. Based on the different structure features, the VAWTs have the ability to fulfil certain energy generation requirements which cannot be achieved by HAWTs. It appears that the structure features of HAWTs and VAWTs, the advantages and

disadvantages of these two types wind turbines, have significant effects on their implementation in urban areas.

2.1.2.1. Horizontal Axis Wind Turbine (HAWT)

The horizontal axis wind turbines (HAWTs) are most commonly used since last decade in the form of wind farms with three aerofoil blades. That the HAWT can be widely used is due to its higher power coefficient than other turbine types. As shown in Fig.2.3, the curve of 'ideal efficiency' is the power coefficient of HAWTs in theory. The high power output of HAWTs happens through $360^{o}$ rotation of the blades and ability of blades to achieve variable pitch angle. The high power output is the main advantages of a HAWT compared with the other wind turbines. However, HAWT also has its disadvantages due to its structure features.

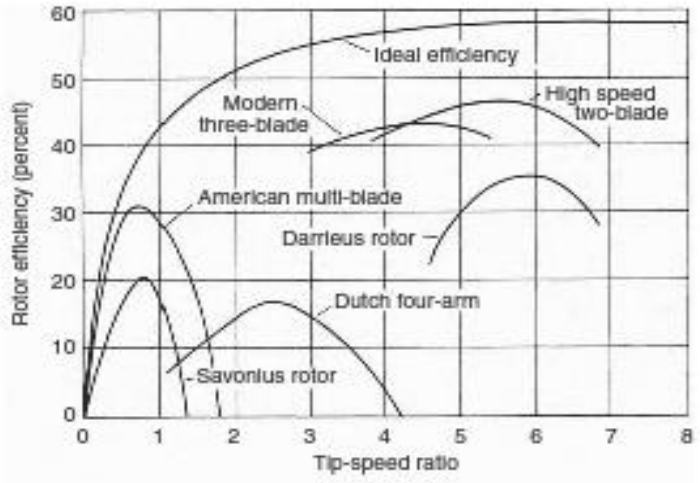


**Fig.2.3. Rotor efficiency against tip speed ratios for different types of wind turbine (Patel, 2005)**

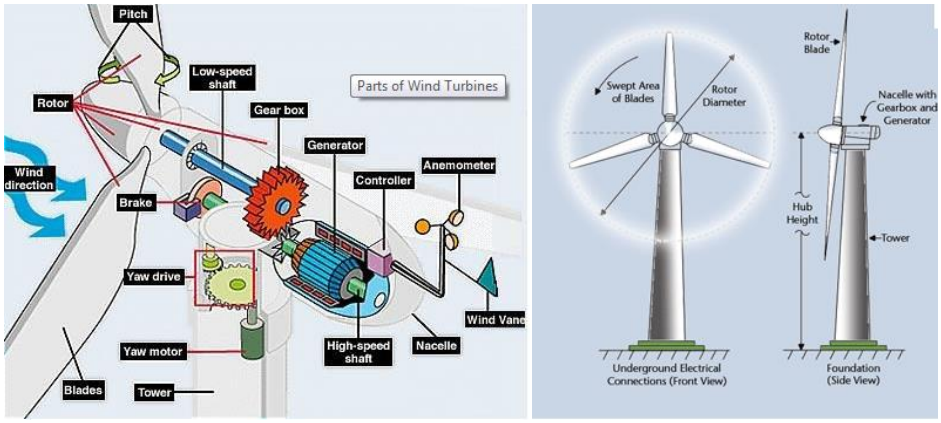


**Fig.2.4. Wind turbine components**

The structure of a modern HAWT is shown in Fig.2.4. The main rotor shaft and the generator are placed on the top of a tower. In order to achieve an optimum power output, the yawing mechanism is required to face the changeable wind directions. The yawing mechanism of HAWTs helps the blades take advantage of the wind velocity through a computer controlled motor in modern wind farms. The height of a tower also will influence the power output of HAWTs. It was found that a higher tower can help a wind turbine reach higher wind velocities in higher altitude and wind shear (Spera, 1994). However, the tall tower of HAWT cannot have a good integration with urban environments and it also will have a high cost of transportation and installation. Moreover, the support tower takes the entire load from the blades, rotor and gear box on the top and this will cause an increase of overall cost. Due to many moving parts, HAWTs require high maintenance (Mittal, Sandhu, & Jain, 2010). The reason that HAWT cannot be widely used in urban areas can be concluded as the high cost of transportation and installation, high maintenance and bad integration with urban environments.

2.1.2.2. Vertical Axis Wind Turbine (VAWT)

The majority research on modern VAWT design was carried out in the late 1970s and early 1980s(Williams, Strakey, & Surdoval, 2005). Then, the interest was lost in VAWT when it

was accepted that HAWTs were more efficient. However, in recent years, the researches about VAWT have become more popular, because there are a number of substantial advantages of VAWTs over HAWTs as follows(Howell, Qin, Edwards, & Durrani, 2010).

- There is no need for VAWTs to constantly yaw into the local wind directions.
- The rotational speed of VAWTs is lower than that of HAWTs and this will make the noise of VAWTs lower than that from HAWTs.
- The manufacture cost of VAWTs' blades could be lower than HAWTs' blades due to the simpler straight constant section blades.
- The VAWTs have a potential operational safety advantage during gust conditions due to the capability to withstand higher winds through changing stalling behaviour

Another major advantage of VAWTs is the low maintenance cost because all the components of VAWTs are located at the ground level so that it is easier and faster to access for maintenance. The self-starting capability is an important issue for a wind turbine to be widely used in urban areas(Van Bussel & Mertens, 2005). However, there is a significant drawback of VAWTs, which is poor self-starting capability (Kirke, 1998). There are three or more blades for a VAWT, but not all the blades will face to the wind direction. When the turbine blade moves parallel to the wind direction, there will be an extra load for the blades with negative or zero torque. VAWTs have the ability to operate effectively in the presence of high unstable and turbulent wind flow patterns, and the ability to make them ideal candidates for small scale applications in urban environment. Their axisymmetric nature allows wind energy extraction during the conditions of rapidly varying wind direction. Their base mounted generator location permits relatively easy maintenance, making them more suitable for small scale urban installation as compared with traditional horizontal axis turbines. There are also two types of vertical axis wind turbines, lift force and drag force, which are divided

by a driving force. The VAWTs were initially started as drag devices (Savonious) and only recently researchers have given emphasis into the lift driven VAWTs after a French engineer, Darrieus, first proposed the lift driven VAWT in 1925 (Hau, 2010). Due to their own features, two types of VAWTs have their advantages and disadvantages used in urban areas.

**Darrieus wind turbines.** The designs of Darrieus wind turbine were first carried out (Paraschivoiu, 2002) in 1931. This type of wind turbines has the highest efficiency among VAWTs because it is lift force wind turbines. However, the starting ability of this type of wind turbines is poor. There are two major types of Darrieus wind turbines, egg-beater type Darrieus wind turbine and Giromill turbine. A typical structure of Darrieus wind turbine is shown in Fig.2.5.(a). The performance of egg-beater type Darrieus wind turbine was good, whose highest power efficiency was 0.42. The production of egg-beater type Darrieus wind turbine was limited due to the complexity of blades, which could lead to high manufacturing costs(Eriksson, Bernhoff, & Leijon, 2008). The Giromill turbine is Darrieus wind turbine with straight blades, and it is applicable for small scale and roof top design. The blades of Giromill turbines can have fixed or variable pitch (Gorelov & Krivospitsky, 2008), which have the potential to overcome the limitation of low starting torque associated with VAWTs (Howell, et al., 2010; M. Islam, Ting, & Fartaj, 2008). The power efficiency of Giromill turbines is 0.23, which is comparatively higher than that of other drag driving force wind turbines.

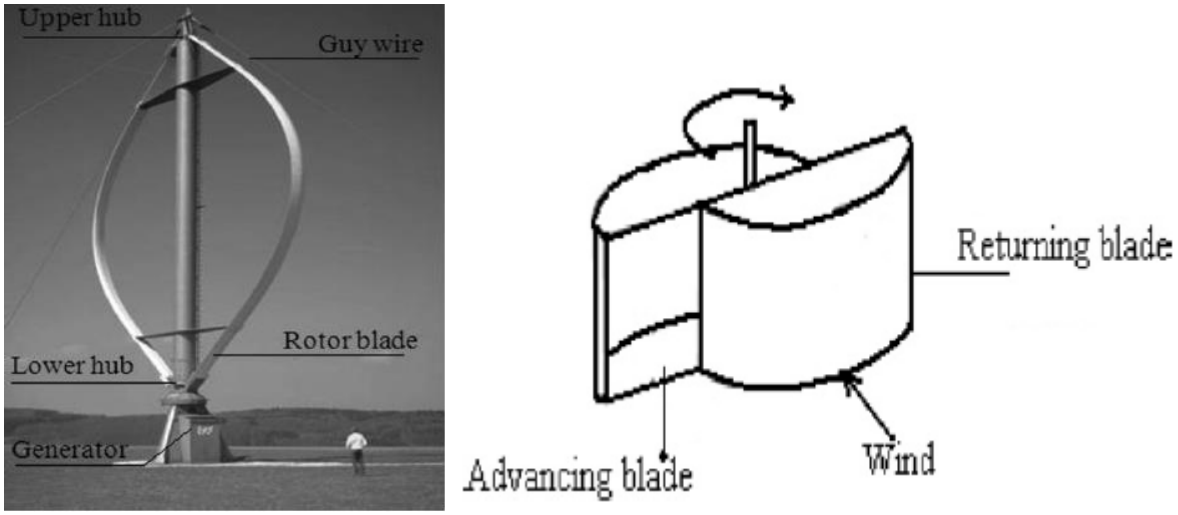


(a) (b)

**Fig.2.5. Two major types of vertical axis wind turbine ( a. Darrieus wind turbine and b. Savonius wind turbine)**

**Savonius wind turbine.** This type of wind turbine is a drag force wind turbine and was presented by S.J. Savonius in the 1920s (Kyozuka, 2008). It usually consists of cup-shaped half or hollow cylinders fixed with a central rotating shaft. A typical structure of Savonius wind turbine is shown in Fig.2.5.(b). The Savonius wind turbine has inherited the advantages of VAWTs and has its own improvement due to structure. The advantages of Savonius wind turbine can be concluded as follows(Akwa, Vielmo, & Petry, 2012; Fujisawa, 1992),

- Simple construction with low cost
- Operation at approaching flow from any directions
- Low angular velocity in operation, which brings low level of noise
- Reduced wear on moving parts
- Different rotor structure options
- High static and dynamic moment

The power efficiency of Savonius wind turbine is from 5% to 20%, which is lower than that of Darrieus wind turbine(Gorelov & Krivospitsky, 2008). Thus, the Savonius wind turbine has not been widely used as commercial wind turbines and is generally used for wind

velocimetry applications. Based upon the recent published results, it was found that Savonius rotor is significantly affected by operational conditions, geometric and air flow parameters (Menet, 2004), which means that Savonius wind turbine is not suitable to be used in urban environment.

## 2.2. Requirements of an Urban Wind Turbine

The wind energy is one of the potentially low-cost renewable sources to meet the requirements of energy consumption in urban areas. The installation and utilisations of wind turbines in urban areas are limited by wind turbine technologies and complex flow conditions in urban areas. In Section 2.1, the limitations of implementing conventional wind turbine were addressed. In order to create an ideal urban wind turbine, urban wind characteristics and requirements for attachment to urban environments were studied.

The wind characteristics in urban areas are strongly affected by urban terrains. Three factors, which are low wind speed, high turbulence intensity and frequently changed flow directions, increase the complexity for wind turbines to achieve good power outputs in an urban area (Makkawi, Celik, & Muneer, 2009). Low wind speed and high turbulence intensity in an urban area are caused by ground topography, which are influenced by a layout of buildings and shapes of buildings roof. Thus, two important issues, location and installation, should be considered when utilising the wind energy in urban areas. It was pointed by Blackmore (Blackmore, 2010) that if a turbine is located in a wrong place on a dwelling roof, it was possible for the power output to diminish to zero for significant periods of time even when the wind blow strongly. In order to utilise wind energy in the urban areas, the flow characters influenced by buildings were studied by many researchers. Three factors, namely, roof shape, building height and urban configuration, were identified to be able to reduce the power output of urban wind turbines. The locations of wind turbines for different roof shapes are critical to

take advantage of the increasing wind speed which leads to more energy to be captured. Three different roof types, pitched, pyramidal and flat roofs, were studied under different directions of approaching flow (Ledo, Kosasih, & Cooper, 2011). The further studies were carried out by Phillips (Phillips & Trust, 2007) to investigate the mounting location for a single wind direction on a gabled roof. More roof types and more locations with various wind directions were also studied. Abohela et al.(Islam Abohela, 2013) found that there was an acceleration effect of various roof types on wind velocity. All different types of roofs could achieve increasing streamwise velocity and have the potential to produce significantly more energy. It was concluded that the power density above the flat roof was greater and more consistent than that above the other roof types. The heights of wind turbine located on buildings were analysed and tested by Mertens (Mertens, 2002). It was found that various building heights would bring similar flow pattern on top of the roof (Islam Abohela, 2013).

However, with considering the effects of ground roughness, it has been proved that the acceleration can be increased with an increase in the building height, which means that high rise buildings will bring higher potentials than low rise buildings. The flow characteristics in urban areas have drawn more attentions in recent years, so that lots of researches about flow characteristics in urban areas have been carried out. It has been reported that the urban configuration significantly affect the flow characteristics (Baik, Park, Chun, & Kim, 2000). The flow character is also affected by an interaction between buildings. There are two groups in the studies of the interaction between buildings. One group treated buildings as roughness elements within cities and the interaction between urban roughness, urban airflows and atmospheric boundary layer characteristic were studied. Second group investigated urban airflow more microscopically within street canyons and urban canopy. Within first group, the initial work was carried out by Grimmond and Oke (Grimmond & Oke, 1999). They reviewed and analysed the wind profiles in various urban areas and summarized available

roughness parameter models. Morphometric methods were implemented in their studies. Several CFD simulations were carried out by Abohela et al. (Islam Abohela, 2013) to determine the effects of various heights of buildings on flow velocity. The simulations proved that the buildings should be higher than surrounding building for installing a wind turbine.

The details of flow around buildings will significantly affect the location of wind turbine. The flow characters around single high building was simulated by Abohela et al.(Islam Abohela, 2013) and the vector plots of flow passing through building were shown in Fig.2.6. It was explained by Murakami et al. (Murakami & Mochida, 1988) that as the flow approached the building, it was divided into four main streams, one stream was deviated over the building, the second stream was deviated down the wind ward facade and the other two streams were deviated to the two sides of the buildings. A stagnation point (St) with highest pressure was formed at flow deviation point and flow changed the direction to lower pressure zone from the stagnation point. Fig.2.6 shows the flow characters through building. A horseshoe vortex was generated in the windward direction of the cube and extended along its sides (V1). There are four main streams, downwards the wind ward façade (S1), above the cube roof (S2) and two sides stream (S3). The approaching flow was separated but reattached again in the leeward direction of the cube (Rx1). It was noticed that the height of stagnation points (St) from ground was proportional to the building height, which was about 0.8h from ground for different buildings. It was found the maximum negative pressure (CpR) occurred at location 0.05h from the windward edge of the roof and the value was -0.97. According to their study, it can be concluded that the free stream approaching building would cause two effects. One is acceleration of free stream flow velocity. The other increases turbulence intensity. The acceleration of flow velocity can increase the power output of a wind turbine. On the contrary, the increasing of turbulence intensity can reduce the power output of a wind turbine. Thus, it is important to consider these two parameters when installing wind turbines in urban areas.

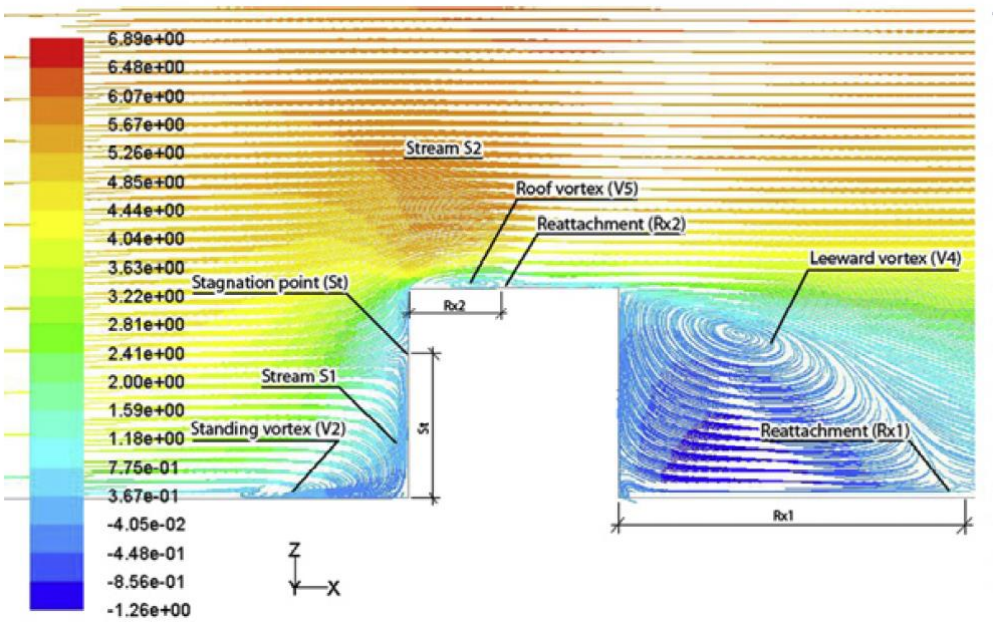


(a)

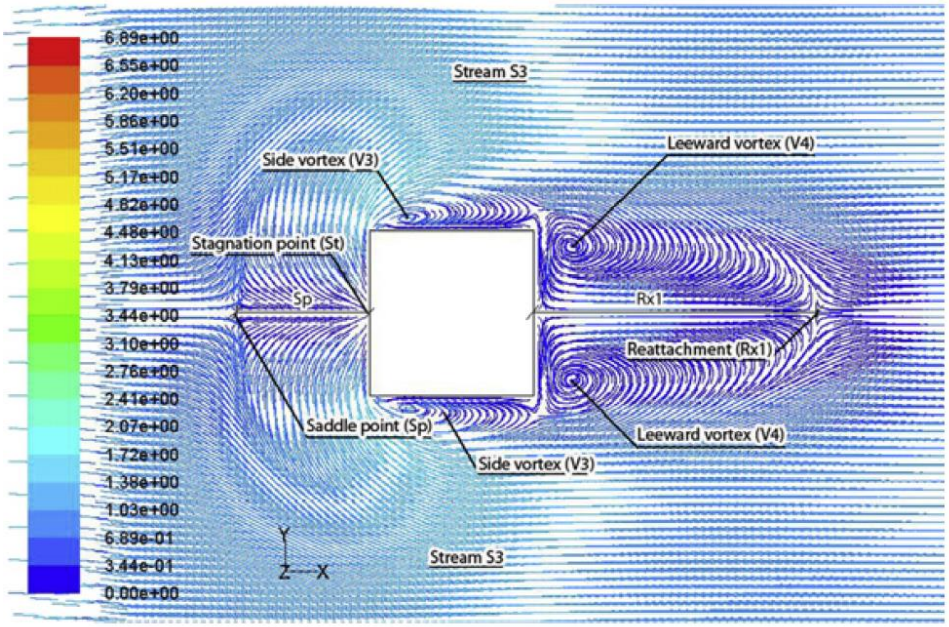


(b)

**Fig.2.6. Flow characters through a building (a) streamwise velocity pathlines passing through the vertical central plane and (b) ground level (Islam Abohela, 2013).**

The other issues that should be considered for an urban wind turbine are caused by urban environments. In considering the performance of urban wind turbines, the integration to buildings should not be underestimated to achieve widespread usage of urban wind turbines.

Since it is placed at high population density areas, the design of urban wind turbine should also consider safety and the effect of noise on people around. The blades of a wind turbine may rotate at a high speed that can cause danger and generate noise. There are two main sources of wind turbine noise. One is mechanical noise which is generated by the fans, generator and gear box due to the vibration of the system. The other is the aerodynamic noise which is caused by the interaction between the rotor and wind due to high rotating speed. The reduction of mechanical noise is almost solved, so that the researchers moved to aerodynamic noise in recent year (Göçmen & Özerdem, 2012). One of the efficient ways to reduce aerodynamic noise is to slow down the rotating speeds of a wind turbine. The high rotating speed of a wind turbine is also the main source to cause danger to surroundings. Thus, the noise and safety issues can be solved if a wind turbine has a low rotating speed. In conclusion, an urban wind turbine should consider the following requirements (Van Bussel & Mertens, 2005).

- System type: static, integration with building/structure, yawing system, with/without collector and/or diffuser;
- System attributes: self-staring, safe, low noise, low vibration, robust design, minimal maintenance, low installation weight, high power per active volume of material;
- Location: aesthetics, building/infrastructure strength, electromagnetic interference with existing electrical installations, space for other equipment e.g. inverters, monitoring devices etc.

The levels of safety and noise should be clarified, so that installation of a wind turbine could cause less cautious of residents. It was reported that there was a negative reputation of urban wind energy which caused by the erroneous installation of rooftop wind systems without

adequate consideration of safety, structural building integrity or turbine performance (Anderson, Whale, Livingston, & Chan, 2008).

## 2.3. Development of Urban Wind Turbines

Utilisation of wind energy in urban areas is an efficient way to deliver carbon savings. There are abundant resources of wind energy in urban area, but the usage of the wind energy is limited by complex wind conditions. In recent years, the wind energy in urban areas has attracted more attentions from researchers. It is proved that in theory over 30% of the UK's electricity supply could be provided by wind by the year 2050 (Britain, 2005). To date, different structures of wind turbines have been successfully installed in the urban or build environment, such as micro HAWT wind turbines, duct wind turbines and so on. These wind turbine strategies were identified to three possible strategies by The EC-funded Project WEB (Campbell et al., 2001).

- Simply siting conventional free-standing wind turbines in an urban environment;
- Retro-fitting wind turbines onto existing buildings;
- Integration of wind turbines into buildings which are specially designed for the purpose.

In this section, a review will be carried out about existing and developing concepts of urban wind turbines. These urban wind turbines will be categorised and introduced based on the three possible strategies.

### 2.3.1. Simply Conventional Wind Turbine

Based on power output, the conventional wind turbines (HAWTs and VAWTs) can be divided into three categories, large turbines (>1 MW), medium turbines (40kM-1MW) and micro turbines (<40kW) (Spera, 1994). The difference between micro wind turbines and

other two wind turbines is that micro wind turbines are located where the power is required. They are usually placed on the top of buildings and used to generate electricity for the isolated homes off the grid. The developments of micro wind turbine technologies have rapidly increased based on the requirements of market. In the section, two types of conventional wind turbines, which are simplified to be used in urban areas, will be introduced.

#### 2.3.1.1. Micro Horizontal Axis Wind Turbine

As the major type of wind turbine, horizontal axis wind turbines (HAWTs) are widely used in wind farms. These wind farms are located in the areas, where dictated by optimum wind conditions. On contrast to large HAWTs, the micro-HAWTs have the applications in roof tops of houses, remote communities and boats (Syngellakis, Carroll, & Robinson, 2006). These places cannot apply the best of wind conditions for wind turbines to generate power. The flows in these areas are made turbulence and slowed down due to obstacles and topology. Thus, the micro-HAWTs should have a good start-up response to low wind speeds in order to achieve maximum possible power. However, the blade size of micro-wind turbines is small and is insufficient to start rotors at a low wind speed. In order to improve their performance, multiple rotor blades are implemented to increase the starting torque (Wood, 2004). By increasing the blade numbers, the rotors of turbines could achieve a quick start and allow the turbines to operate at much lower cut-in wind speeds. Due to operating in lower cut-in wind speeds, power production of the micro-wind turbines could be increased. Also, it is important to optimise the characteristics of rotor, which include the chord, twist distribution, number of blades, choice of aerofoil shape and tip speed ratio (TSR). It is reported that the power coefficients of wind turbines could reach close to the Betz limit of 59.2% by blade optimisation(Chappell & Enterprises). However, it is essential for HAWT to operate in yaw control systems, which are costly and require high level of maintenance.

#### 2.3.1.2. Micro Vertical Axis Wind Turbine

Vertical axis wind turbines (VAWTs) also play an important role in the Micro-wind turbine market, although horizontal axis wind turbines (Gunnell, Platt, & Hawton) are considered more efficient in operation than vertical axis wind turbines (VAWT). Due to the structure feature, VAWTs can offer greater advantages in safety and operation when implemented in urban areas. VAWTs are much more suitable to urban environments due to their inherent axisymmetric design and allowing the gearbox and generator to be located on the ground (Dayan, 2006). According to this, the other two important advantages can be achieved. One is easy access to facilitate turbine maintenance, and the other is reduction of loads on the turbine tower to reduce material installation costs. The most widely used micro VAWT is Savonius wind turbine due to its low cost and reduced environment impacts. The Savonius wind turbines operate essentially due to wind drag forces and also take contributions of lifting forces. They can work in strong wind conditions when most of lift wind turbines must be stopped (OD Vries, 1983). The geometry of Savonius wind turbine blade is essential to improve its performance. Thus, various types of Savonius wind turbine blades have been investigated and two remarkable types, Bach-type rotor and semi-circular blades, have had the maximum power coefficient of 25%. There are two reasons that the usage of Savonius wind turbine is still not widespread. The performance of Savonius wind turbine is strongly affected by the flow conditions and flow parameters, which are not controllable in urban areas. Due to slow-running behaviour that the blades run at the same order as wind velocity, it is difficult for Savonius wind turbines to produce sufficient electric energy (Menet, 2004).

### 2.3.2. Retro-Fitting Wind Turbine

Retro-fitting wind turbines are a group of small scale of conventional HAWTs and VAWTs with some attached parts that have been designed and implemented onto these conventional wind turbines to improve their suitability and efficiency in urban areas. There are two most

popular retro-fitting wind turbines. One is diffuser wind turbine(Gilbert, et al., 1978), which is to improve the performance of small HAWTs. Another is zephyr wind turbine(K. Pope, et al., 2010), which is to increase the power output of VAWTs.

2.3.2.1. Diffuser Horizontal Axis Wind Turbine

The structure feature of diffuser wind turbine is based on horizontal axis wind turbine (Gunnell, et al.) around with a diffuser structure is implemented to collect and concentrate wind flow (as shown in Fig.2.7). The initial idea of diffuser wind turbine was proposed and examined by Gilbert et al.(Gilbert, et al., 1978) in 1978 and Igra (Igra, 1981) in 1981. In their studies, a large open angle diffuser was used to achieve wind energy concentration and the boundary layer control method was employed to prevent a pressure loss due to flow separation so that the mass flow inside the diffuser could be increased. The wind energy is proportional to the wind speed cubed. Thus, a slight increase in the velocity of approaching flow to a wind turbine could achieve significantly power output improvement. The further work was carried out by Bet and Grassmann. They developed a shrouded wind turbine with a wing-profiled ring structure, which improved system power output by a factor of 2.0 compared with the bare wind turbine. Ohya et al. (Abe, et al., 2005; Abe & Ohya, 2004; Ohya, Karasudani, Sakurai, Abe, & Inoue, 2008) carried out the cases of a flanged diffuser wind turbine in both computational and experimental investigations. The flange part was implemented at the diffuser outlet, and the flange in the near wake of the diffuser can generate a low-pressure region. Thus, more mass flow can be drawn into the diffuser to improve the power output of the wind turbine. The flanged diffuser wind turbine was tested in real condition, and it was proved that the flanged diffuser wind turbine can be improved four to five times in terms of output power compared with the conventional wind turbine (Ohya, et al., 2008). Also it was examined that the diffuser structure could help wind turbine system to achieve significant improvements in noise reduction, safety factor increment and

fast response to various wind directions (Abe, et al., 2005). The suitability and efficiency of HAWTs used in urban areas can be improved.

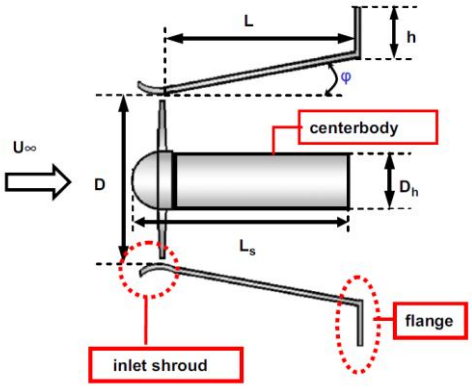


**Fig.2.7. Flanged diffuser wind turbine (Ohya, et al., 2008)**

2.3.2.2. Zephyr Vertical Axis Wind Turbine with Stator Vanes

It was reported that power output of VAWT was dramatically lower than that of HAWT. In order to improve the performance of VAWT, many researches were carried out. One of the remarkable improvements was zephyr vertical axis wind turbine, which implemented stator vanes (as shown in Fig.2.8). The stator vanes are used to optimise flow conditions approaching the wind turbine. The flow was first led through a ring of stationary stator blades, which allow the wind to leave at a particular angle of incidence and achieve an acceleration of velocity. Thus, the flow can strike the rotor blades in a dominant direction to improve the wind turbine power output. With implementation of stator vanes, the flow turbulence can be reduced thereby decreasing aerodynamic loading on turbine blades (K. Pope, et al., 2010). The theoretical and practical analysis were carried out by Pope et al.(K. Pope, et al., 2010), the power coefficient is determined about 0.12, which is too low to be accepted for commercial application. However, the parameters of prototype, which include blade design, stator vane design, distance between stator ring and rotor, etc. can be optimised to improve the power coefficient of whole system. Pope et al.(K. Pope, et al., 2010) derived equations

which related the power coefficient with TSR. The results showed that at 0.4 TSR the maximum value of power coefficient can be obtained while it decreases afterwards with an increase of TSR. The results are helpful for further improvement of the prototype.

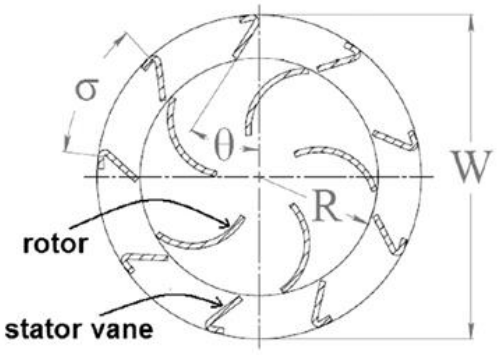


**Fig.2.8. Sketch of zephyr wind turbine with stator vanes(K. Pope, et al., 2010)**

### 2.3.3. Specially Designed Wind Turbines

Even improved by the attached structures, there are still some limitations of conventional wind turbines inherent from their structural features. In recent years, many researches in innovations of urban wind turbines were carried out. These new wind turbines are specially designed for using in urban environment with considering advantages of conventional wind turbines and complex flow conditions in urban areas. There are three remarkable outcomes of innovation, duct wind turbine, crossflex wind turbine and vertical resistance wind turbine. These new wind turbines are specially designed for using in urban environment with considering advantages of conventional wind turbines and complex flow conditions in urban areas, so that they could take advantage of flow conditions.

#### 2.3.3.1. Duct Wind Turbine

The ducted wind turbine was designed to be an alteration to conventional wind turbines used in urban areas. The original concept was from a patent by Webster (Webster, 1979) as shown

in Fig.2.9.The duct was used to protect the wind turbine from an extreme turbulence generated by buildings, at the expense of directional sensitivity. High pressure was formed on vertical walls facing the on-coming wind, and low pressure was formed around the roof of building. As have been well known, the wind speed and direction can be expressed by a function of pressure difference.

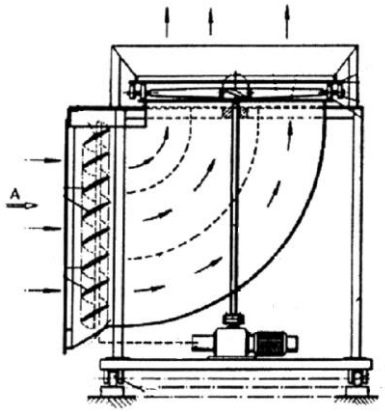


**Fig.2.9. Original ducted wind turbine from patent by Webster (Webster, 1979)**

The duct wind turbine takes advantage of pressure differentials produced by the wind flow around and over a building to drive air through the ducted wind turbine. In order to determine and improve the power output of ducted wind turbine, many researches were carried out. A single unit of duct wind turbine was tested for a long period (AD Grant, 1994) and its effectiveness and robustness in operation have been proved. To determine the power output of duct wind turbine, wind tunnel tests about curved and straight ducts (without turbines) in a rectangular building model were carried out by Dannecker and Grant (Dannecker & Grant, 2002), and the potential of ducted wind turbine was reported. The mathematical model was developed by Grant (A. Grant, et al., 2008) to predict power outputs under the typical operating conditions. The mathematical model was examined by experimentalwork and its accuracy has been validated. It is a viable alternative to achieve attaching small conventional

machines to the roofs of existing buildings. The potential of duct structure is large so it is possible to excess of the conventional Betz limit by improving the duct structure.

2.3.3.2. Crossflex Wind Turbine

The crossflex wind turbine was designed by Sharpe and Proven (Sharpe & Proven, 2010) to meet the requirements of turbines in urban conditions. It was a new development of Darrieus type wind turbine in innovation of flexible blade system. The vertical shaft was implemented on crossflex wind turbine to work in various flow directions. Two or more flexible aerofoil blades were attached to the top and bottom of rotating shaft. The design concept of crossflex wind turbine is shown in Fig.2.10. Its efficiency is improved by using a low solidity and low internal mass design blades. The structure of crossflex wind turbine enables to achieve not only self-starting ability, but also to reduce the loads on the bearings and shafts. The supporting frame of a crossflex wind turbine is strong so that vibrations can be reduced. The crossflex wind turbine can be installed at walls or corners on a building so that a great installed capacity per building can be achieved. The most important is that crossflex wind turbine has a good integration with buildings. The theoretical modelling of crossflex wind turbine was carried out by Sharp and Proven based on the multiple streamtube momentum balance approach (Sharpe & Proven, 2010). The prototypes of crossflex wind turbine were already tested at Newberry tower in Glassgow, Scotland. However, it has been found that the application of crossflex wind turbine is only suitable for high rise buildings, but it cannot be installed in wind farm arrangements or low height buildings. Through the experimental study, it is determined that the crossflex wind turbine achieves its highest power output when flow velocity is higher than 14m/s. Hence, it is suggested that the installation of this type of turbine is suitable only in the area where free stream velocity is greater than 14m/s. The further work should be carried out to improve this design for working in low flow speed conditions.

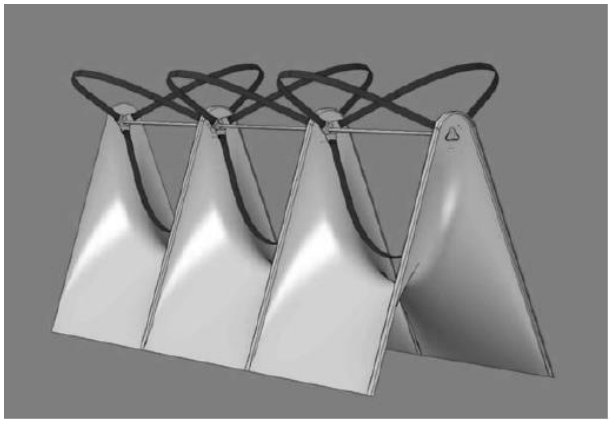

**Fig.2.10. Concept of crossflex wind turbine (Sharpe & Proven, 2010)**

2.3.3.3. Vertical Resistance Wind Turbine

The vertical resistance wind turbine is a typical structure of VAWT and is a drag force based system. It was proved that VAWTs had the ability to be suited in urban environment due to their better function in the turbulent wind conditions found in a built-up area (Dayan, 2006; Mertens, 2002). Especially for drag force based systems, they can be expected to be less sensitive to turbulence and less noisy. There is a long history about using vertical resistance wind turbine. It was recorded in 9$^{th}$ Century AD in the area of Sistan in eastern Iran on the border to Afghanistan (Hau & Platz, 2008). The vertical resistance wind turbine was redesigned for urban environment by Muller *et al*.(Müller, Jentsch, & Stoddart, 2009). Two important improvements were proposed, which were implementation of disks and utilising pressure difference. Two disks were placed at the top and bottom of the turbine body to increase the drag coefficient. According to theory, the drag coefficient can be increased from 1.2 to 2, which means 29.6% increase of maximum efficiency (Prandti, 1925). The structure of a vertical axis resistance wind turbine is shown in Fig.2.11. During the rotating process, high-pressure zone and low-pressure zone were, respectively, generated on the side of the obstacle facing the flow direction zone and on the lee side. The pressure difference between high-pressure zone and low—pressure zone could significantly affect the energy output of the vertical resistance type wind turbine. By using resistance type energy converters, it was found

that the pressure difference could increase. Thus, the overall performance of the wind turbine could be improved. The theoretical and experimental work about a specially designed wind turbine were carried out by Muller et al.(Müller, et al., 2009). It was determined that the maximum converter efficiency of the resistance vertical axis wind turbine was about 48% - 61% in theoretical analysis and measured about 42% in an experiment. It is also suggested that the wind turbine system could achieve 6% to 7% additional efficiency by increasing the blade number from four to six. The most important advantage of the vertical resistance axis wind turbine is simplicity of its components compared with other urban wind turbines. As a specially designed, resistance vertical axis wind turbine had a good integration with high rise buildings.

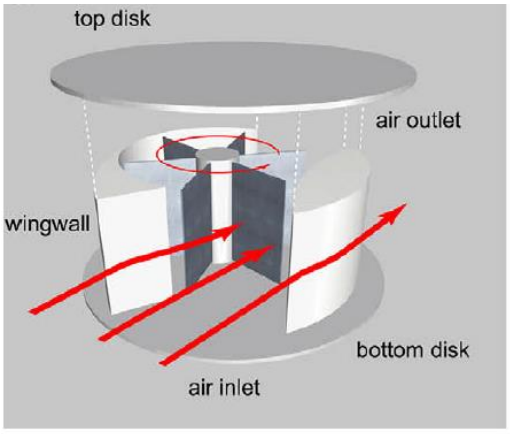


**Fig.2.11. Concept of vertical axis resistance wind turbine(Müller, et al., 2009)**

## 2.4. Discussion

In this section, the reasons that limited the wide application of the existing wind turbines in urban areas are discussed. The technologies of conventional wind turbines, which include horizontal axis wind turbine (HAWT) and vertical axis wind turbine (VAWT), have been rapidly developed for several decades. The performance of conventional wind turbines has been significantly improved. However, the usages of wind turbines are still not widespread in urban areas due to the structure limitations of conventional wind turbines. The structure

features of HAWTs and VAWTs have given these two types their own advantages to be used in urban areas. A review on the advantages of conventional wind turbines to be implemented in urban areas has been carried out. The comprehensive estimation is addressed in Table 2-1 with comparing every requirement of wind turbine working in urban areas.

| | VAWT | HAWT | Requirements of Urban Wind turbine. |
|---|---|---|---|
| Tower sway | No | Yes | Tower should not be implemented on urban wind turbines to achieve good integration with urban environments. |
| Yaw mechanism | No | Yes | Yaw mechanism should not be used for urban wind turbines, because the complexity of operation will reduce the widespread. |
| Self-starting | No | No | It is important for urban wind turbine to have self-starting ability, especially in low wind speed condition. |
| Blade structures | Simple | Complex | The complex blade structure will increase the manufacture cost, which is not good for wind turbine widespread. |
| Generator location | On ground | Not on Ground | The generator should be placed on ground level or roof top for easily maintenance. |
| Height from ground | Small | Large | The high location will make the maintenance not easily, and increase maintenance cost. |
| Blade's operation space | Small | Large | The blade's operation space should be as small as possible due to the space limitation in urban area. |
| Noise produced | Low | High | Due to implement in urban areas, the level of noise should keep low. |
| Wind direction | Independent | Dependent | The flows in urban areas are frequently changed. The wind turbines should independent on wind directions. |
| Safety | Less | Less | Due to wind turbines will be implement in The safety is an important issue to be considered |
| Theoretical efficiency | About 59% | About 59% | The theoretical efficiency shows the potential of wind turbine to do further improvement. |
| Actual efficiency | 5% - 25% | 30% - 50% | It is a critical issue to evaluate the performance of wind turbine. High efficiency will lead more power generated in unit area. |

**Table 2-1. Performance estimation of HAWT and VAWT(MR Islam, et al., 2013; Mittal, et al., 2010; Walker, 2011)**

In order to be widely used in urban areas, a wind turbine should meet six requirements, which are low manufacture cost, easy operation, low maintenance, good performance, good integration and high safety. The manufacture cost is depended on the complexity of blades and tower structure. The wind turbine with simple blades structure and no tower part can significantly reduce the manufacture cost. According to Table 2-1, it can be found that the structure of VAWTs can achieve lower manufacture cost than that of HAWTs. The operation, which needs considering yaw mechanism, self-starting ability and limitation of wind directions, should be easy for people without professional knowledge to operate. The VAWTs can work in any directions of approaching flows without yaw mechanism, but they are poor in self-starting. Thus, the VAWTs are more suitable than HAWTs being used in

urban areas due to operation issues. In order to achieve a wide application, the maintenance should be low. According to this, the generator needs to be located on the ground level for easy maintenance which can reduce maintenance cost. Also, the level of noise generated by VAWTs is lower than HAWTs due to their low tip speed ratio (TSR). It will be easily acceptable of VAWTs to be used in an urban area. It can be found the suitability of VAWTs is better than HAWTs in manufacture, operation, maintenance and noise. The space is limited in urban areas. Therefore the high efficiency is required for a wind turbine to generate more power output in a unit area. However, the efficiency of VAWTs is much lower than that of HAWTs, and it is about 50% of HAWTs' power output. This is the main drawbacks of VAWTs to be widely used. The safety is also an important issue due to the urban wind turbine will be placed in high population density in urban areas. Thus, the blades of HAWTs and VAWTs should be protected, which can reduce the damage of blades in high wind flow conditions. However, the safety factor of these two types of wind turbines is not good enough. It is suggested that the conventional wind turbines are not suitable to be used in urban areas due to their structure limitations.

The researches about implementing wind turbine in urban areas have drawn extensive attentions over last decade. The technologies and design concepts of urban wind turbines have been significantly developed. The urban wind turbines can be divided in three groups which are simply conventional wind turbines, retro-fitting wind turbines and specially designed wind turbines. Some remarkable works are compared by considering integration, maintenance, safety, manufacture, performance and noise. The details of their performances are shown in Table 2- 2.

| | Integration | Maintenance | Safety | Manufacture | Performance | Limitation |
|---|---|---|---|---|---|---|
| Micro-HAWT | Bad | High | Low | High | Good | The yaw mechanics are required to achieve best performance |
| Savonius WT | Bad | Low | Low | Low | Bad | Low power coefficient |
| Diffuser HAWT | Bad | Medium | Medium | High | Good | The system should be placed high with hub structure |
| Zephyr VAWT | Bad | Low | High | High | Good | Complex construction and Occupies large area |
| Ducted WT | Good | Low | High | Low | Good | Limited by wind directions |
| Crossflex WT | Good | High | Low | High | Good | The best performance achieved at 14m/s of approaching flow |
| Vertical Resistant WT | Good | Low | High | Low | Good | Only designed in theory. |

**Table 2-2. Summary of wind turbine configurations**

From Table 2-2, it can be found that there are improvements for every optimised wind turbine, but the limitations are still remaining. However, these improvements can show some good ideas for development of a real urban wind turbine. The improvement of Diffuser and stator vanes highlights the importance of external structure to increase the performance of wind turbine. Before wind approaching turbine blades, the flow can be modified by these external structures to increase the flow velocities or to control the direction of approaching flow towards to blades. Moreover, the flow from any directions can be led to a unified direction to avoid frequently changing direction flow in urban areas.

The utilisation of wind energy in urban areas is an efficient way to reduce the $CO_2$ level and energy shortage. The problem is that the conventional wind turbines are not suitable to be used in urban areas. Even through several researches have been carried out to improve the performance of conventional wind turbines and to develop novel structure wind turbine, there are still limitations of wind turbines to meet the requirements of an urban wind turbine. Thus, a novel wind turbine is needed and designed with considering all requirements of urban wind turbine. The methods from previous works to improve the performance of wind turbines can be considered and implemented in novel urban wind turbines.

## 2.5. Summary

In this chapter, a critical review of conventional wind turbines has been carried out. It is evident that conventional wind turbines are not suitable for urban areas due to urban environments. Thus, an innovation of urban wind turbines is needed to utilise wind energy in urban areas. A study of requirements of an urban wind turbine has been addressed and the requirements are laid out. The researches about different types of urban wind turbines have been studied. The highlights and drawbacks of these urban wind turbines are analysed, and the highlights have been estimated and used for designing the novel wind turbine.

# Chapter 3 – Research Methodologies

This chapter will conduct a review of turbine blades and methodologies that used to validate the performance of wind turbines.

## 3.1. Wind Turbine Blades

The structure of a rotor is critical to the power output of a wind turbine because wind turbine power production depends on the interaction between the rotor and the wind. The wind is considered to be a combination of the mean wind flow and turbulent fluctuations. The analysis of wind turbine rotor performance was originally carried out by Betz (Betz, 1926) and Glauert (Glauert, 1935) in the 1920s and 1930s. Then, the theory was developed and expanded for solution by digital computers by Wilson et al. (Wilson & Lissaman, 1974) and O Vries (O. Vries, 1979). In the study of rotor aerodynamic features, momentum theory and blade element theory are combined to calculate the performance characteristics of an annular section of the rotor. The performance of the whole rotor was determined by integrating the values obtained from each annular section(Lanzafame & Messina, 2007).

The performance of a wind turbine rotor is usually characterised by power coefficient ($C_p$), which is expressed as,

$$C_P = \frac{P}{\frac{1}{2}\rho U^3 A} = \frac{Rotor \quad Power}{Power \quad in \quad the \quad wind} \qquad (3.1)$$

The ideal power output of a wind turbine rotor is about 59%, which was determined by Betz in 1926 (Betz, 1926). The analysis was carried out in ideal conditions which had the following assumptions:

- Homogenous, incompressible, steady state fluid flow;
- No frictional drag;
- An infinite number of blades;
- Uniform thrust over the disc or rotor area;
- A non-rotating wake;

  The static pressure far upstream and far downstream of the rotor is equal to the undisturbed ambient static pressure

The Betz limit of 59% is the maximum ideal power output coefficient of a wind turbine. However, the maximum achievable power coefficient can be reduced by three aspects:

- Rotation of the wake behind the rotor;
- Finite number of blades and associated tip loses;
- Non-zero aerodynamic drag.

The aerofoil has been implemented on a wind turbine system to generate mechanical forces due to the relative motion of the aerofoil and a surrounding fluid. The wind energy can be captured through the aerofoils of blade. The cross-sections shape of wind turbine blades is important for obtaining the desire aerodynamic performances, which include the maximum desired rotor power, the assumed aerofoil properties and strength considerations. The cross-section of a wind turbine blade is shown as Fig.3.1. The mean camber line is the locus of points halfway between the upper and lower surfaces of the aerofoil. The most forward and rearward points of the mean camber line are on the leading and trailing edges, respectively. The straight line connecting the leading and trailing edge is the chord line with the length c. The camber is the distance between the mean camber line and the chord line, measured perpendicular to the chord line. The thickness is the distance between the upper and lower surfaces and is also measured perpendicular to the chord line. Finally, the angle of attack, $\alpha$,

is defined as the angle between the relative wind ($U_{rel}$) and the chord line. The span of aerofoil is defined as the length of the aerofoil perpendicular to its cross-section. The following parameters have effects on the aerodynamic performance of an aerofoil:

- The leading edge radius;
- Mean camber line;
- Maximum thickness and thickness distribution of the profile;
- The trailing edge angle.

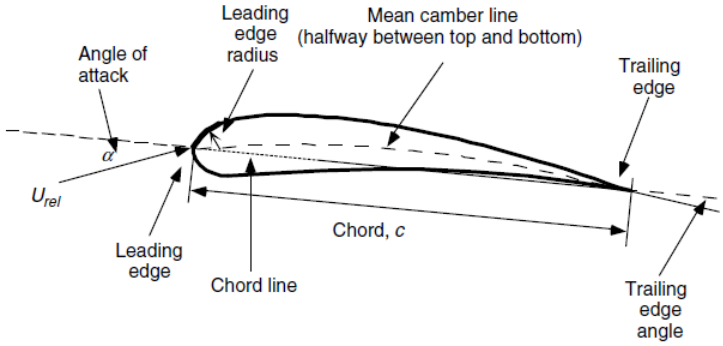


**Fig.3.1. Cross-section of aerofoil (Bertin & Smith, 1989)**

Based on the structure of wind turbine blades, there is a distribution of forces on a section of aerofoil when air flows over the aerofoil surface. The velocity in the convex surface of aerofoil is increased, which leads to low pressure. Meanwhile, the air flow is slowed by the viscous friction between the air and the aerofoil surface. By the effects of pressure difference between upper and lower surfaces, and friction forces, two forces and one momentum can be generated on the chord, which act at a distance of c/4 from the leading edge as shown in Fig.3.2. The two forces and one moment are defined as:

- Lift force – It is defined to be the force perpendicular to direction of the oncoming air flow. The lift force is caused by the pressure difference on the upper and lower aerofoil surface.

- Drag force – It is defined to be the force parallel to the direction of the oncoming air flow. The drag force is caused by both viscous friction forces on aerofoil surface and pressure difference between aerofoil surfaces facing toward and away from the oncoming flow.
- Pitching moment – It is defined to be moment about an axis perpendicular to the aerofoil cross-section.

At beginning, when the air flow reaches aerofoil leading edge, the air flow along the chord surface is accelerated and pressure drops, which results in a negative pressure gradient at the front of chord. When the air flow moves to the trailing edge, the velocity of air flow is decreased and pressure near the chord increases, which results in a positive pressure gradient. If the aerofoil design and the angle of attack of a specific blade are given, there is a net lift force, which is caused by the air speeding up more over the upper surface than over the lower surface of the aerofoil.

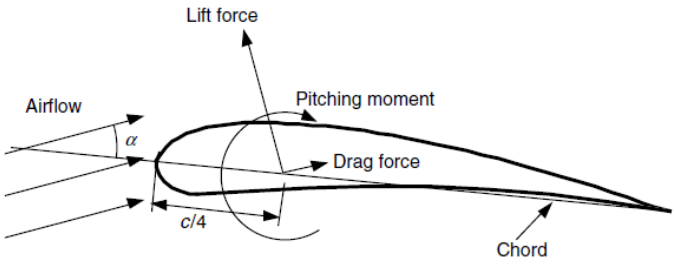


**Fig.3.2. Forces and moments on aerofoil(Bertin & Smith, 1989)**

The two-dimensional lift coefficient, drag coefficient, pitching moment coefficient and pressure coefficient can be expressed as $C_l$, $C_d$, $C_m$ and $C_p$ respectively. The function of each coefficient is shown as,

$$C_l = \frac{Lift \quad Force/unit \quad length}{Dynamic \quad force/unit \quad length} = \frac{L/l}{\frac{1}{2}\rho U^2 c} \tag{3.2}$$

$$C_d = \frac{Drag \quad force/unit \quad length}{Dynamic \quad force/unit \quad length} = \frac{D/l}{\frac{1}{2}\rho U^2 c} \tag{3.3}$$

$$C_m = \frac{Pitching \quad moment}{Dynamic \quad moment} = \frac{M}{\frac{1}{2}\rho U^2 Ac} \tag{3.4}$$

$$C_p = \frac{p_{total} - p_{dynamic}}{\frac{1}{2}\rho U^2} = \frac{Static \quad pressure}{Dynamic \quad pressure} \tag{3.5}$$

where $\rho$ is the density of air, $U$ is the velocity of free stream air flow, $A$ is the projected aerofoil area (chord × span), $c$ is the aerofoil chord length and $l$ is the aerofoil span, L is the lift force and D is the drag force, $p_{total}$ is total pressure and $p_{dynamic}$ is dynamic pressure.

There are other important dimensionless coefficients of a rotor section, which include power coefficient, thrust coefficient, tip speed ratio and pressure coefficient:

$$C_P = \frac{P}{\frac{1}{2}\rho U^3 A} = \frac{Rotor \quad power}{Power \quad in \quad the \quad wind} \tag{3.6}$$

$$C_T = \frac{T}{\frac{1}{2}\rho U^2 A} = \frac{Thrust \quad force}{Dynamic \quad force} \tag{3.7}$$

$$\lambda = \Omega R/U \tag{3.8}$$

where $P$ is power generated by rotor, $U$ is velocity of approaching flow, $\rho$ is air density, $A$ is area of blade, $T$ is thrust force of blades, $\Omega$ is angular velocity, $R$ is radius of rotor,

While flow goes through aerofoil, there are three regimes, attached flow regime, high lift/stall development regime and flat plate/fully stalled regime. The performance of these three flow regimes are presented by lift curve and drag curve as shown in Fig.3.3.

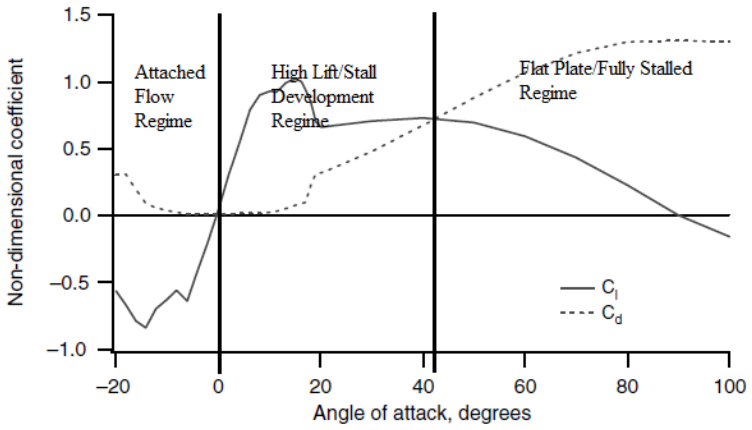


**Fig.3.3. Performance of lift and drag in three flow regimes**

In the attached flow regime, which happened at the negative angle of attack of aerofoil (-20° to 0° in Fig.3.3), the flow is attached to the upper surface of the aerofoil and lift increases with an increase of the angle of attack, but drag is relatively low. Eggleston et al. and Miley et al. (Eggleston & Stoddard, 1987; Miley & Texas, 1982) carried out a series of studies and have shown that the lift coefficient at low angles of attack can be increased and drag can often be decreased by using a cambered aerofoil.

In the high lift/stall development regime, which coursed at low and medium positive angle of attack of aerofoil (0° to about 42° in Fig.3.3), the flow performance is divided into two phases by stall point. The stall happens when the angle of attack reaches a certain value (about 16° in Fig.3.3), and then the separation of the boundary layer on the upper surface takes place. A wake is formed above the aerofoil and it reduces lift and increases drag. The power output of wind turbine in high winds is limited by this condition. When wind speed increases, stall progresses outboard along the span of the blade, causing lift reduced and drag increased. However, there is nearly constant power output as the wind speed increases above a certain value in a well-designed wind turbine(Burton, Sharpe, Jenkins, & Bossanyi, 2002).

In the Flat plate/Fully stalled regime, which happened at the high angel of attack of aerofoil (42° to 90°), the lift keeps decreasing and the drag keeps increasing. The lift force is reduced to zero at about 90°.

In modern commercial wind turbine blades, the aerofoils with high maximum lift coefficients, low pitching moment and low drag, are preferred (Moriarty & Hansen, 2005). Especially for HAWT, the blade tip is designed using a thin aerofoil to achieve high lift to drag ration, and the root region is designed using a thick version of the same aerofoil for structural support(Tangler, 2000). The study of wind turbine blades gives a general view to design the blades of novel wind turbine.

## 3.3. Methodologies of Determining Wind Turbine Performance

Two methods are usually used to analyse the aerodynamic performances of wind turbines. One is computational fluid dynamic (CFD), and the other is wind tunnel test. CFD is used for design process, which can provide a qualitative prediction with less time consuming. Wind tunnel testing is used to simulate the real conditions, which may be expensive and time consuming. Thus, the performance of novel wind turbine will be determined and improved using CFD, and CFD results will be validated by wind tunnel results. The methodologies of CFD and wind tunnel will be introduced in this section.

### 3.3.1. Computational Fluid Dynamics (CFD)

Computational fluid dynamics (CFD) is an efficient way to solve and analyse problems that involves fluid flow problems, using numerical methods and algorithms. With the development of computer resources, the application of CFD has been significantly increased in aerospace and wind energy over last two decades. Since a wind tunnel experiment with a large scale model is quite expensive, CFD simulation becomes more useful. Also, setting up a wind tunnel experiment takes quite a long period of time, which makes CFD simulation more

efficient. The processes of CFD method can be summarised as follow (Versteeg & Malalasekera, 2007):

- Modifying and defining of geometry boundaries.
- Dividing fluid volume into discrete cells, the mesh. The sizes of mesh cells could be various, and be uniform or non-uniform.
- Defining physical conditions, which include equation of motions, materials, viscous regimes etc.
- Selecting of boundary conditions, specify the fluid behaviour and properties at the boundary of the domain.
- Solving the simulation using the equations by using iteration process.
- Visualization of the resulting solution.

The mathematical model of a fluid dynamic problem is based on the equations of continuity, momentum and energy conservation. These equations is called Navier-Stokes (N-S) equations. Thus, the fundamental basis for solving CFD problems is the N-S equations which are used to define any single-phase fluid flow. The N-S equations are nonlinear and complex. When dealing with specific problem, N-S equations should be simplified with an introduction of the minimum amount of complexity while capturing the essence of the relevant physics. Many methods based on N-S equations can be used to solve to aerodynamic problems related to wind turbines, which include direct numerical simulation (DNS), large eddy simulation (LES), detached eddy simulations (DES) and Reynolds Averaged Navier Stokes (RANS). It is reported that DNS, LES and DES methods need more computational resources and are time consuming. Compared with other models, the RANS equations are widely used to solve the aerodynamic problems of wind turbines. In RANS equations, the mean flow can be considered as an incompressible flow or compressible flow. The RANS equations can be

expressed by two equations, continuity equation and equation of motion as shown in equations 3.47 and 3.48.

Continuity

$$\nabla \bullet \vec{u} = 0 \tag{3.47}$$

Equation of Motion

$$\rho \frac{\partial \vec{u}}{\partial t} = -\rho \vec{u} \bullet \nabla \vec{u} + \mu \nabla^2 \vec{u} - \nabla p + \vec{F} \tag{3.48}$$

where $u$ is the flow velocity, $\rho$ is the fluid density, $p$ is the pressure, $F$ is body forces acting on the fluid. The continuity equation is used to ensure that mass flow is always conserved. Thus, there will be no increase in the mass within the control volume for a steady flow. The equation of motion is used to express the balance between unsteadiness in mean flow, the convection by mean flow and mean body force. Each term in equation of motion can be seen in Fig.3.10.

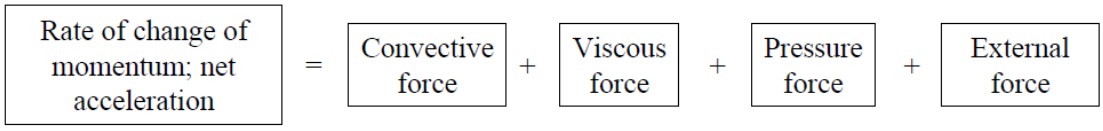


**Fig.3.10. The terms in N-S euquation**

In order to obtain a reasonable accurate solution, three key issues should be validated, which are mesh quality, turbulence model and simulation convergence. The analysis grid should be sufficiently fine to avoid any grid resolution dependence of the simulation results. The correct turbulence model should also be selected to capture flow features in simulation. If a simple turbulence model and a rather coarse grid system are used for a CFD simulation, the obtained airflow rate will not be so reliable since the energy dissipation process is not always simulated accurately(Kato, Murakami, Takahashi, & Gyobu, 1997).

The calculation procedure in a CFD simulation is iterative process, so that the simulation should be guaranteed to converge in order to make sure that the results of the equation coefficients are constant. The studies of turbulence model, mesh quality and simulation convergence will be carried out in following sections.

#### 3.3.1.1. Meshing

In the CFD simulations, the starting point for all problems is a geometry which describes the physics shape of the problem to be analysed. Before an aerodynamic analysis of geometry, there is an important procedure called meshing. A mesh is a discrete representation of the geometry of the problem and it is critical to CFD simulations. The generated mesh should preserve the correct geometry forms of various objects in the simulation with little amount of manual interaction and be capable to facilitate the computational model to capture the characteristics of flow regions. The quality of mesh will affect the rate of convergence, solution accuracy and CPU time required. Thus, there is a significant effect of mesh on CFD simulation results. The process of a mesh generation is complicated and time consuming. The mesh generation should consider the mesh refinement, mesh type and time step. A balance between mesh quality and time consumption should be determined. Main sources of mesh to cause errors can be concluded as follows (Cignoni, Montani, & Scopigno, 1998).

- Too coarse mesh
- High skewness
- Large jumps in volume between adjacent cells
- Large aspect ratios
- Interpolation errors at non-conformal interfaces
- Inappropriate boundary layer mesh

In order to limit the errors, four sub-factors should be validated when generating mesh, which are mesh type, mesh size, mesh skewness and aspect ratios.

Mesh type depends on geometric complexity, flow field and element types supported by a specific solver (Johnson & Tezduyar, 1999). Two different mesh types, tetrahedral mesh and hexahedral mesh are most widely used in CFD simulations.

The mesh skewness is defined by two methods. One is based on the equilateral volume. The mesh skewness can be calculated by equation $Skewness = \frac{optimal\ \ cell\ \ size - cell\ \ size}{optimal\ \ cell\ \ size}$ (The sketch is shown in Fig.3.11 a). This method could only be applied to triangles and tetrahedral mesh type. The other method is based on the deviation from a normalized equilateral angle. The mesh skewness can be expressed as $Skewness(for\ \ a\ \ quad) = \max[\frac{\theta_{\max} - 90}{90}, \frac{90 - \theta_{\min}}{90}]$ (The sketch is shown in Fig.3.11 b). This method can be applied to all cells and face shapes. However, it is always used for prisms and pyramids. The skewness range is from 0 (best) to 1 (worst).

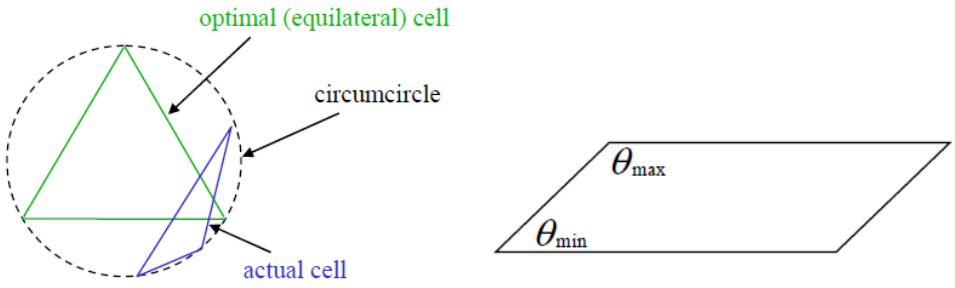


**Fig.3.11. Sketches for determination of skewness**

The mesh cell aspect ratio is the ratio of longest edge length to shortest edge length. It should be near unity where flow is 3-dimensional. A change in mesh cell size should be gradual and

the maximum change in grid spacing should not exceed 20% (Ruppert, 1995). If there are rapid changes in cell volume, larger truncation errors will be resultant.

3.3.1.2. Turbulence Models

Recent advances in computational techniques have considerably increased the use of numerical models, a demand that is encountered by a growing range of commercial and academic CFD software. In a computational procedure, a turbulence model was used to define the system of mean flow equations. The turbulence models are essential to determine the accurate CFD simulation results. The flow condition strongly depends on the turbulence when turbulence appears and it will be the dominant over all other flow phenomena (Kumar, Gupta, & Banerjee, 1998). For turbulence model applications, the selected turbulence model should be accurate, simple and economical to run, while capturing the essence of the relevant physics (Wilcox, 1998). There is no universal turbulence model which can be implemented into all conditions. Thus, the features of different turbulence models were studied. As mentioned in Section 3.3.1, the RANS equations are widely used to analyse the aerodynamic performance of wind turbines. Based on RANS equations, the classical turbulence model can be divided into four groups

- Zero equation model: mixing length model
- One equation model: Spalart-Almaras
- Two equation models: k-ε style models (standard, RNG and realizable), k-ω model and ASM
- Seven equation mode: Reynolds stress model.

To simulate all turbulent motions in a complex flow field is infeasible due to limitations of current computational resources. This is due to the necessity of all grid cells in the domain being smaller than the smallest turbulent motion and that time steps in an unsteady

calculation are smaller than the fastest turbulent motion (Parsons, Wiggs, Walker, Ferguson, & Garvey, 2004).

Even a usage of CFD simulations has extraordinary advantages; there is still a strong need for validation and assessment of the data obtained from a simulation. It is not merely the feedback process of formalizing knowledge and testing if theory is in conflict with reliable data, but numerical approximations, parameterisation schemes and the choice of boundary conditions can also introduce errors in simulated data sets that should be evaluated against measured data(Mohammadi & Pironneau, 1993).

3.3.1.3. Simulation Convergence

Convergence is an important factor to judge the performance of CFD simulation results. It is stated as the solution of the system of algebraic equations approaching the true solution of the partial differential equations having the same initial and boundary conditions as the refined grid system. The performance of the CFD solutions is strongly dependent on whether the errors and uncertainties are identified and qualified. In order to achieve convergence, the numerical method should satisfy two properties, consistency and stability. The consistency is an important property and concerns the discretization of the partial differential equations where the approximation performed should diminish or become accurate if the finite quantities, such as the time step $\Delta t$ and mesh spacing $\Delta x$, $\Delta y$ and $\Delta z$, tend to zero. The stability also strongly governs the numerical solution, and it concerns the growth or decay of errors introduced at any stage during the computation. For most of the commercial CFD codes, the algebraic equations in the system are solved by iteration. In the iteration processes, three important aspects should be abided to deal with CFD codes(Blazek, 2001). Firstly, the simulation can be treated as convergence when the momentum equation, energy equation and other equations achieve a specified tolerance at every nodal position. Secondly, there are no

more changes of residual and other numerical schemes with further iterations, the convergence will be deemed to be achieved. Finally, the balances of overall mass, momentum, energy and scalar are obtained.

Residuals are used to monitor the behaviour of a numerical process that deflects performance of convergence for CFD simulations. If there are large tolerance values of residuals during a simulation process, it will be considered that the simulation results are rather coarse or not sufficiently converged. In general, the residual should be reduced by three orders of magnitude during the iteration process to achieve a qualitative convergence. If so, it is considered that the major flow features are sufficiently established. However, all transport variables, which include energy and scalar species, are required with less convergence tolerance to achieve much stricter convergence. The convergence tolerance of energy and scalar species should be decreased to $10^{-6}$ and $10^{-5}$, respectively, to achieve quantitative convergence (Stern, Wilson, & Shao, 2006). In a CFD simulation, several factors such as poorly constructed mesh, improper solver settings and nonphysical boundary conditions, affect the convergence performance. Of course, the effects of these factors can be reduced by improvements of properties setting. There is another strategy to improve CFD convergence, using under-relaxation factors. The under-relaxation factors are used to stabilize the numerical calculations of governing equations. In order to accelerate the convergence process, good initial conditions should be set up to reduce computational efforts and resources. The under-relaxation factors can be used to accelerate the convergence. However, it should be noticed that a converged solution does not mean an accurate solution.

By applying CFD methodologies, the solutions are approximate and carry numerical errors. The distinction between error and uncertainty should be distinguished. The errors can be defined as a recognisable deficiency that is not due to lack of knowledge while uncertainty

can be defined as a potential deficiency that is due to lack of knowledge. When dealing with numerical solutions, some prevalent sources of errors can be divided into following classifications:

- Discretisation error, which is caused by the difference between the exact solution of the modelled equations and a numerical solution with a limited time and space resolution. Two important factors, the density of the mesh and distribution of the grid nodal points, strongly affect the accuracy of results. However, it is determined that the smaller mesh size or time step in transient problems, the smaller the error, and thus the more accurate the approximation.
- Round-off error, which is caused by the difference between the machine accuracy of a computer and the true value of a variable. The round-off error could be accumulated and will lead to a serious error. A more powerful computer can be used to reduce the round-off error.
- Iteration or convergence error, which is caused by the difference between a fully converged solution of a finite number of grid points and a solution that has not fully achieved convergence. The iteration process of solution should be fully completed and convergence tolerances should be reduced to minimise the convergence error.
- Physical-modelling error, which is caused by uncertainty in the formulation of the mathematical models and deliberate simplifications of the models. Due to the lack of sufficient knowledge to numerical model, it is impossible to select exact equations for solution. There are four sources of uncertainty in physical models. A) the phenomenon is not thoroughly understood; B) there are some degree of uncertainty caused by parameters employed in the model; C) the uncertainty is introduced when appropriate models are simplified; D) the models should be confirmed by experiment. The validation studies can be used to exam the physical-modelling errors.

- Human error, it includes two aspects. One is caused by human mistakes made in programming, which is directly caused by programmer operation and the errors can be removed. The other error is due to application of the code in a less-than-accurate or improper manner. If the level of options available is increased, the potential for usage errors could be increased as well. The human errors could only be reduced through training and accumulating of experience about software operation.

In order to increase the credibility of CFD simulation, detailed analysis should be performed to quantify the modelling and numerical uncertainties in the simulation. Two procedures, verification and validation, are used to quantitatively estimate the inherent errors and uncertainties of a CFD solution. Verification can be defined as a process for assessing the numerical simulation uncertainty and when conditions are permitted, estimating the sign and magnitude of the numerical simulation error and the uncertainty in that estimated error. It verifies procedure, the primarily input parameters, which include geometry, initial conditions and boundary conditions, should be carefully checked and systematically documented. Validation can be defined as a process for assessing simulation model uncertainty by using benchmark experimental data and when conditions are permitted, estimating the sign and magnitude of the simulation modelling error itself. In validation procedure, the results from CFD simulations are compared with experiments that span the range of conditions. Thus, the simulation results will be validated by wind tunnel results in this study.

### 3.3.2. Wind Tunnel Test and Its Application

A wind tunnel is an instrument which is used to measure the aerodynamic properties, such as forces, moments and pressure distribution, of the body placed in the test section. The inner structure of wind tunnel is shaped to achieve steady uniform airflow. A wind tunnel structure usually consists of several elements, the wind tunnel shell, the speed control unit and balance

system used to measure forces and moments(Bradshaw & Pankhurst, 1964). There are two basic types of wind tunnels which are open circuit wind tunnel and closed circuit wind tunnel. There are two basic test-section configurations which are open test section and closed test section. Each type of wind tunnel has its advantages and disadvantages.

A wind tunnel test is an important tool for aerodynamic analysis of wind turbines. It has been used to simulate the real condition and validate the CFD results. A wind tunnel experiment, on the contrary, can reproduce turbulent flow far easier than CFD since it utilizes real physical phenomena. It has been proven that it usually provides useful and reliable predictions of the airflow rate and pressure distributions around building openings. It is reasonable to use wind tunnel testing to analyse the overall airflow rate around an object or wind pressure distributions around a building instead of CFD.

The solid blockage effect is a common phenomenon can be found in a wind tunnel test, which produces an increase in the local wind velocity in a test section. Solid blockage effect is caused by a reduction in the test-section that makes flow to be disturbed compared with the freestream. The magnitude of a solid blockage is expressed by a blockage ratio, which is defined as a swept area of a model to the wind tunnel cross-section. There is a range of blockage ratio from 1% to 10%, that effects of solid blockage can be ignored due to low effect on mean flow (Barlow, Rae, & Pope, 1999). Both the closed test-section and the open test-section can provide large variations when referring to blockage allowances. Due to the ability to leak flow and expand the flow around objects within the test section, the open test section wind tunnel has the capability to allow the flow conditions inside tunnel to be less affected by a larger blockage ratio. The closed test section wind tunnels are more sensitive to solid blockage, but the effects of solid blockage can be corrected by using blockage correction factor(A. Pope, 1954). The blockage correction factor is defined as the sum of the

velocity increment (blockage factor) caused by wake blockage and solid blockage. There are two main correction factors.

- **Pope and Harper blockage correction factor**

This method was carried out by Pope and Harper in 1966(Barlow, et al., 1999), and two equations were defined as $\varepsilon_t = solid\ \ blockage + wake\ \ blockage = \varepsilon_{sb} + \varepsilon_{wb}$ and $\varepsilon_t = \frac{1}{4}\frac{\mathrm{mod}\,el\ \ frontal\ \ area}{test\ \ \mathrm{sec}tion\ \ area}$. According to these two equations, the measured data can be modified as,

Velocity correction $$U = U_u(1+\varepsilon_t) \quad (3.49)$$

Dynamic pressure correction $$q = q_u(1+2\varepsilon_t) \quad (3.50)$$

Reynolds number correction $$R = R_u(1+\varepsilon_t) \quad (3.51)$$

Drag coefficient correction $$C_{D0} = C_{D0_u}(1-3\varepsilon_{sb}-2\varepsilon_{wb}) \quad (3.52)$$

where $U_u$ is measured flow velocity, $q_u$ is measured dynamic pressure, $R_u$ is experiment Reynolds number and $C_{D0u}$ is measured drag coefficient.

- **Maskell correction**

The problems about non-streamline flow bodies, which include bluff-body and partially stalled shapes, were first addressed by Maskell in 1963(Maskell, 1963). It was found that there were remarkable differences of high-lift characteristics for a particular wing aircraft tested in different wind tunnels. According to Maskell's research, a more convincing existence of this interference factor and the need for corrections were established. The further research was carried out by Alexander in 1978(Alexander, 1978), and he did further development of Maskell's method by comparing the drag of flat plates and the

drag of Savonius rotors. The relationship between flat plates and rotors of m (m=B/S) is shown in Fig.3.12. For small values of blockage ration (S/C≤0.045), the value m given by Maskell is 3.15. However, it is suggested by Alexander that the value of m falls close to 2.0 for 30% blockage due to restriction on the wake by the tunnel walls at high S/C values.

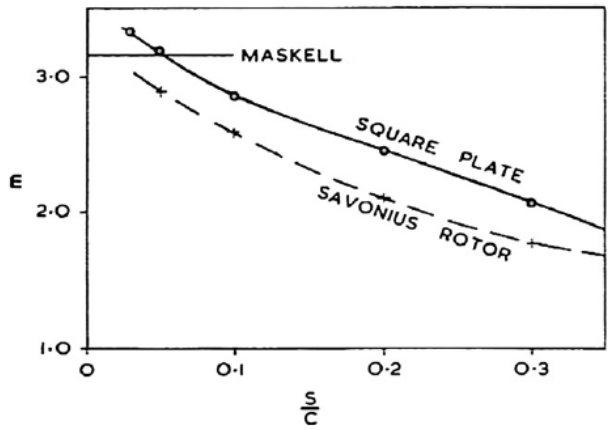


**Fig.3.12. Flat plates and rotors relationship of m vs. A/C (Alexander, 1978)**

According to Alexander's work, the corrected wind velocity can be expressed as,

$$\frac{U_c^2}{U^2} = \frac{1}{1 - m(A/C)} \tag{3.53}$$

where $U_c$ is the corrected wind velocity, $U$ is the undisturbed wind velocity, $A$ is the testing objective frontal area, $C$ is the wind tunnel test section cross section area.

Pressure is an important aspect of studying the aerodynamic performance of structures. The measurement of the pressure could be divided into measuring static pressure and total pressure. There are two methods to measure pressure, pitot tube and pressure transducer.

Both total and static pressure have to be measured over a wide range of Mach and Reynolds numbers to define the forces on bodies or walls and the local magnitude and direction of the fluid velocity.

$$Static\ Pressure\ P_s \rightarrow Wall\ Pressure\ P_w$$

$$Total\ Pressure\ P_T\ (Stagnation\ or\ Reservoir\ Pressure)$$

$$P_T = P_S + P_{Dynamic} \tag{3.54}$$

$$P_T = P_S + \frac{1}{2}\rho U^2 \tag{3.55}$$

where $P_T$ is total pressure, $P_s$ is static pressure, $P_{Dynamic}$ is dynamic pressure, ısity of air and U is the velocity of flow.

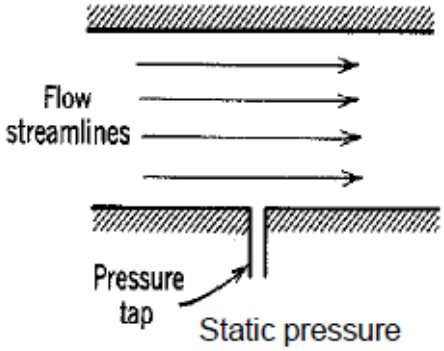


**Fig.3.13. Wall pressure taps for static pressure measurement**

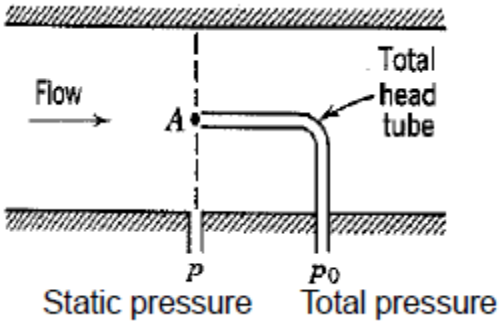


**Fig.3.14. Simultaneous measurements of total and static pressures**

Static pressure measurement can be seen in Fig.3.13. There are four sources of errors in static pressure measurement, eddies developing in the cavity, fluid turbulence, mach number effects and stagnation of the fluid in the holes depending on orifice geometry and burrs (R. W. Miller,

1983). Total pressure measurement can be shown in Fig.3.14. There are six sources of errors in total pressure measurement, which are incident effect, Reynolds number effect, velocity gradient effect, wall proximity effect, turbulence effect and Mach number effect.

Pitot tube is a common tool used to measure pressure, including total pressure and static pressure. Even more, with a digital anemometer, the velocity of flow could be measured. Pitot tubes are not very sensitive to angles of attack which caused by the nose shape and Mach number. Thus, the measured total pressure deviates less than 1% of the dynamic pressure from the true one (Klopfenstein Jr, 1998).

Turbulent also affects the accuracy of pitot tube. It may influence pitot tube reading in two ways. One is the fluctuating velocity component which influences the direction of the flow approaching the orifice, and the other is the fluctuating velocity components which may contribute to the stagnation pressure. The measured velocity is the sum of the mean velocity and the fluctuating components $u', v' and\ w'$, it can be expressed as,

$$U_{total} = U_{mean} + \sqrt{(u')^2 + (v')^2 + (w')^2} \tag{3.56}$$

This results for incompressible flows, into a stagnation pressure defined by

$$P_0 = P_s + \frac{1}{2}\rho U_{total}^2 \tag{3.57}$$

Mach number is another factor which affects the accuracy of pitot tube. However, Mach number variation does not substantially affect the pitot tube pressure measurements if the flow is subsonic. In the supersonic Mach number condition, the shock waves appear and results in pressure lost so that a pitot tube pressure reading is below the isentropic stagnation pressure. Total pressure measurement corrections in supersonic flows are based on the assumption that the shock is normal to the flow. Turbulence intensities of 20%, which are high, will result into a maximum pressure errors of 2% (Lee, 1975).

## 3.4. Summary

In this chapter, the fundamentals of wind turbine blades were introduced. The BEM theory that is widely used to validate the aerodynamic performances of turbine blades has been studied. Two major methods, Computational Fluid Dynamic (CFD) simulation and wind tunnel testing, which are widely used to determine the aerodynamic performances of wind turbines, have been addressed. It has been noticed that the accuracy of CFD results strongly depends on mesh, turbulence models and simulation convergence. The apparatus of wind tunnel also affects the results of wind tunnel test. The CFD simulation and wind tunnel test will be used to determine the aerodynamic performances of the novel wind turbine. The BEM theory will give a reference to analyse the flow characteristics of the novel wind turbine. However, the simulation conditions and wind tunnel apparatus need to be adjusted before investigating the novel wind turbine.

# Chapter 4 – Investigation of the Novel Wind Turbine

In this Chapter, the concept design of a novel wind turbine will be introduced and the flow characteristics of a novel wind turbine prototype will be determined by using CFD simulation and wind tunnel test. The suitability of the novel wind turbine used in urban areas will be validated.

## 4.1. Concept Design of a Novel Wind Turbine

An innovation of wind turbine structure has been carried out to meet the requirements of an urban wind turbine. A completely new wind turbine structure, which did not inherit the drawbacks of HAWTs and VAWTs, has been designed. The specifically designed wind turbine was named as novel shroud wind turbine and it was designed with consideration for all the requirements of urban wind turbines, such as integration, manufacture, maintenance, safety, performance and noise. Before introducing concept of the novel wind turbine, three highlights from previous wind turbines (Abe, et al., 2005; Müller, et al., 2009; K. Pope, et al., 2010) were addressed and implemented on the novel wind turbine.

- Flow acceleration structure. The power outputs of urban wind turbines were limited by low flow velocities in urban areas. It was proved that diffuser structure could significantly improve the power output of HAWTs through wind energy concentration. Thus, the flow acceleration structure is needed to improve the power output of the novel wind turbine.
- Flow guided structure. The direction of flow can be modified by guide vanes before approaching blades to achieve best angle of attack, so that the power output of the wind turbine can be improved. The flow direction in urban areas may frequently

change. Thus, it was considered the possibility to modify various directions of flow to a unified direction. By doing this, the requirements of wind turbine blades can be reduced.

- Location. The roof top of high building is a good option for an urban wind turbine. Due to the space limitation in urban areas, the roof top of building can be utilised without taking up the spaces for building. It was also proved that high building can provide high velocity of wind flow. Thus, the novel wind turbine was designed to be located on roof top of high buildings.

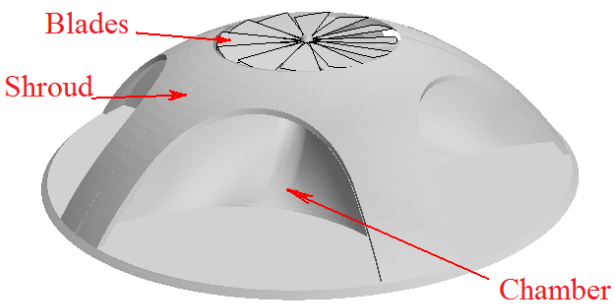


**Fig.4.1. Concept of a novel wind turbine**

The design concept of the novel wind turbine was firstly carried out in 2008(SURESHAN, 2008). A typical structure of a novel wind turbine can be seen in Fig. 4.1. A novel wind turbine system consists of two parts, turbine shroud and turbine blades. The turbine shroud is a dome structure with chambers, and the blades are simple twisted structure located at the top of shroud outlet. The blades can be protected by shroud instead of being exposed to surroundings. The safety of the novel wind turbine can be improved, even if the blades rotate at high speed. The scale of the novel wind turbine can be changed to be installed on different buildings. The design of shroud was considered with appearance and integration with urban environments. The generator and other components can be placed inside the shroud to be

protected. Also, the novel wind turbine does not need hub structure and it will be easy to access for maintenance. The shroud consists of several chambers, which are located along the circumference of shroud to capture flows from any directions. The flows from any direction are led to the vertical outlet through the chambers. Thus, the performances of novel shroud wind turbine are not affected by the frequently changing flow directions in urban areas. The complex flow conditions in urban area can be simplified to one constant direction flow, so that the requirements of the novel wind turbine blades can be relaxed. The simplicity of wind turbine blades can make it possible to reduce its manufacture cost. In order to improve the performance of novel shroud wind turbine, each single chamber was designed as an acceleration structure. The flow can be accelerated through the chamber. The concentration of wind energy is achieved by the chamber, so that the potential of system power output can be improved. An image of a novel shroud wind turbine placed in an urban environment can be shown as Fig.4.2.

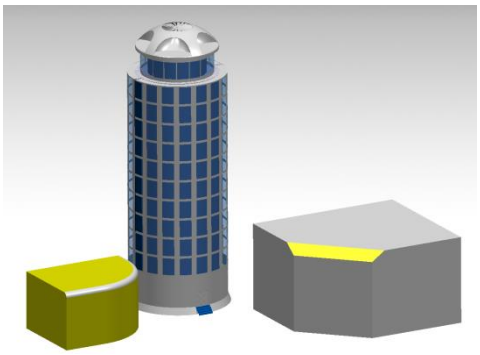

**Fig.4.2. Location of the novel wind turbine in an urban environment**

## 4.2. The Model of the Novel Wind Turbine

As introduced, the novel wind turbine consists of two parts, namely shroud and blades. The shroud is used to improve the suitability of the novel wind turbine to be installed in urban

environments. Thus, the performance of shroud is critical to achieve success of the novel wind turbine. The performance of shroud will be assessed in two aspects. One is the ability to unify different flow directions to a single vertical direction, and the other is the ability to accelerate the flow. These two aspects are essential for an urban wind turbine because its power output is limited by frequently changing direction and low speed of the flow in urban areas. According to the design concept, a CAD model of the shroud part of the novel wind turbine was created in CATIA V5 R20 as shown in Fig.4.3. The model contains four chambers to collect winds from different directions. The model was created in 500mm radius of base ($R_{base}$) 200mm height (H) and 175mm radius of outlet ($R_{outlet}$). The technical drawing of the prototype was shown in Appendix I.

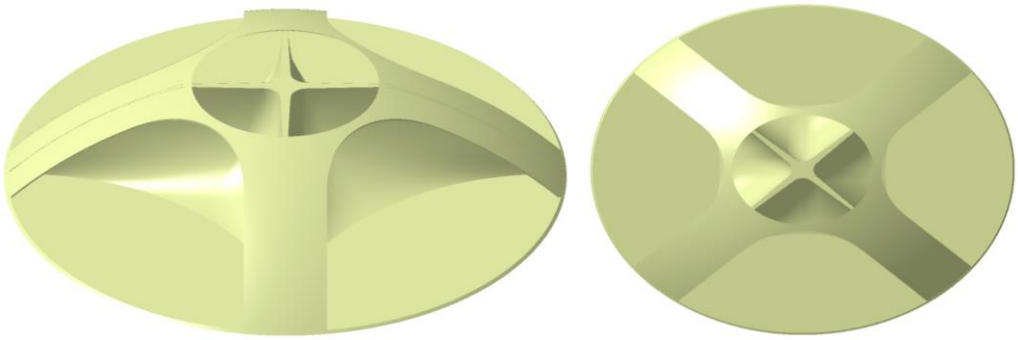

**Fig.4.3. CAD model of the structure of the novel shroud**

The shroud can be divided into two parts, namely internal shape and broad. The structures of internal shape and broad are shown in Fig.4.4 and Fig.4.5, respectively. The internal shape was designed to lead the flow from various horizontal directions to the vertical outlet and the broad part was used to cover the internal shape to avoid flow splitting.

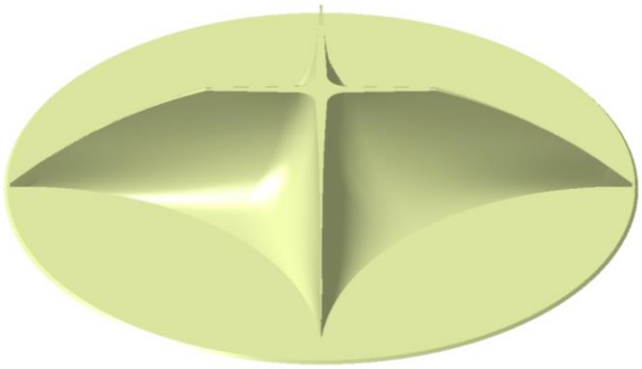

**Fig.4.4. Structure of internal shape**

**Fig.4.5. Structure of broad**

The dimensions of internal shape were shown in Fig.4.6. From the front view in Fig.4.6, it can be seen that the whole shroud was divided into four sections. The diameter ($D_{base}$) of the shroud is 1000mm. The flow from horizontal direction was led into chamber and started to be altered to vertical at 300mm (L) after entering chamber. The leading curve that alters flow from horizontal to vertical is tangential to axis. As shown in Section view B-B in Fig.4.6, the leading curve is also tangential to vertical axis to achieve vertical flow. The height (H) of the shroud is 200mm.

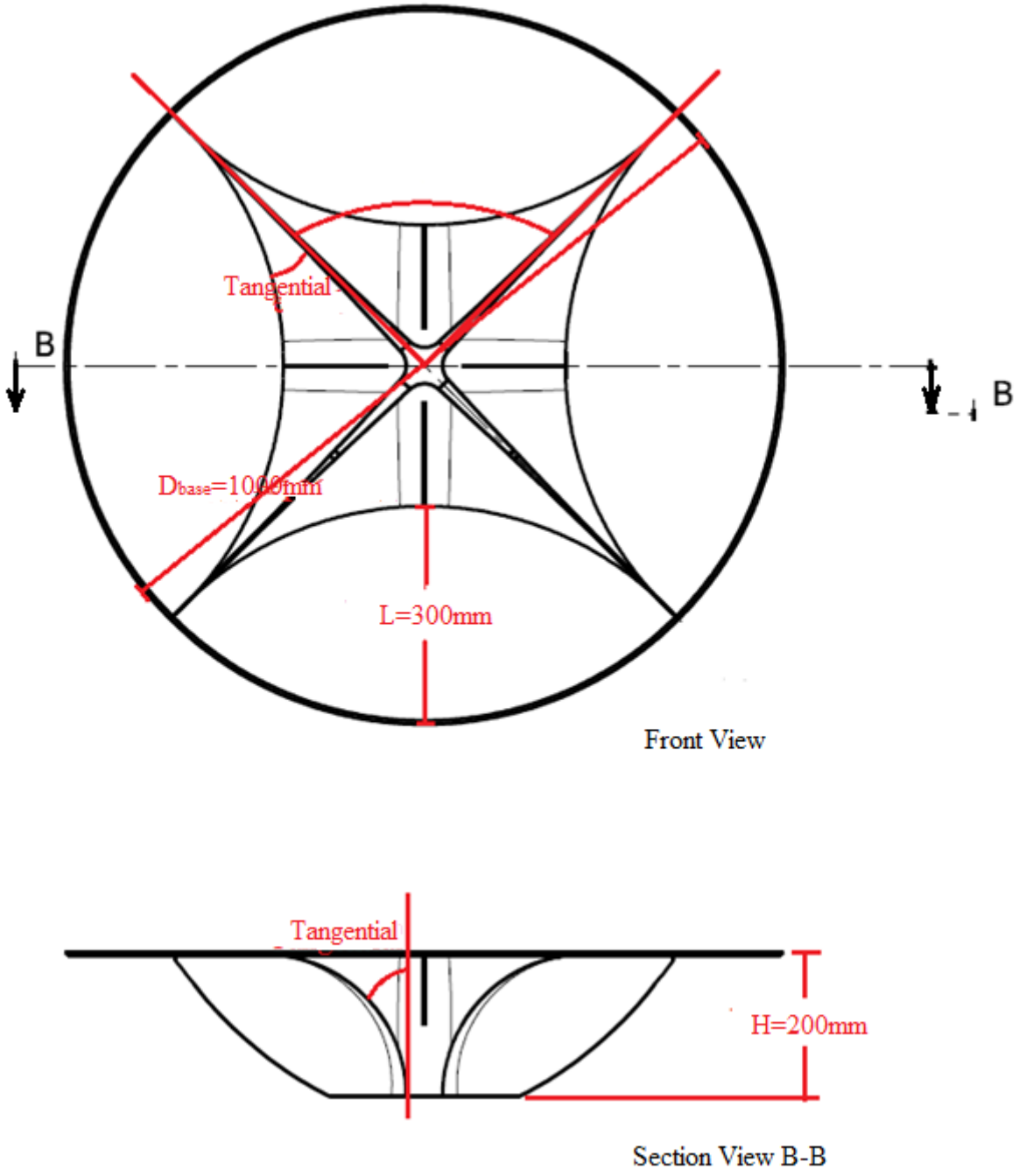


**Fig.4.6. Dimensions of internal shape of a typical shroud**

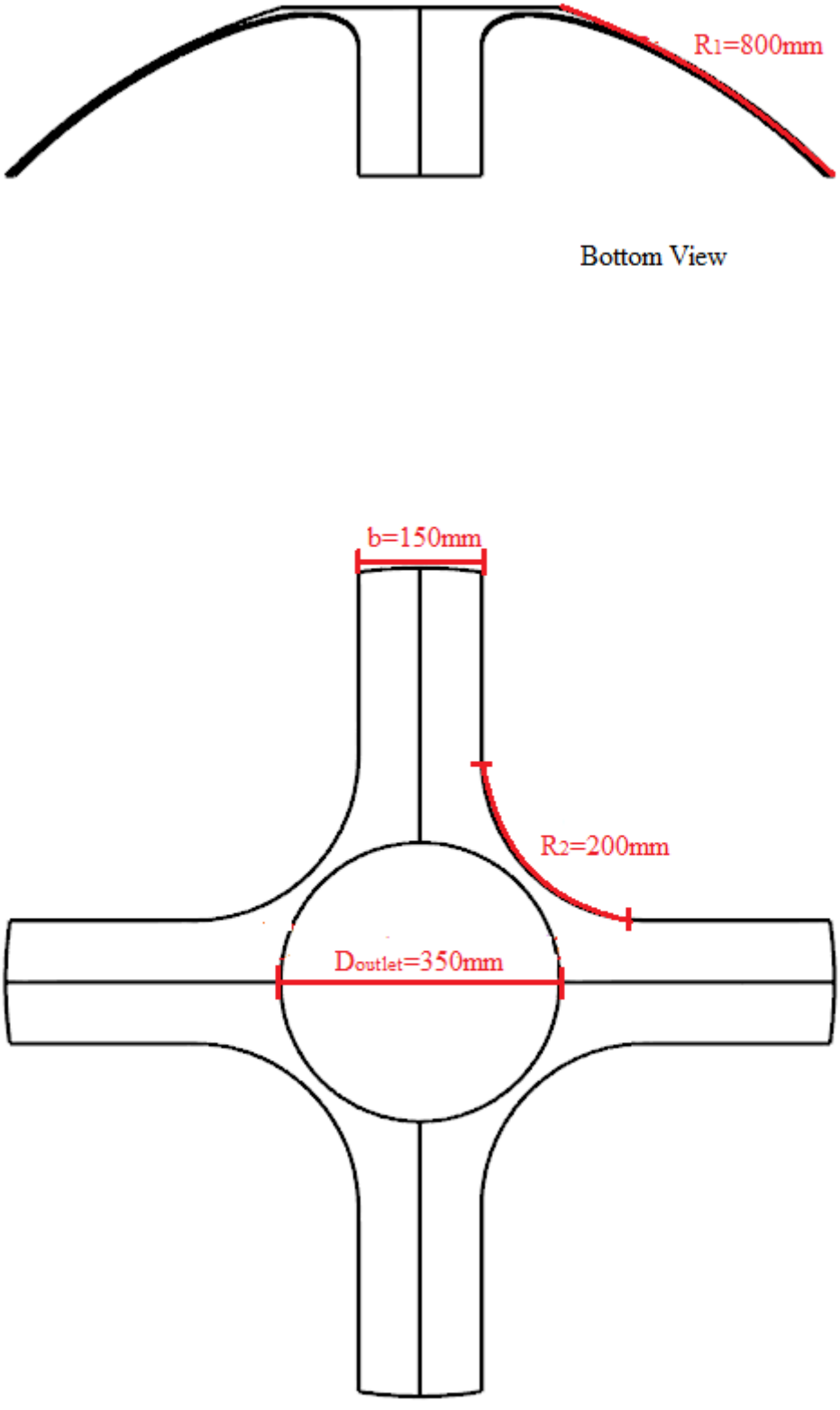


**Fig.4.7. Dimensions of broad**

The dimensions of broad are shown in Fig.4.7. The four chamber model has a 800mm radius ($R_1$). The diameter of the outlet depends on the dimension of broad and the four chamber model has the outlet with 300mm diameter ($D_{outlet}$). The broad width is used to avoid flow split out before starting to turn to vertical, and it is 150mm for original model. The broad width cannot be unlimited increased, since it may block the flow to go into a chamber and reduce the performance of flow concentration. The value of cutting radius ($R_2$) is used to control the shroud width covered, and the large $R_2$ will give the shroud more covered range.

## 4.3. CFD Modelling of the Novel Wind Turbine

In order to determine the flow characteristics of shroud, the computational fluid dynamic (CFD) method was used to investigate its performance. The CFD simulation is a fast way to analyse the fluid dynamic problems, but the accuracy of CFD simulation strongly depends on the mesh conditions and physical conditions. Thus, the validations of simulation settings were carried out before analysing the shroud. Commercial CFD software package Star-CCM+ was used to do the simulation.

### 4.3.1. Mesh Validation

In Star-CCM+, three mesh models, which are Polyhedral, Tetrahedral and Trimmer, can be used to generate a volume mesh. The polyhedral meshes provide a balanced solution for a complex mesh generation problem. It is easy and efficient to build, and requires no more surface preparation than Tetrahedral and Trimmer mesh. Trimmer mesh is usually used for simple mesh generation problems to produce grid. The polyhedral cells typically create an average of 14 cell faces. The mesh cells generated by polyhedral meshes contain

approximately five times fewer cells than a trimmer mesh for a given starting surface(Guide, 2009). Thus, the mesh type in this study was set as Polyhedral.

The total number of mesh cell will significantly affect the accuracy of CFD results. Coarse mesh will reduce the accuracy of results, and fine mesh will achieve more accurate results. However, the mesh size could not be refined infinitely. The more mesh cells are used, the more computer resources will be needed. In order to determine a suitable mesh size setting, various base mesh sizes were tested. The velocity at a specific point as shown in Fig.4.8 was used to compare the effects of number of mesh cell on accuracy of simulation. The velocities at vertical direction were measured for comparison purpose.

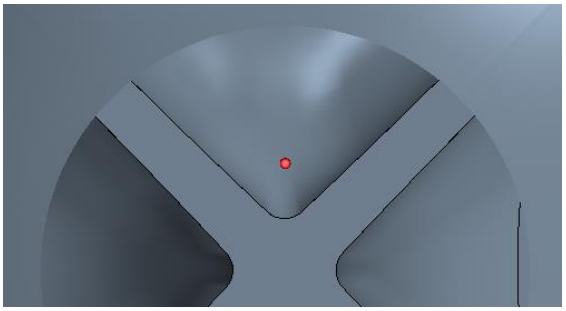

**Fig.4.8. The location of calibration point**

The CPU time is mainly considered for validation purposes. The most suitable size will be chosen by considering accuracy and resource usage. A typical four chamber model (details see appendix I) with a specified size of domain was used for the validation. The variable results which were measured by using different numbers of mesh cell are shown in Table 4-1.

| Cell Number | CPU Time (s) | Velocity (m/s) |
|---|---|---|
| **508356** | 42163 | 9.693 |
| **593082** | 50267 | 9.797 |
| **702472** | 59830 | 9.872 |
| **857355** | 77213 | 9.964 |
| **1192215** | 103468 | 10.031 |
| **1575355** | 133021 | 10.151 |
| **1970652** | 185305 | 10.183 |
| **2598948** | 249446 | 10.198 |
| **3902964** | 354498 | 10.205 |
| **5537220** | 485887 | 10.222 |

**Table 4-1.The effects of various mesh sizes on simulation CPU time and accuracy**

According to the results from Table 4-1, two plots were created to validate the accuracy of simulation results using various mesh sizes. One plot shows the time consumption of simulations against number of cells, which is presented in Fig.4.9. The other plot shows the velocity at the given point against number of cells, which is presented in Fig.4.10.

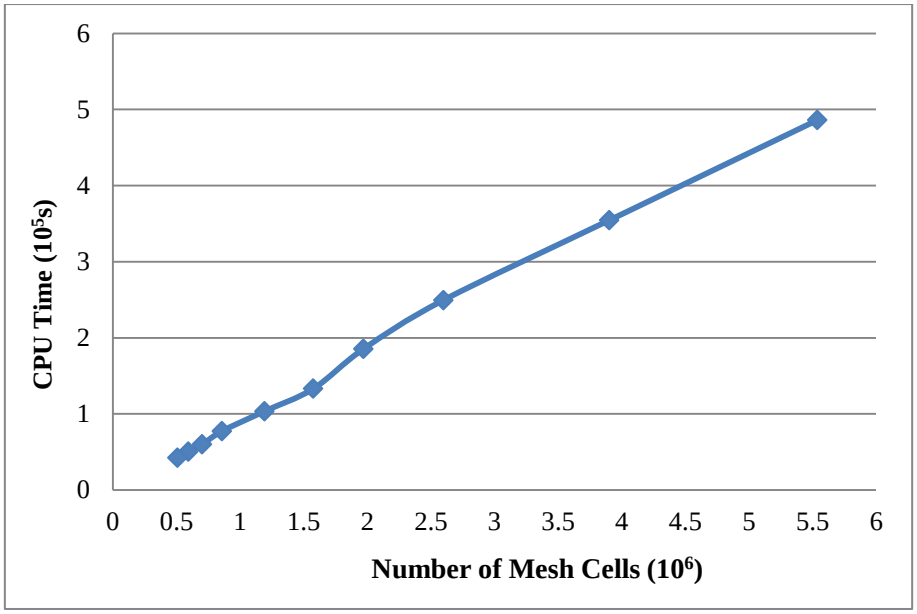


**Fig.4.9. CPU time vs. number of mesh cells**

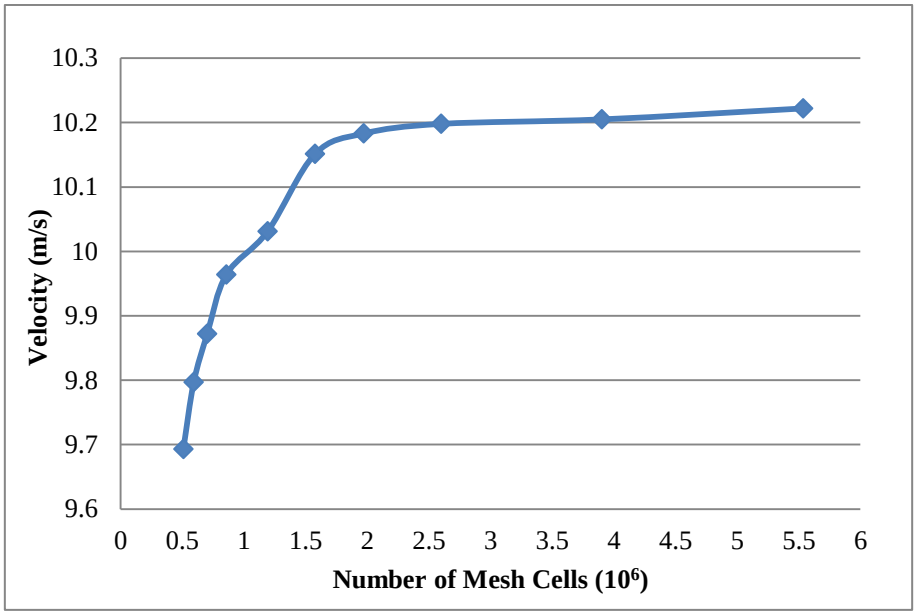


**Fig.4.10. Velocity at the point vs. number of mesh cells**

According to Fig.4.9, it can be found that the CPU time is proportional to the number of mesh cells. There is a significant increase of CPU time due to an increase of mesh cells. The gradient of increasing function is about 0.9. The accuracy of simulation was presented by the velocity at one specific point, and the velocity was measured and plotted against the number

of mesh cells as shown in Fig.4.10. It can be found the accuracy of measurement increases with mesh cells. However, it can be seen that from about $4\times10^6$ mesh cells, the increase of velocity slows down. The velocity increases for about 0.039m/s, which is about 0.38%, compared with velocity measured from $5.5\times10^6$ mesh cells simulation. However, there is a significant increase of CPU time between the simulations, which are due to these two base mesh sizes. The CPU time increased from 185305s to 485887s, which is about 1.62 times increase. The tolerance of results is reduced to a small value since $4 \times 10^6$ mesh cell. The accuracy of the results is acceptable using about $4\times10^6$ mesh cells, but the CPU time is continuing to significantly increase. Thus, the $4\times10^6$ mesh cells will be used for simulations, which can provide accurate results with reasonable time consuming.

### 4.3.2. Physical Validation

The flow field in this study has been identified. Two different solvers can be chosen from Star-CCM+ settings, which are segregated solver and coupled solver. Because the simulation problems are based on low Mach number, the segregated flow solver with constant density of air was used. It was suggested that choosing the segregated flow solver for incompressible or mildly compressible flow (Guide, 2009). Also, the algorithm of segregated flow uses less memory than the coupled flow algorithm. According to the flow properties, Reynolds averaged Navier-Stokes equations were employed and the flow was set as incompressible in this study.

The turbulent model was set as standard K-Epsilon model. In this study, the standard K-Epsilon model was specified as standard low-Reynolds Number K-Epsilon mode, which has an identical coefficient to the standard K-Epsilon model and also can provide additional damping functions that allow the standard K-Epsilon model to be applied in the viscous-affected regions near walls(Avva, Smith, & Singhal, 1990).

### 4.3.3. Convergence

The convergence is an important factor to judge the performance of CFD simulation results.. The algebraic equations are solved by iteration in Star-CCM+. The residuals are used to monitor the behaviour of numerical process in Star-CCM+, and an example of residuals monitor plot is shown in Fig. 4.11. Due to mesh and physical conditions in this study, the iteration steps were set as 2000 that is enough for simulations to achieve convergence. The simulation requires 40 hours to achieve convergence by running on a work station of Intel Core i7-2600S with 2 parallel processors. The residual of all the simulations have been reduced to less than five orders of the magnitude to achieve simulation convergence(Carle & Fagan, 1996). The under-relaxation factors of velocity are reduced to 0.6 to improve the stability and convergence rate of the iteration process (Van Doormaal & Raithby, 1984).

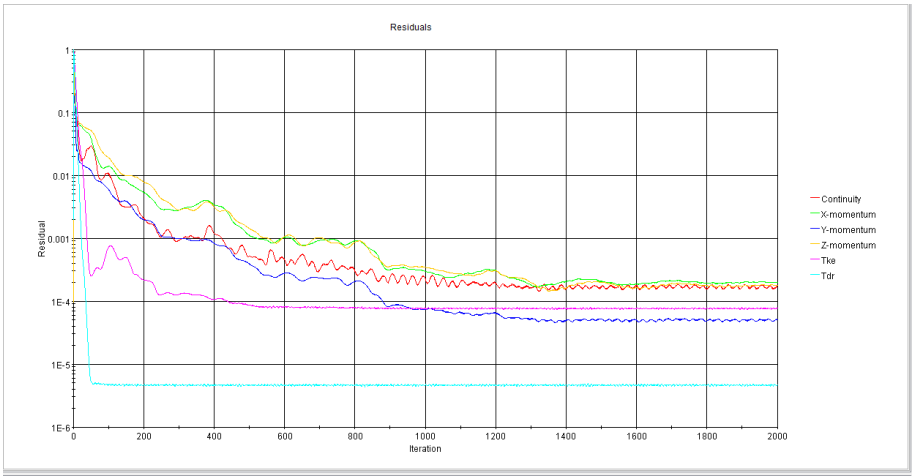


**Fig.4.11. Convergence Monitor**

### 4.3.4. Computational Conditions

A three dimensional (3D) steady state analysis was carried out using the computational fluid dynamics (CFD) method to determine the flow characteristics of the shroud. The computational conditions are shown in Fig.4.12. The flow was assumed to be a steady flow. As shown in Fig.4.12, h, d and D, respectively, denote model height, base diameter and outlet

diameter. The simulation settings were validated in Section 4.3.1 and Section 4.3.2. The settings have been used to do all the simulations in this thesis. For the inlet boundary condition, a uniform flow with 1% of free stream turbulence, which as wind tunnel flow condition, was specified. At the outlet boundary, the boundary type was set as pressure outlet. The walls were specified as slip and the ground was set as no-slip. The flow characteristics around is more interesting. Thus, finer mesh was used around the shroud. There were about 4,000,000 cells in total used for the simulations. The meshed domain and a meshed shroud model which was extracted from the meshing system are shown in Fig.4.13.

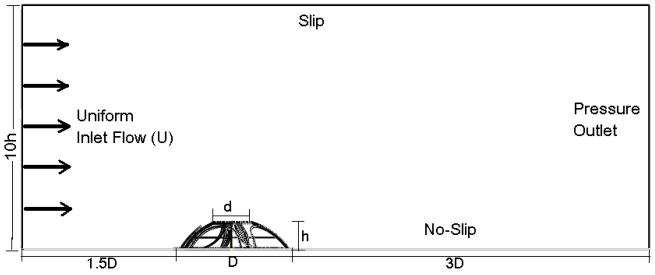


**Fig.4.12. Computational modeling conditions**

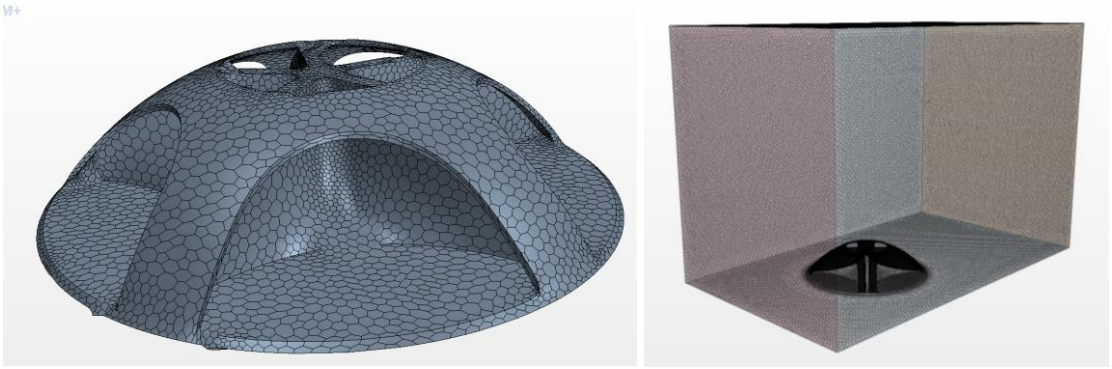

(a) (b)

**Fig.4.13. Simulation meshing. (a) a meshed shroud, (b) a mesh domain**

## 4.4. Wind Tunnel Apparatus for the Novel Wind Turbine

The wind tunnel test was carried out to validate the computational fluid dynamic (CFD) results. The wind tunnel tests of the shroud were carried out under controlled test parameters, such as a flow speed and the angle of approaching flow. The wind tunnel tests were performed in an open jet closed return wind tunnel at the University of Hertfordshire. This wind tunnel has a jet of 480mm diameter, with a maximum wind velocity of 55m/s. The flow turbulence intensity was less than 1%, and the flow uniformity was greater than 99%. As shown in Fig.4.14, the model of the wind turbine shroud was placed at the wind tunnel test section about 500mm upwind from the jet in order to achieve steady and central direction flow. The free stream velocities were specified in a range of 2m/s to 12 m/s to perform the wind flow in an urban area. The flow velocity within the test section was measured with a pitot tube connected to the test section. The specific tiny pitot tubes were used to measure the flow velocities at the outlet of the shroud. The pitot tubes were connected with a digital manometer and the values of velocities could be read from the digital manometer.

**Fig.4.14. A tested sample in wind tunnel test section**

The accuracy of tiny pitot tubes was tested in a wide range of flow velocities, from 1m/s to 20m/s, in steady flow. The results from a tiny pitot tube were compared with commercial pitot tube results. It was found the errors between the tiny pitot tube and the commerical pitot tube were less than 2% in high flow velocities (as shown in Table 4-3). It is acceptable to suggest that the geometry parameter of tiny pitot tubes is suitable for measuring the flow parameters in and around the shroud.

| Commercial Pitot Tube (m/s) | Tiny Pitot Tube (m/s) | Error (%) |
|---|---|---|
| 2 | 2 | 0 |
| 3 | 3 | 0 |
| 4 | 4 | 0 |
| 5 | 5 | 0 |
| 6 | 5.9 | 1.7 |
| 7 | 6.9 | 1.4 |
| 8 | 8 | 0 |
| 9 | 8.9 | 1.1 |
| 10 | 9.9 | 1 |
| 11 | 10.9 | 0.9 |
| 12 | 11.8 | 1.7 |
| 13 | 12.9 | 0.77 |
| 14 | 13.8 | 1.4 |
| 15 | 14.8 | 1.3 |
| 16 | 15.8 | 1.25 |
| 17 | 16.7 | 1.76 |
| 18 | 17.7 | 1.67 |
| 19 | 18.6 | 2.1 |
| 20 | 19.5 | 2.5 |

**Table.4-3. Validation of tiny pitot tubes**

The shroud model was rotated and tested in variable directions and velocities of the approaching flows in order to simulate different conditions that an urban wind turbine could face in urban enviroments. The velocity at its vertical outlet of the shround is a critical factor defining the capability of wind energy concentration of the shroud structure. As shown in Fig.4.15, five sampling points at the outlet of a chamber were selected and measured. The coordinates of these five points can be seen in Appendix B. These five points were selected because their positions were typical to reflect the velocity distribution within the outlet of a

chamber, based upon the computational simulation results. Their aerodynamic parameters can illustrate the flow feature at the outlet, such as the maximum and minimum flow velocities. Based on the symmetry structure of shroud, the model was tested for $45^{o}$ with an interval of $15^{o}$. For each direction of the free stream flow, the model was tested in the flow velocity range from 2m/s to 10m/s with an increment of 1m/s.

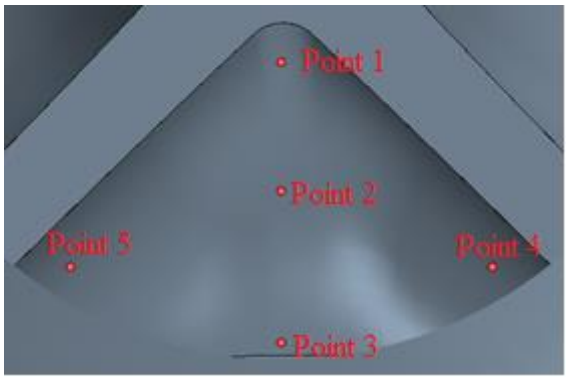


**Fig.4.15. Locations of measureing points in wind tunnel test**

## 4.5. Computational Fluid Dynamic (CFD) Results

The Reynolds number of the novel wind turbine is defined as,

$$\mathrm{Re} = \frac{\rho V D}{\mu} \qquad (4.1)$$

where $\rho$ is the density of air, $V$ is velocity of approaching flow, $D$ is diameter of the shroud and $\mu$ is dynamic viscosity of the fluid.

In order to simulate flow characteristics in urban areas, the simulations were conducted at a range of flow velocity from 1m/s to 10m/s in 0° direction and under different directions from 0° to 180° of approaching flows with an increment of 15°. The testing flow range included the low speed condition in urban areas and various directions of approaching flows were used to simulate frequent changing flow direction in urban areas. The reference of 0° approaching flow is shown in Fig.4.16 and the model is rotated anti-clockwise with an increment of 15° .

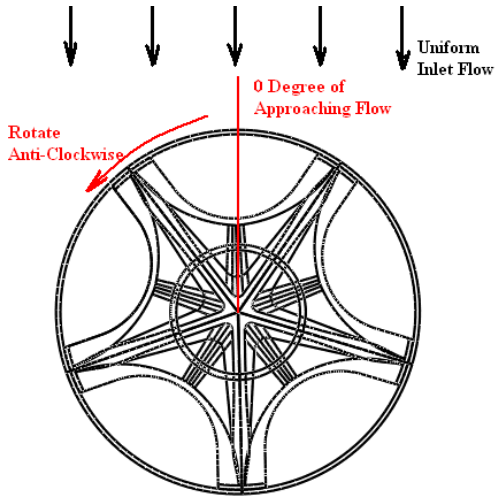


**Fig.4.16. Model testing condition**

The shroud was designed to capture wind flow from different directions and accelerate the flow velocity so that the flow characteristics at the shroud outlet were used to estimate the capability of wind energy concentration of the shroud. The flow velocities, which include average flow velocity and maximum flow velocity, at shroud outlet were measured. The average flow velocity can be used to estimate the power output that can be generated by a wind turbine, and the value of power output can be calculated from $P = \frac{1}{2}\rho A V^3$. For the novel wind turbine, the $A$ is defined as the aerodynamically useful area of the shroud outlet. It was noticed that the mass flows through the shroud outlet were different for various directions of approaching flow. Thus, the aerodynamically useful area of the shroud outlet can be expressed as $A_{useful} = \frac{n}{N} A_{shroud-outlet}$. $N$ is the total number region that the shroud outlet was divided into, and $n$ is the number of regions that mass flow went through. The value of the maximum velocity was measured within the aerodynamically useful area and the value of the average velocity was calculated due to the flow velocity in the aerodynamically useful area.

According to Blade Element Momentum (BEM) theory, the location of maximum velocity might improve the performance of blades. Both the values and locations of maximum

velocity will be measured and determined. The flow characteristics of the shroud in different directions and velocities of approaching flows were determined as a ratio of maximum velocity versus inlet velocity of approaching flow and average velocity against inlet velocity of approaching flow. The maximum increase ratio and average increase ratio, respectively, are calculated by $U_{max}/U_{approaching}$ and $U_{average}/U_{approaching}$. The average velocity ratios and maximum velocity ratios for various flow directions in a wide velocity range were shown in Fig.4.17 and Fig.4.18 respectively.

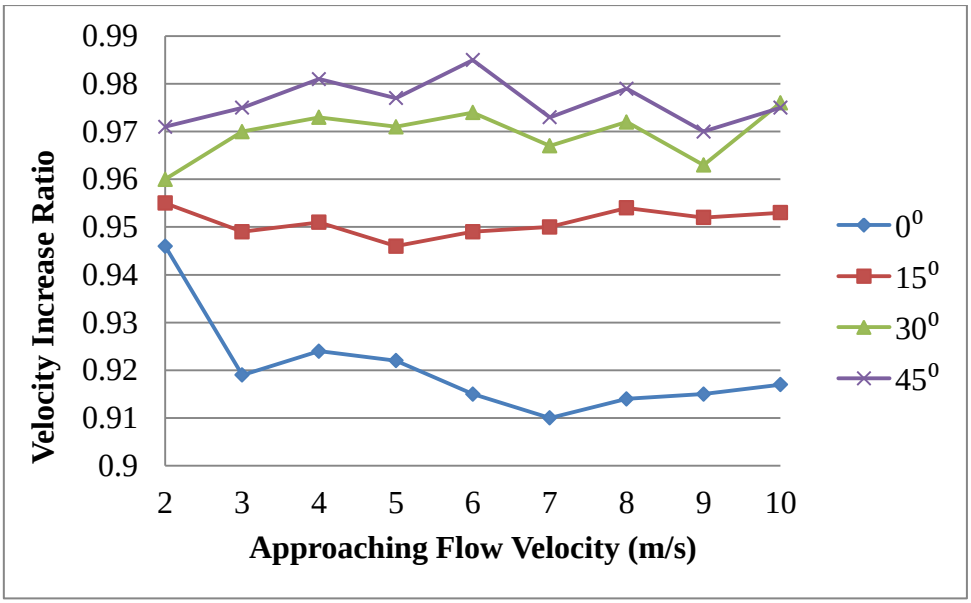


**Fig.4.17. Average velocity increasing ratio against approaching flow speed**

The average velocity increasing ratios at the shroud outlet area were used to present the total energy can be generated from the flow. As shown from Fig.4.17, the average velocity increasing ratios are about 0.92, 0.95, 0.97 and 0.98, respectively, at $0^o$, $15^o$, $30^o$ and $45^o$ of approaching flows. There is no significant alteration of average velocity increasing ratio under various approaching flow speeds. The wind energy concentration of the shroud is not affected by approaching flow velocity. According to Fig.4.17, it can be determined that the direction alteration process of approaching flow can be achieved. The flow from any directions can be led to the vertical outlet with about 5% velocity loss, which will cause 15%

energy loss. The average velocities at outlet area are less than those at the approaching flow area, but the problem of frequently changing wind directions can be solved with implementing the shroud. However, the power output of the novel wind turbine is not only depended on the average velocities at outlet, but also is affected by the location and values of maximum velocity at outlet.

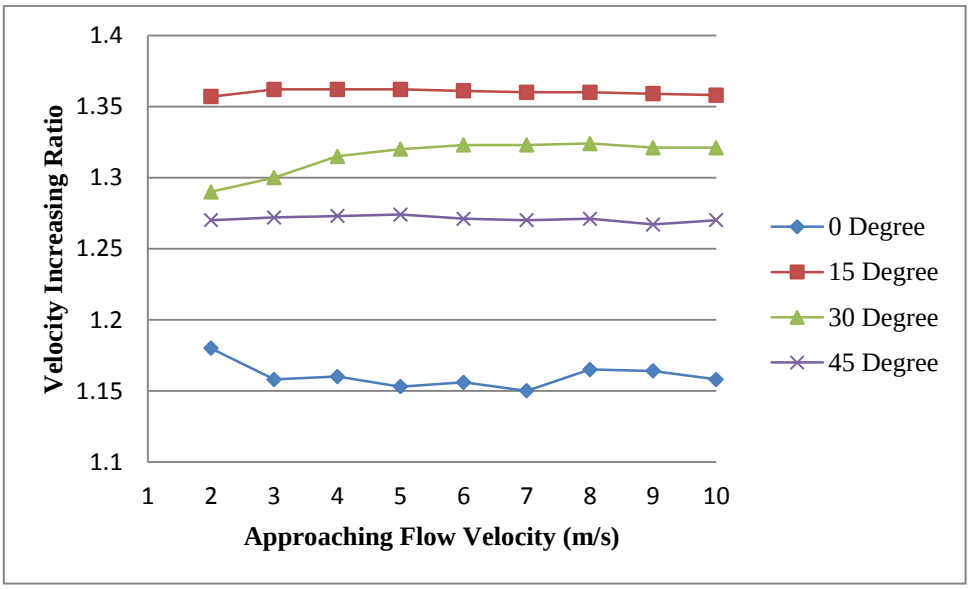


**Fig.4.18. Maximum velocity increasing ratio versus approaching flow speed**

The maximum velocities at the outlet layer of shroud were measured, and the maximum velocity increase ratios were calculated. According to Fig.4.18, the maximum velocity increasing ratios are 1.15, 1.36, 1.325 and 1.275 at $0^o$, $15^o$, $30^o$ and $45^o$ of approaching flows, respectively. The maximum velocities at various directions of flows are higher than the velocity of approaching flow. It proves that there are high velocity regions at the outlet area for different conditions. The locations of these high velocity regions are essential to improve the power output of the novel wind turbine. The high velocity regions are located at blade tips which can generate large forces at the blade tip. Due to the blade element momentum (BEM)

theory, the large forces acted near blade tips will generate more torque to contribute to power output of a wind turbine. This feature will be detailed in Chapter Five.

The flow characteristics inside the chamber is an important issue to do further improvements of the system.The flow behaviour inside the chamber was therefore studied. The model was simulated in different velocities of approaching flows at 0°. In order to visualise the flow performance inside the chamber, flow velocities along three different streamlines inside the chamber were measured. The locations of these three streamlines are shown in Fig.4.19, and coordinates of 15 points on each layer are listed in Appendix C.

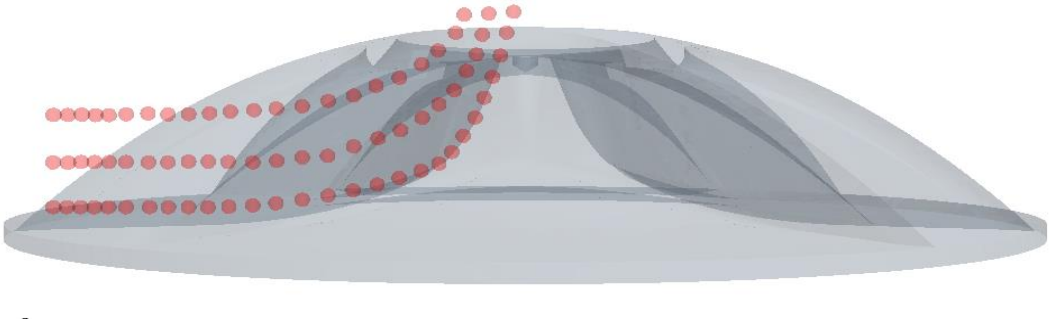

**Fig.4.19. Point distribution inside a chamber**

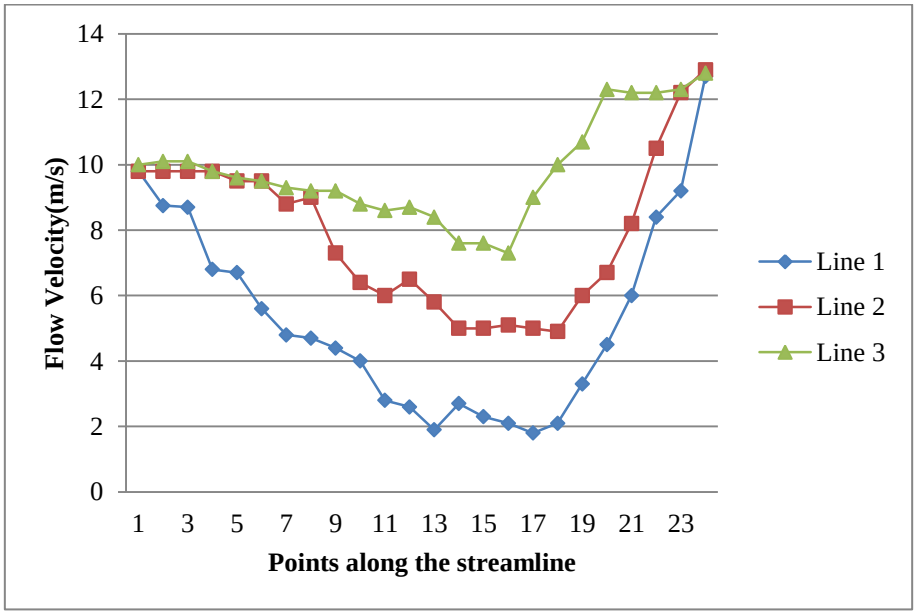


**Fig.4.20. Plot of velocity distribution across a chamber**

The velocities along these three layers are plotted in Fig.4.20. As shown in Fig.4.20, the alteration of flow through chamber can be seen. The flows in different layers have similar trends, which were decreased after entering the chamber then accelerated near the chamber outlet. Before entering the chamber, the flow velocities at different layers were the same as those of approaching flow, which are 10m/s. The velocities started to reduce after the flow went into the chamber. The worst case happened at lowest layer, which is near the surface of chamber. The reduction may be caused by the viscous friction near the surface of shroud inside the chamber during a flow alteration process. The velocity at the lowest layer was dragged down so that the velocities at other layers were reduced as well. When the flow went near the chamber outlet, the velocities started to accelerate significantly. This is because the alteration process of flow had completed, and the compressed process started. It is suggested that these phenomena happened after flow direction turned to vertical. Thus, it may be possible to improve the flow acceleration of shroud by increasing the vertical height.

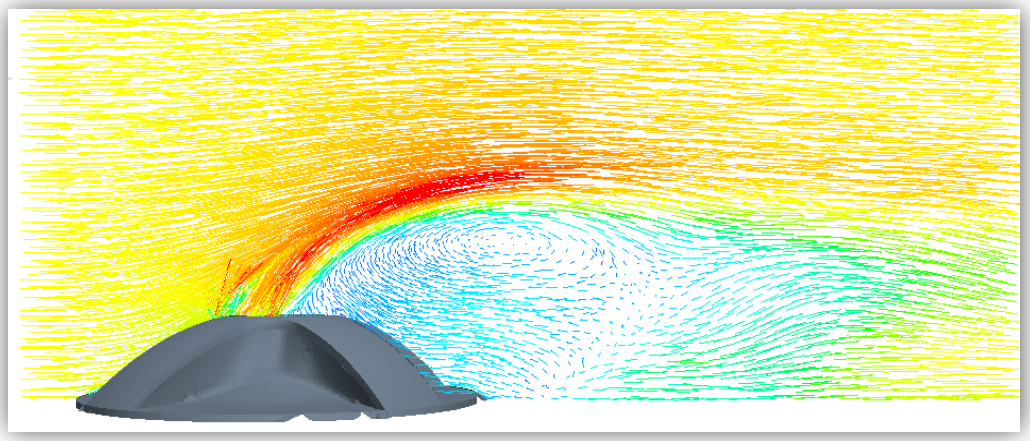

**Fig.4.21. Vector field of flow through a chamber of the novel wind turbine**

A study of flow around the novel wind turbine shroud was carried out. The vector of flow through novel wind turbine shroud is plotted, and vector field of flow has been shown in Fig.4.21. It was found out that the flow at the outlet area was affected by free stream flow after the flow through the chamber. Thus, the flow direction at the outlet was affected. The flow velocity around wind turbine system is accelerated because of sphere structure of the wind turbine system. With this effect, the pressure at the outlet can be reduced. Hence, it is an important feature to improve the flow acceleration of shroud by decreasing pressure at the outlet. The pressure decrease at outlet will generate a low pressure region, so that more mass flow can be draw into the chamber. This will be helpful for further improvement of shroud.

## 4.6. Wind Tunnel Testing Results

The wind tunnel tests were carried out to validate computational fluid dynamic (CFD) results. The velocities at five points located at the shroud outlet layer were measured and compared with CFD results.. Each group of data was tested and measured five times, and the average values are calculated to reduce the errors of wind tunnel tests. The error analysis of wind tunnel data was shown in Fig.4.22.

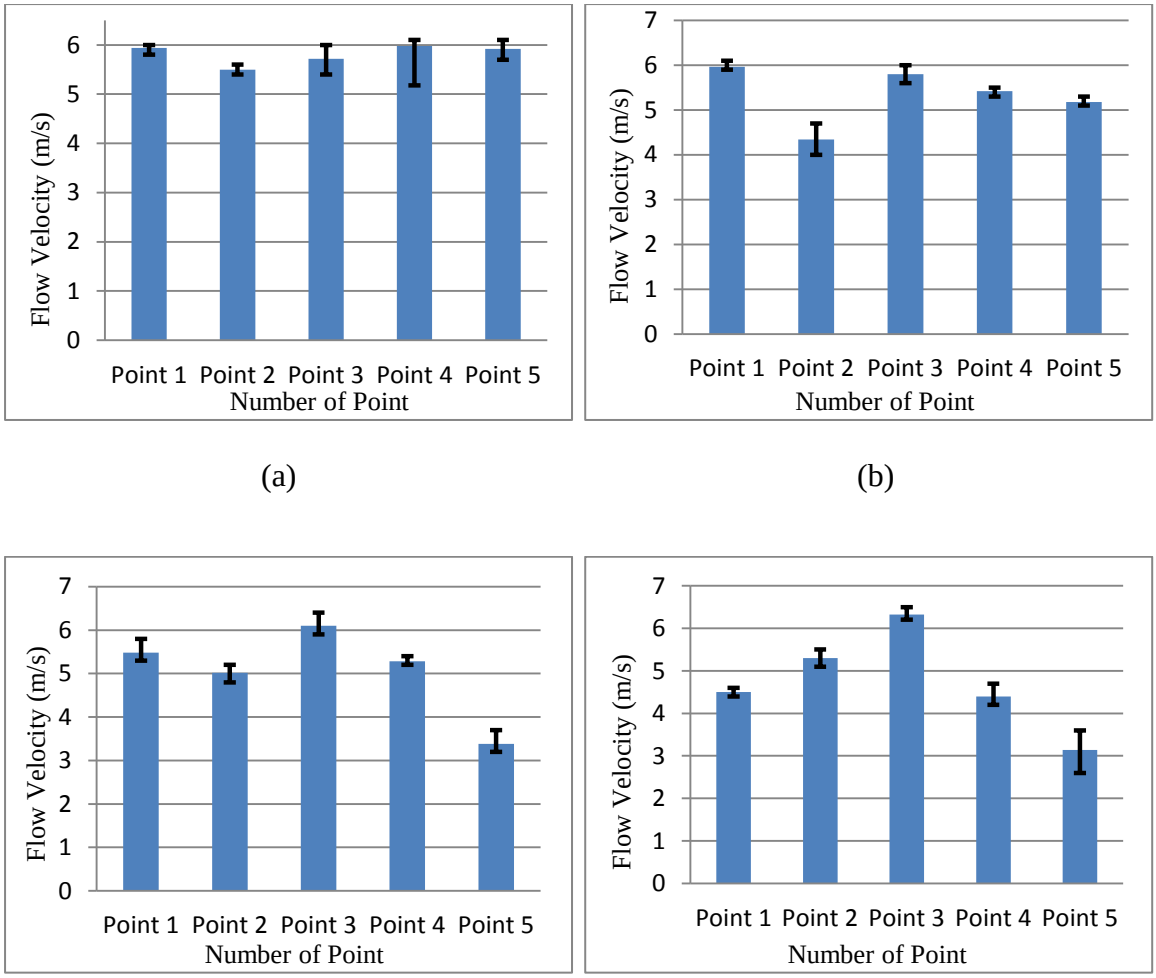


**Fig.4.22. Error analysis of wind tunnel results in 5m/s approaching flow from different directions (a). 0° of approaching flow (b). 15° of approaching flow (c). 30° of approaching flow (d). 45° of approaching flow**

From Fig.4.22, it can be seen that the relative errors of wind tunnel results are about 5%, which is in an acceptable range, in most of points under different directions of approaching flow. The main reason is the minimum scale which can be read from the digital manometer. However, it also can be seen in Fig.4.22 (d) that the relative error at point 5 is about 15%, which is slightly higher than that of other points. The reason is that the strong turbulence flow, which reduces the accuracy of pitot tube, is around point 5.

The locations of these five points were chosen by the CFD prediction, and their locations include high velocity regions and low velocity regions at an outlet. Thus, the average values

of these five points are used to present the average velocity at the outlet layer and the maximum values of these five points are used to present the maximum velocity at the outlet layer. The average velocity increase ratios and maximum velocity increase ratios of wind tunnel test under various directions of approaching flow were shown in Fig.4.23 and Fig.4.24.

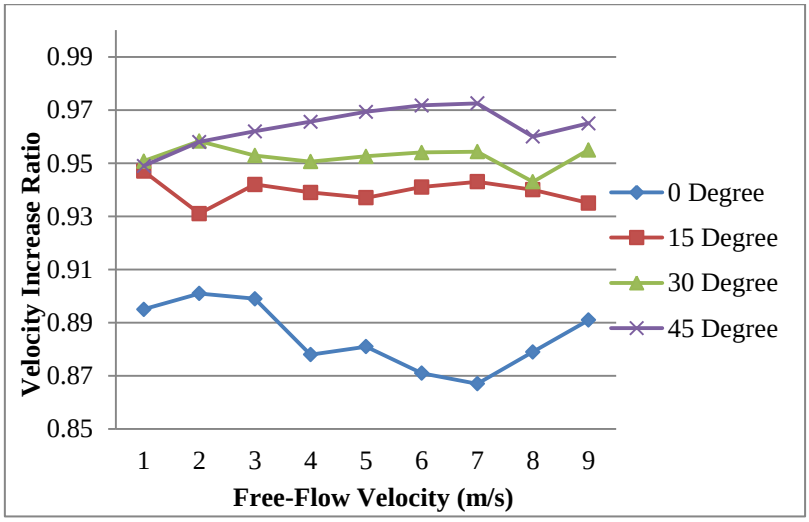


**Fig.4.23. Wind tunnel results of average increase ratio of prototype in different angle**

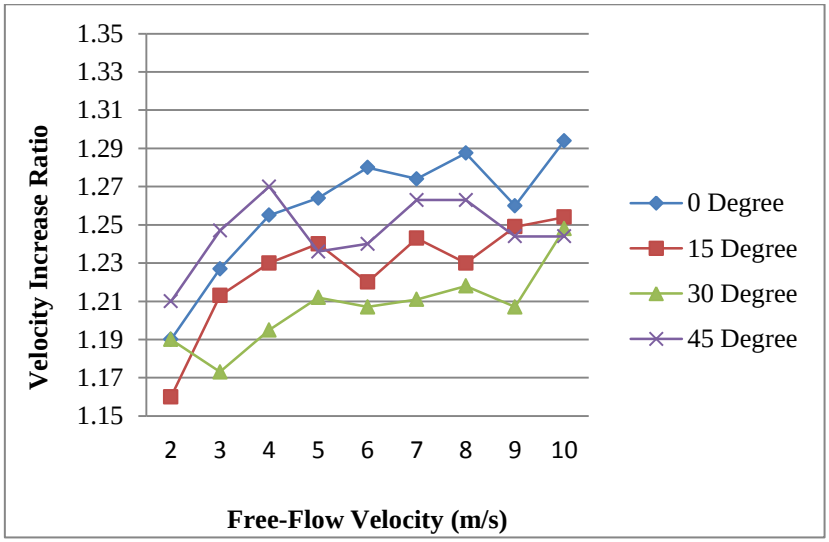


**Fig.4.24. Wind tunnel results of maximum increase ratio of prototype in different angle**

From Fig.4.23 and Fig.4.24, it can be seen that the CFD predictions are matched with wind tunnel results. However, the differences of maximum increase ratios between CFD simulations and wind tunnel test cannot be neglected. The reason caused the differences is

that the maximum flow velocity may not be included in those five points. The novel wind turbine shroud can work in different directions velocities of approaching flows. The shroud was satisfied with design requirements that achieved flow alteration and acceleration in some regions at outlet. The suitability of novel shroud wind turbine was proved by CFD simulation and wind tunnel test. A comprehensive comparison between CFD and wind tunnel results were carried out. The velocities at the five points under 0° of approaching flow were compared in Fig.4.25. The wind tunnel testing data of four chamber model can be seen in Appendix E.

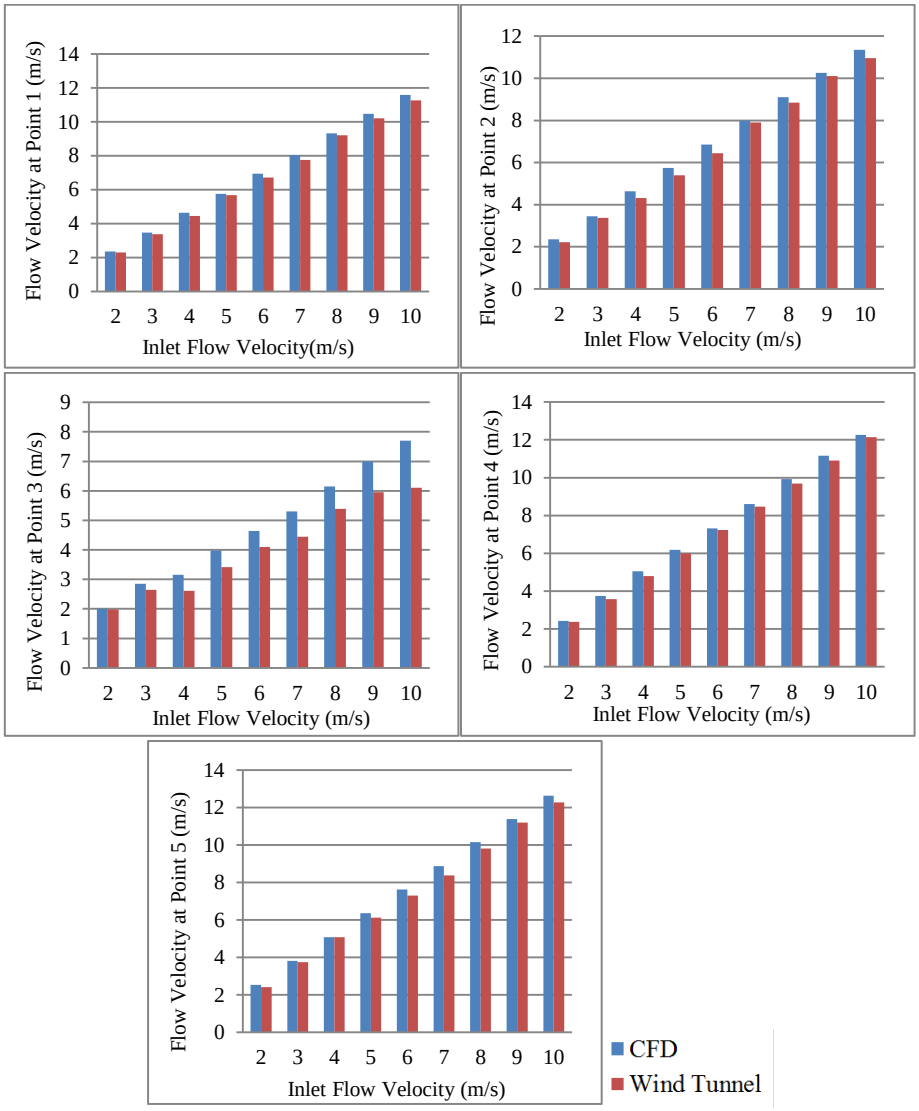


**Fig.4.25. Velocities at the five points under 0° of inlet flow**

It is clear that the results of CFD simulations and wind tunnel test achieved good correlation. The errors between CFD results and wind tunnel results are less than 5% for most of points, but the errors of point 3 under 0° of approaching flow are slightly higher, which is about 10%. The errors at point 3 may be caused by the unsteady flow in the region. Due to unsteady flow, the turbulence level was increased, and the accuracy of tiny pitot tubes was reduced. This can be proved from vector plot at shroud outlet.

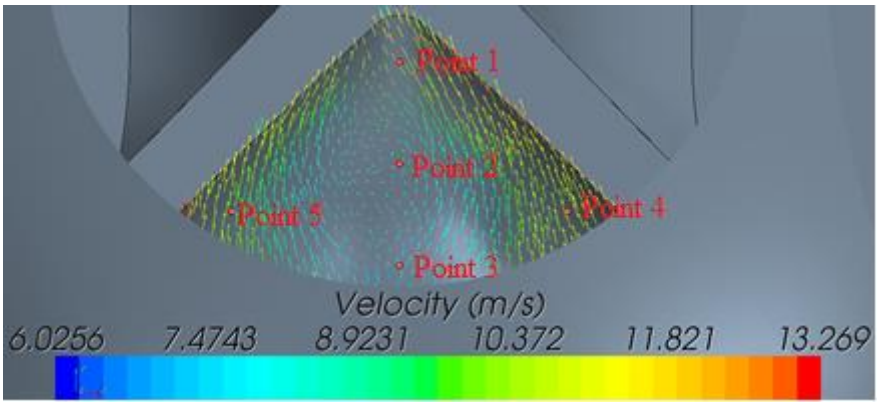


**Fig.4.26. Vector plots at outlet under 10m/s approaching flow at 0°**

The flow conditions at the five points can be seen from Fig.4.26. The flows at the point 1, 2, 4 and 5 were much steadier than flow at point 3. It is proved that the accuracy of wind tunnel results at point 3 was affected by turbulence. The velocities comparisons at other directions inlet flow (15°, 30° and 45°) also achieved good correlation between CFD simulation and wind tunnel test. The large errors happened at unsteady flow regions, the results can be seen at Appendix E.

## 4.7. Summary

The flow characteristics of shroud were investigated numerically and experimentally. The CFD simulation results showed the suitability and potential of the novel shroud wind turbine to be used in urban areas. The simulation results have shown a good agreement with the experimental data from different directions of approaching flow and various flow velocities.

Based on the results, the following improvements of the novel shroud wind turbine can be drawn:

- The frequently changed direction flow in urban areas can be unified. One of the problems that limited the wide spread of urban wind turbines is frequently changed direction flow. By implementation of a shroud, the flow from any directions can be led to a given vertical direction. Thus, the power output of the novel wind turbine cannot be affected by flow direction.
- The wind energy concentration can be achieved by a shroud. Due to this feature, the low speed condition which limited the performance of urban wind turbine can be solved. The maximum velocity is about 1.2 times of approaching flow which can result in 3 times increment of potential of power output.
- There is a good correlation between CFD results and wind tunnel results. The results of CFD simulations were validated by wind tunnel results. The tolerance between CFD and wind tunnel results is less than 10%. Thus, the further prediction of novel wind turbine performance can be carried out based on the current CFD settings.
- The flow characteristics inside chamber were studied. It was determined that the velocity of flow inside chamber had a decreasing process, and then started to accelerate. Thus, the flow acceleration of shroud can be improved by extend accelerating process which will be carried out in Chapter Six.

The novel wind turbine is an innovation of urban wind turbines, which was designed based on the requirements of an urban wind turbine. It consists of two parts, namely shroud and blades. In this chapter, the design details of shroud are introduced and its suitability to be

used in urban areas has been proved. The design characteristics of the novel wind turbine can achieve flow acceleration and flow alteration, which are essential for an urban wind turbine. The flow characteristics at shroud outlet were determined in Computational Fluid Dynamic (CFD) simulation, and validated in wind tunnel test. It was found that there is a good correlation between CFD and wind tunnel results. The flow features around and inside shroud were studied, and they will be useful for optimisation process.

# Chapter 5 – Determination of Shroud Chamber Numbers

## 5.1. Introduction

The total amount of wind energy can be expressed as (Matsushima, Takagi, & Muroyama, 2006),

$$P = \frac{1}{2}\rho A U^3 \qquad (5.1)$$

where the $P$ is the power output of a wind turbine, $\rho$ is density of air, $A$ is the flow area through the turbine blades and $U$ is wind speed. Thus, enlarging flow area or accelerating flow velocity can effectively increase the total power possibly produced by a wind turbine. In Chapter Four, it has been proved that the velocity acceleration of flow can be achieved within each chamber. This chapter will focus on enlarging a flow area to improve the potential of power output of novel wind turbine.

## 5.2. Concept to Enlarge the Flow Area

A typical structure of four chamber model is shown in Fig.5.1. The area in red circle is the outlet of shroud. It can be seen that the outlet area of shroud is divided into four sub-outlets shown in green area due to the number of chambers. Each sub-outlet is the outlet of a single chamber. The total amount of wind energy through the outlet of shroud is critical to validate the capability of energy concentration of the shroud. In the working condition, the flow may go through one or two sub-outlets under various directions of flow which means only 1/4 to 1/2 area of the outlet of shroud is filled with flow as shown in Fig.5.2. If the flow area at the outlet of shroud can be enlarged and flow characteristics are kept constant, the potential of power output of the novel wind turbine can be improved.

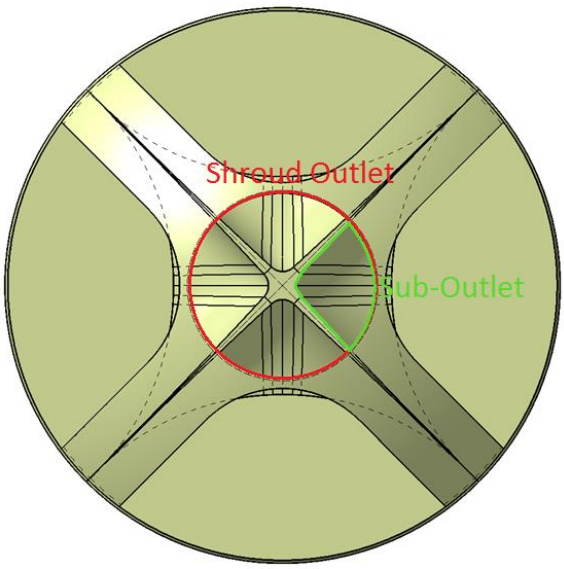


**Fig.5.1. A typical four chamber model**

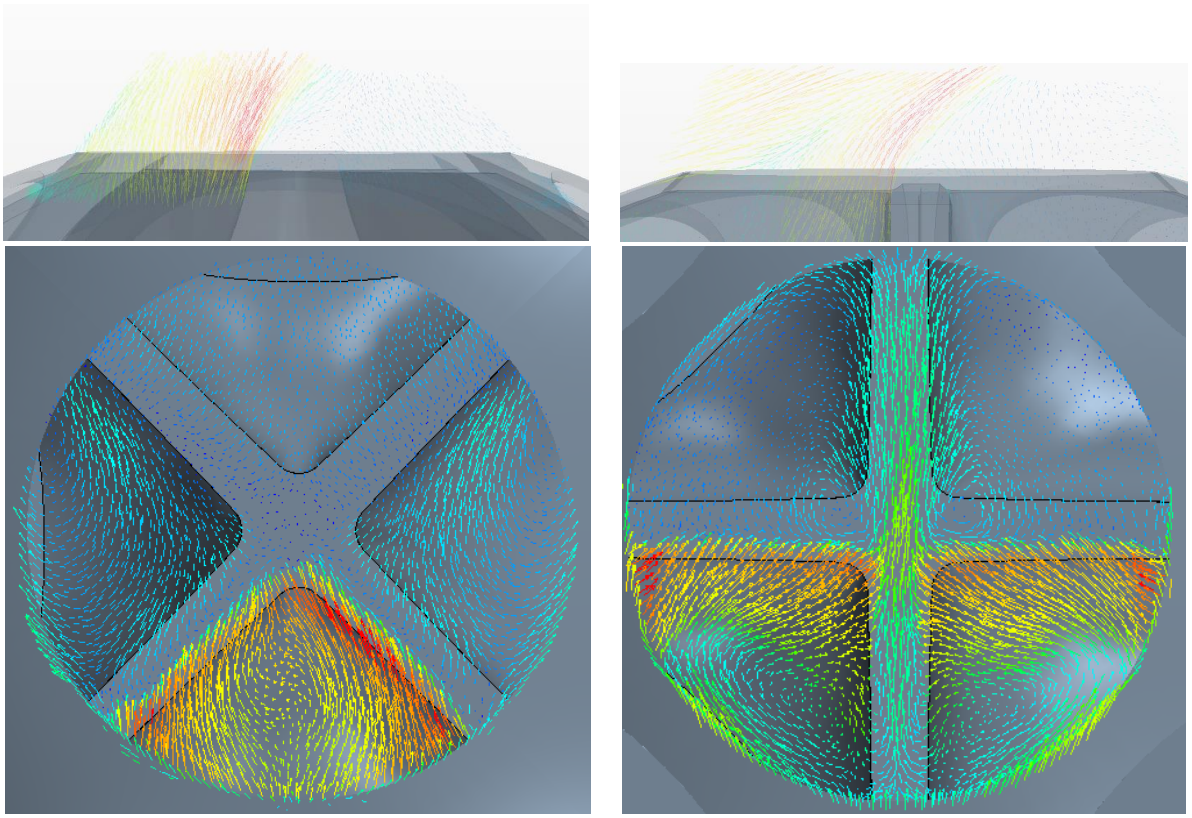

(a) (b)

**Fig.5.2. Vector plots of a four chamber model in different directions of approaching flow. (a) 0° of approaching flow (b) 45° of approaching flow**

In order to increase the total amount of wind energy captured by shroud, three different models which have various numbers of chambers were created and tested to determine the

effects on enlarging the flow areas. The geometries of these three models were shown in Fig.5.3. The dimensions of these three models are detailed in Appendix I, Appendix J and Appendix K. In this section, the study has been focused on the area that flow goes through the outlet of the shroud. These three models have the same diameter of outlet ($D_{outlet}$) which means the outlet area of different models is same. The outlet areas ($A_{outlet}$) of different models can be split to several regions due to various numbers of chambers. In order to validate the effects of number of chamber on the area that flow goes through, these three models will be analysed by CFD method and flow velocity and flow area at the outlet will be measured and compared.

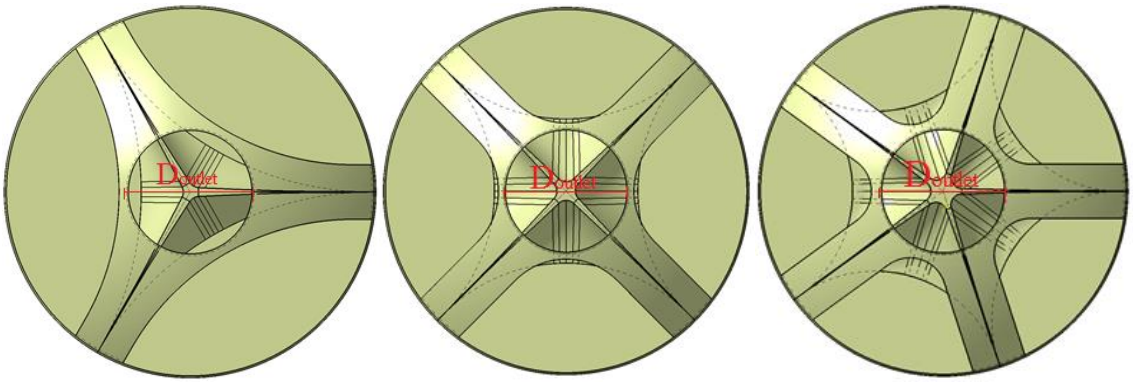


(a) (b) (c)

**Fig.5.3. Models with various number of chambers. (a). three chamber model (b) four chamber mode (c) five chamber model)**

## 5.2. Computational Fluid Dynamic (CFD) Results

As mentioned in Section 5.1, the areas that flow goes through the outlets of shroud vary due to different directions of approaching flow. Thus, these three models were simulated in various directions of approaching flow from $0^o$ to $180^o$ with an interval of $15^o$. The velocity of approaching flow is constant, 10m/s. The average velocity and maximum velocity at the outlet of different models were measured and compared. The areas, which flow goes through under different approach directions, were determined and compared. The value of average

velocity and flow area can be substituted into equation (5.1) to evaluate the total amount of wind energy. The value and location of maximum velocity are also essential to increase the power output of a wind turbine which will be discussed in Section 5.3. The model that could apply highest flow velocity and largest flow area should have the best capability in wind energy concentration.

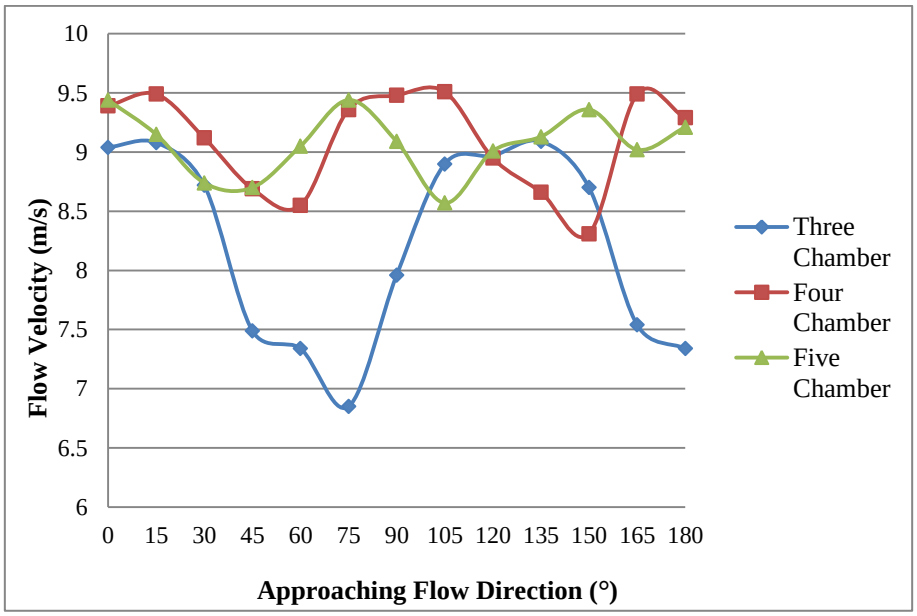


**Fig.5.4. Average velocity at the outlets of different models**

Fig.5.4 shows the average velocity at the outlets from three models with various numbers of chambers. It can be found that the values of average velocity of these models repeated every 120º, 90º and 72º for three chamber model, four chamber model and five chamber model, respectively. The repetition is due to the number of chamber of different models. Thus, the performance of whole model can be predicted by testing one chamber. The values of average velocity of four and five chambers models are similar, which achieved 9.5m/s of best value and 8.5m/s of worst value. The three chamber model had the worst average velocity among these three models. Especially, from 40º to 80º, the average velocity of three chambers model is lower than 7.5m/s. It should be noticed that the performance of three chambers model repeated every 120º. According to this, the low average flow velocity at the outlet of three

chamber model would happen 1/3 duration of overall performances. This drawback will significantly reduce the wind energy concentration of the three chambers model. It is suggested that both four and five chamber models achieved better average velocity at the outlet than three chamber model did.

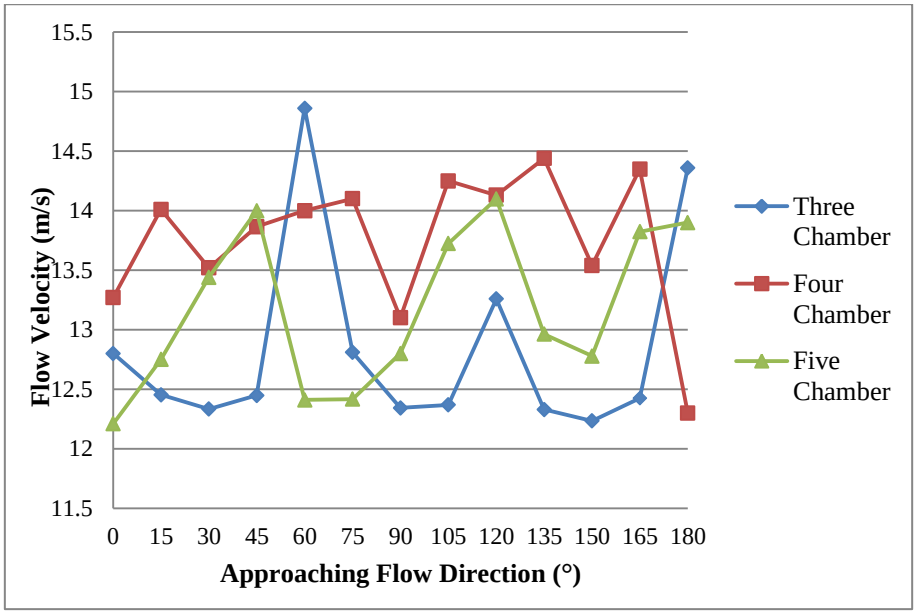


**Fig.5.5. Maximum velocity at outlet for the three models**

The maximum velocities of these three models under various directions of approaching flow are shown in Fig.5.5. It can be seen that the maximum velocities of these three models were fluctuated with approaching flow directions. Also, it was noticed that the maximum velocity does not have the exactly same periodicity with the flow direction. The reason might be caused by mesh generation at shroud outlet. More mesh cells should be employed around shroud outlet to capture more accuracy results. The maximum velocity fluctuations of three chamber model are more significant than the velocities of the other two models. The maximum velocity at the outlet of three chamber model reached highest value nearly 15m/s and lowest values about 12.4m/s. The maximum velocities at the outlet of the other two models are steadier than that of three chambers model. The maximum velocity values of various directions are from 12.3m/s to 14.5m/s for four chamber model, and from 12.2m/s to

14m/s for five chamber model. However, the highest maximum velocity value of three chamber model happened in a sudden increase in a specific direction of the approaching flow. Under the other directions of approaching flow, the values of maximum velocity of three chambers model are similar to or lower than the values of maximum velocity of the other two models. Thus, it is suggested that the flow characteristics at the outlet of four and five chamber models are better than three chamber model.

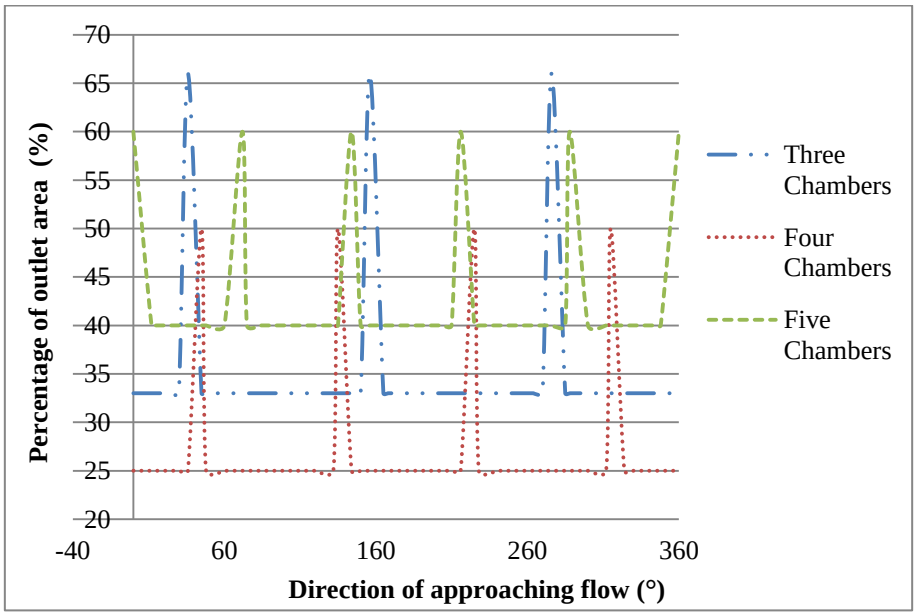


**Fig.5.6. The percentage of outlet area that flow goes through under various directions of approaching flow**

As described in equation (5.1), the total wind energy can be captured from the wind flow is proportional to the area flow going through and cubed with flow velocity. According to flow average and maximum velocities as shown in Fig.5.4 and Fig.5.5, it is evident that the four and five chamber models have had higher value of maximum and average velocities than three chamber model has. There is no significant difference between four chamber model and five chamber model due to the velocities validation.

The areas that flow through the outlet of the three models under various directions of approaching flows were determined as shown in Fig.5.6. According to the same diameter,

these three models have an identical outlet area. Thus, the comparison is based on the percentages of the outlet area that that flow goes through. The working area is the region that included vertical direction flow and the values of the working area were recorded due to the vector plots at shroud outlet. As shown in Fig.5.5, the working areas of three, four, five chamber models are 33%, 25% and 40% in most directions. The total amount of wind energy that can be captured is proportional to the working areas. Thus, the total amount of wind energy that can be captured from five chamber model is about 7% and 15% higher than three and four chamber models due to enlarging flow area at the outlet. It also can be seen that the flow area at the outlet can be increased to 66%, 50% and 60% for three, four and five chamber, respectively, in some specific directions. This phenomenon is more frequently happened for five chambers model than other two models, because of the chamber number.

In conclusion, the total amount of wind energy that can be captured by five chamber model is more than that of three and four chamber models due to the differences in flow velocity and flow area. The four and five chamber models have had similar flow velocity values at the outlet, but had higher values of average and maximum velocities than the velocity values of three chamber model. However, the area of the outlet that the flow goes through four chambers model is smaller than that in five chamber model under most directions of approaching flow. Therefore, it is suggested that the five chamber model is selected and further optimisation is needed.

## 5.3. The Flow Characteristics of the Five Chambers Model

Before the optimisation process, the flow characteristic of the five chamber model was studied using CFD simulation and wind tunnel test. The shroud was designed to unify and accelerate the wind flow from various directions. Thus, the shroud should have the ability to work in a wide range of velocities and under various flow directions. The performance of the

shroud was evaluated by the velocity increase ratios which are maximum velocity increase ratio ($U_{\max} / U_{approaching}$) and average velocity increase ratio ($U_{average} / U_{approaching}$). The model was investigated under different directions of approaching flow to simulate frequently changing wind direction in urban areas. According to Blade Element Momentum theory (BEM), the locations of maximum velocities at the outlet shroud will significantly affect the total power generated torque of the novel wind turbine blades. Thus, the vector plots at shroud outlet layer were measured and validated.

### 5.3.1. Computational Fluid Dynamic Modelling

In CFD modelling, the shroud was simulated under the different velocities of free stream flow varied from 1m/s to 18m/s and under the different directions of free stream flow from $0^o$ to $180^o$. Fig.5.7. shows the relationship of velocity increase ratio against different free stream flow velocities. It can be found that the maximum and average velocity increase ratios in different velocities of approaching flows are similar and nearly constant. This implies that the flow alteration and flow acceleration of the shroud is not affected by different incoming flow velocities. It is suggested that the new wind turbine system can work in an urban area with wind velocity as 1m/s. However, the differences between the maximum increase ratios and the average velocity increase ratios are significant under 0° of approaching flow. This indicates that there is an uneven flow inside the chamber.

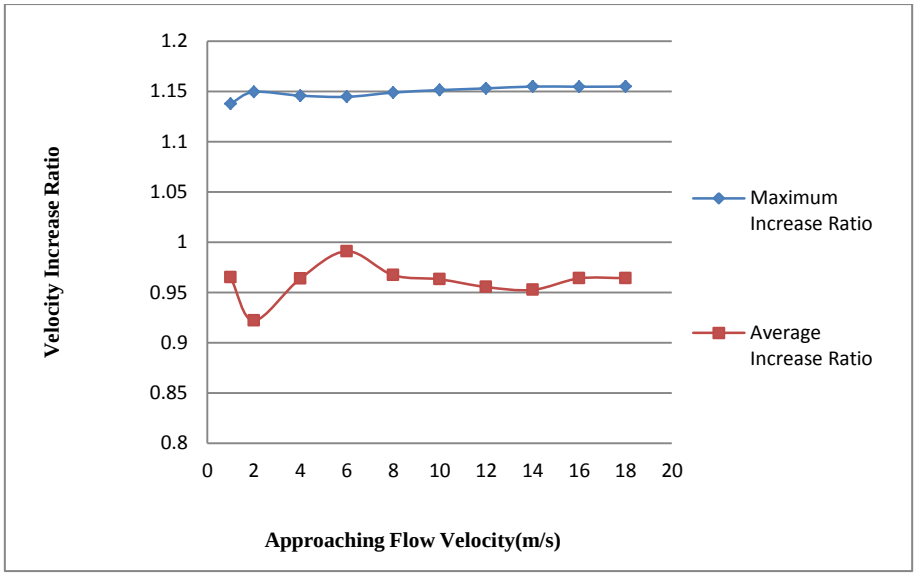


**Fig.5.7. Velocity increase ratio of different velocities of approaching flow at 0°**

In an urban area, the wind directions could vary frequently over time so the different directions of approaching flow need to be simulated. The shroud of five chamber model is symmetrical and its flow characteristics repeat every 72°. Thus, the performance of the whole shroud structure could be predicted by simulating the flow directions from $0^o$ to $180^o$ with an interval of $12^o$ in a given approaching flow velocity, such as 10m/s.

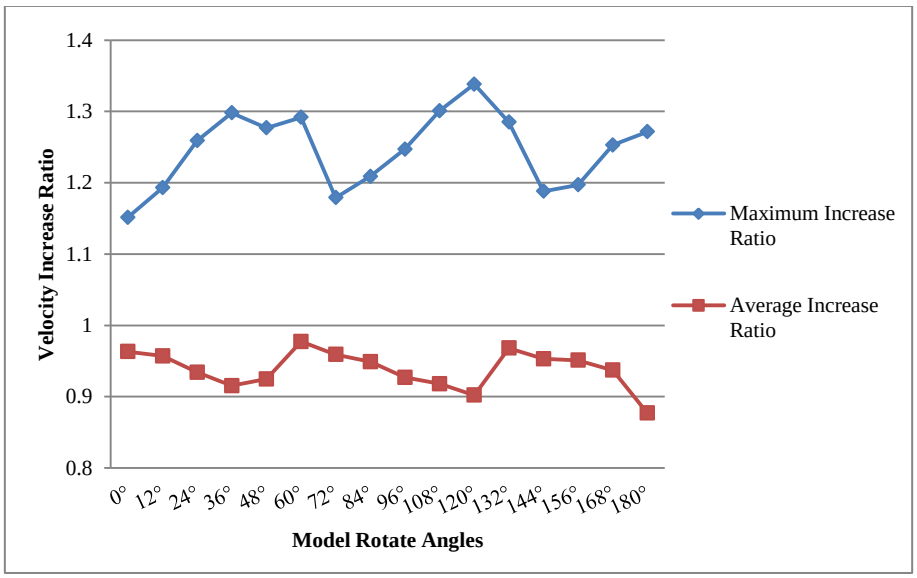


**Fig.5.8. Velocity increase ratio of different directions of approaching flow at the velocity of 10m/s**

Fig.5.8 shows the maximum and average velocity increase ratios at the different angles of approaching flow. The velocity increase ratios of the shroud vary in different directions. According to Fig.5.8, the shroud could lead flows from any direction to the vertical outlet with an acceleration of velocity. However, it is noticed that the flow velocities at the outlet of the shroud is fluctuated with different directions of approaching flow. The average velocity increase ratio is about 0.95, which is near the same as that of the approaching flows. The maximum velocity increase ratios are about from 1.15 to 1.3 for some regions at the outlet layer. The location of these high velocity regions will increase the torque that generated by blades, so that the power output of novel wind turbine can be increased. The reason of this will be discussed later. In Fig.5.8, it is observed that the peak value of maximum velocity increase ratio occurs when an average velocity increase ratio is at the low valley. This indicates that the flow swirls inside the chamber. In some directions of approaching flow, the vortices inside the chamber are significant and result in a lower average velocity increase ratio at the outlet. The performance pattern of the shroud is repeated at an approximate interval of $72^{o}$ which is the range that flow can be captured by a chamber. It was noticed that there is an opposite trend for the maximum increase ratio and average increase ratio. The reason is that the wind flows are compressed to achieve high value of maximum increase ration. During the compression process, some wind flows slip out of shroud, so that the average increase ratio is reduced.

The vortices inside the chamber might be generated during a flow alteration process. In order to visualise the flow characteristics inside chamber, a plane section was created in the middle of chamber. A plane section was created as shown in Fig.5.9 and the vector plot in the plane section was created as shown in Fig.5.10. According to Fig.5.10, it can be seen that the entrance flows from different directions were led to the vertical outlet through the chamber. The structure of a chamber was designed as a diffuser to achieve a concentration of wind

energy. During this process, the flow was accelerated at the outlet layer where the turbine blades will be located. However, it also can be seen that a strong vortex was generated during a flow alteration process. The flow velocity was dragged down until the flow finished its alteration. The flow feature inside the chamber is important. In order to determine the wind flow behaviour inside the chamber, the flow velocity distribution is plotted in Fig.5.10. These three curves of flow velocity versus the positions were obtained at the symmetrical plane of the chamber as shown in Fig.5.10. The coordinates of 15 points on each curve were shown in Appendix C. Curve one, curve two and curve three, respectively, illustrated the flow behaviour at the bottom section, the middle section and the top section within the chamber.

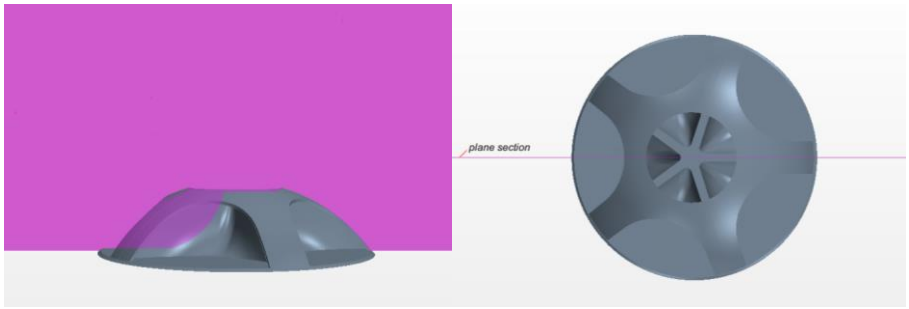


**Fig.5.9. Location of a plane section**

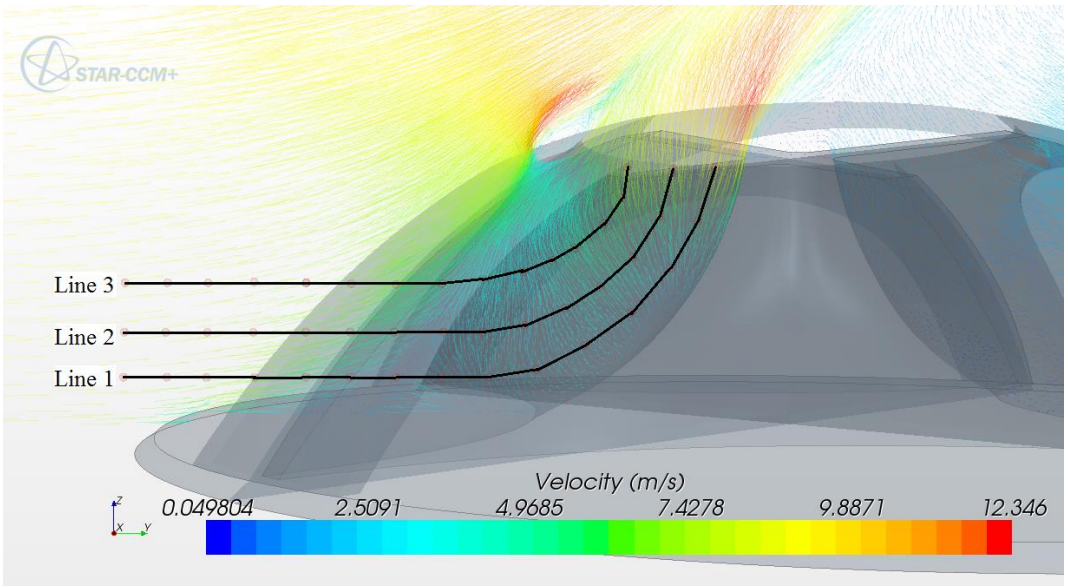


**Fig.5.10. Vector plot of flow distribution in the symmetrical plane of a chamber at the zero degree approaching flow**

As shown in Fig.5.11, the flow trend in different sections indicated that the flow velocity started to decrease when the flow entered the chamber and kept the trend across the horizontal section of the chamber. When the flow reached the vertical part within the chamber, it began to be accelerated and reached the maximum value at the outlet. The flow feature of five chamber model was similar as that of four chamber model, which is caused by the similar internal shapes of these two models.

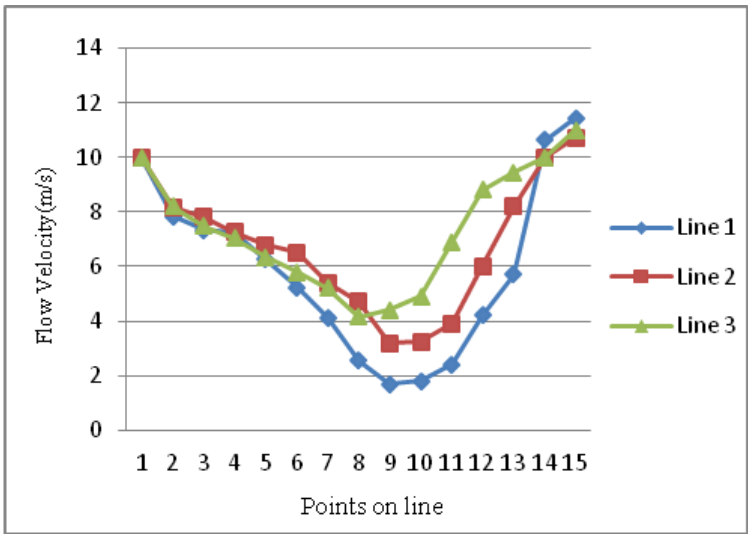


**Fig.5.11. Velocity distribution inside a chamber**

The flow feature inside a chamber is also important for a location of turbine blades. The blade should be placed at highest flow velocity layer to achieve the best performance. As shown in Fig.5.11, there were vortices inside the chamber which force the flow turning to the vertical direction where the outlet is located. However, the flow velocity was decreased in this process. The vortices were caused by the internal structure of the chamber. In further work, it is necessary to conduct an optimisation of internal structure of a chamber so that the intensity of vertices inside the chamber can be reduced. Due to this, the flow acceleration of the shroud can be improved.

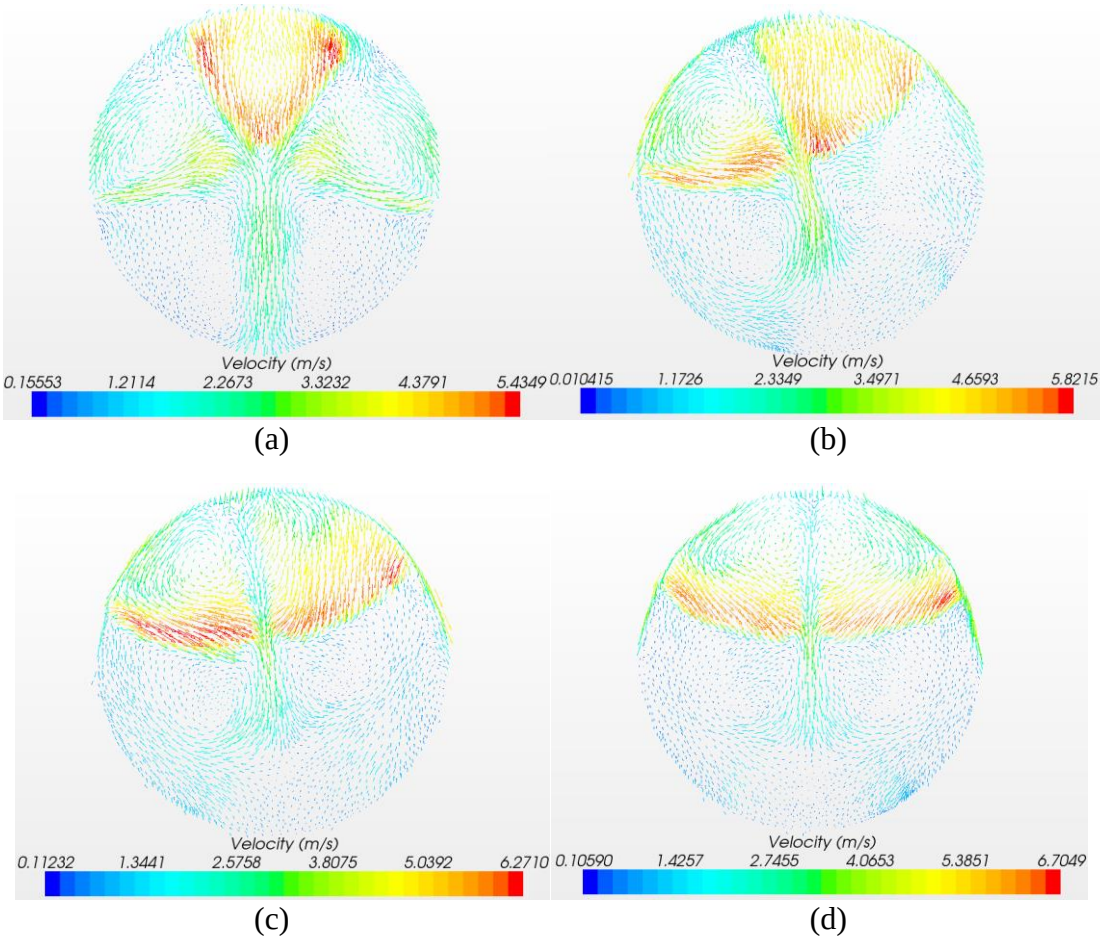


**Fig5.12. Flow distribution at the outlet of shroud (at 5m/s approaching flow).(a). 0° of approaching flow, (b) 12° of approaching flow, (c) 24° of approaching flow, (d) 36° of approaching flow**

The flow vector at the shroud outlet is presented to determine the flow characteristic at the location where the turbine blades will be placed. It was mentioned that the locations of high velocity region would significantly affect the power output of novel shroud wind turbine. Depended on the directions of approaching flow, flows from two or three sub-outlets will provide a driving force. The distributions of velocities at the outlet are shown in Fig.5.12. It is noticed that the area of the outlet can be divided into several regions with different values of flow velocities. With different strength of velocities at the outlet, the forces applied on the each blade are different. With this feature, the static balance of the blades could be easily broken, and the self-starting ability of the blades could be improved.

Due to vortices inside the chamber, the velocities at the outlet vary and this is the reason that the average velocity increase ratio is lower than the maximum velocity increase ratio. However, the locations of high velocity points are important. As shown in Fig.5.11, these high velocity regions are distributed along the edge of each sub-outlet, which should provide a high value of momentum at the blade tip. The locations of the highest velocities are also critical to the performance of the blades. The high flow velocity regions at blade tips are important for blades to achieve a high power output. The power output can be calculated from the following equation:

$$P(W) = T \times 2\pi n \tag{5.2}$$

where $P$ is the power output of wind turbine, n is the rotational speed of wind turbine and $T$ is the torque generated by blades. Based on blade element momentum (BEM) theory, the torque (T) can be expressed as follows:

$$dT = \rho V \omega r^2 2\pi r dr \tag{5.3}$$

where $\rho$ is the density, $V$ is the absolute velocity, $\omega$ is the wake rotational speed, $r$ is the radius of blade.

The contribution to the total power from each element is:

$$dP = \Omega dT \tag{5.4}$$

where $\Omega$ is the blade rotational speed.

The total power from the rotor is:

$$P = \int_{r_h}^{R} \Omega \rho V \omega 2\pi r^3 dr \qquad (5.5)$$

where $R$ is the blade tip radius, and $r_h$ is the hub radius.

From equation (5.2) to equation (5.5), it can be seen that the value of torque is proportional to velocity ($V$) and cubed with radius of blade ($r$). Thus, the force acted on the location where far from rotating axis could provide larger torque for generating power output. At the shroud outlet, the maximum velocities occur at the tip of blades. This means that the large value of r was forced by high flow velocities, so that high value of torque will be generated at the blade tips. The blade element calculations suggest that most of the starting torque is generated near the hub, whereas most power producing torque come from the tip region (Wright & Wood, 2004). The flow conditions at the outlet of shroud could generate high power producing torque for power output so that the power output of the novel wind turbine could be increased.

### 5.3.2. Comparison Wind Tunnel Result with CFD Results

After the flow characteristics at five chambers shroud outlet were determined. The wind tunnel test was carried out to validate these flow characteristics from CFD simulation results. The apparatus of wind tunnel were introduced in Section 3.3. As shown in Fig.5.12, seven points were chosen on one sub-outlet layer of the shroud, and the velocities at these seven points were measured five times. The average values of velocity were calculated and compared with the CFD results. The coordinates of these seven points are detailed in Appendix D.

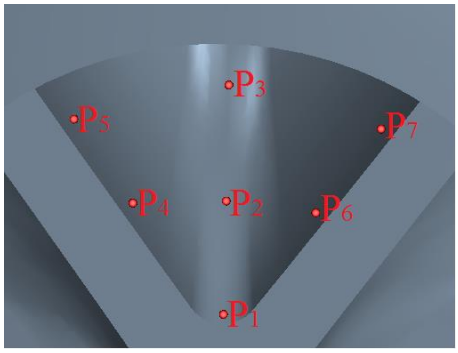


**Fig.5.13. Locations of seven points at outlet**

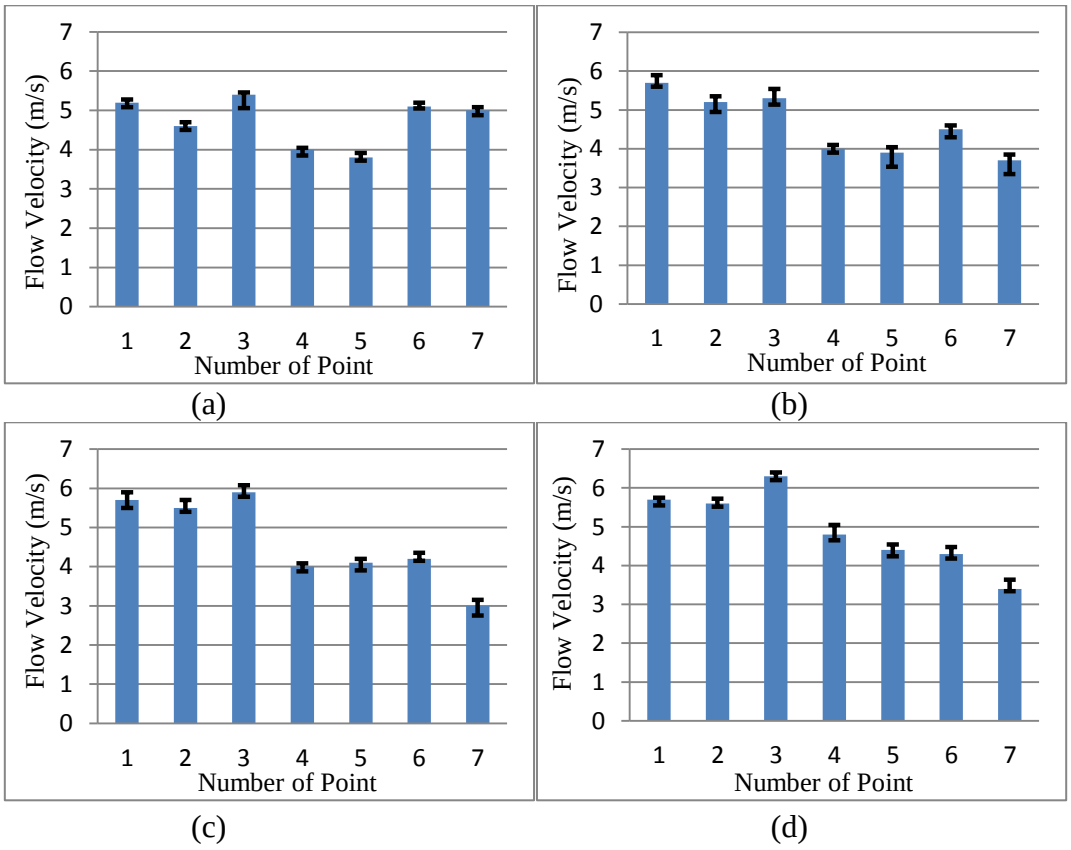


**Fig.5.14. Wind tunnel results in 5m/s approaching flow from various directions (a). 0° of approaching flow (b). 12° of approaching flow (c). 24° of approaching flow (d). 36° of approaching flow**

The error analysis of wind tunnel results is shown in Fig.5.14. It can be seen that the relative error of wind tunnel results at most of points is about 5%, which is in the acceptable range. These errors are mainly caused by the minimum scale of manometer. However, the relative

errors at few specific points are about 10% to 15%, which is caused by the strong turbulence around these points. The accuracy of pitot tube was affected by the turbulence.

Fig.5.15 and Fig.5.16 shows the comparison of computational results with experimental results. The flow velocities at the seven points on the sub-outlet layer shown in Fig.5.13 are selected and studied. The results from computational simulation and wind tunnel tests in a specific degree of $0^o$ and velocity of approaching flow are compared as shown in Fig.5.13. It is evident that there is a good correlation between the experimental and computational results. Both computational and experimental results give the similar velocities on these points although there are still small differences between CFD results and wind tunnel test results. They could be caused by the effect of turbulence flow on the accuracy of pitot tube readings. It is evident that the present CFD simulation gives satisfactory predictions of the flow behaviour through the new wind turbine shroud. The detailed data of the wind tunnel tests can be seen in Appendix F.

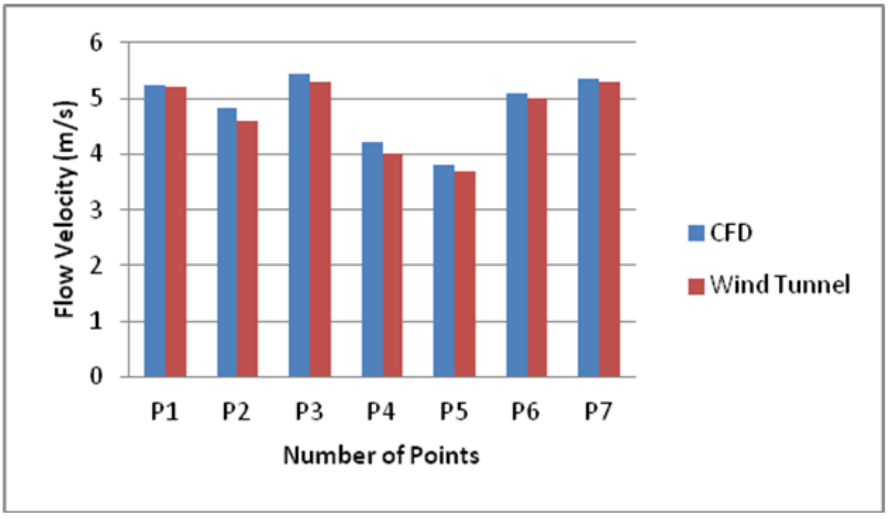


**Fig.5.15. Comparison of velocity at points (at 5m/s free stream flow)**

The results in Fig.5.15 match with the prediction of velocity vector distribution shown in Fig.5.12. The velocity vector distributions of free stream flow at 10m/s at $0^o$ is shown in

Fig.5.12 (a). It can be seen that the flow velocities at points 2-3 and points 6-7 in the outlet (see Fig.5.13) have higher values of velocities and these points are also located around the boundary of one sub-outlet. This flow feature at the outlet of shroud achieved a high torque so that the power output of the new wind turbine could be improved. As shown in Fig.5.15, the maximum flow velocity was achieved at points 1 and minimum flow velocity happened at point 5. It is suggested that the flow vortices generated inside a chamber have resulted in low velocities at points 4-5.

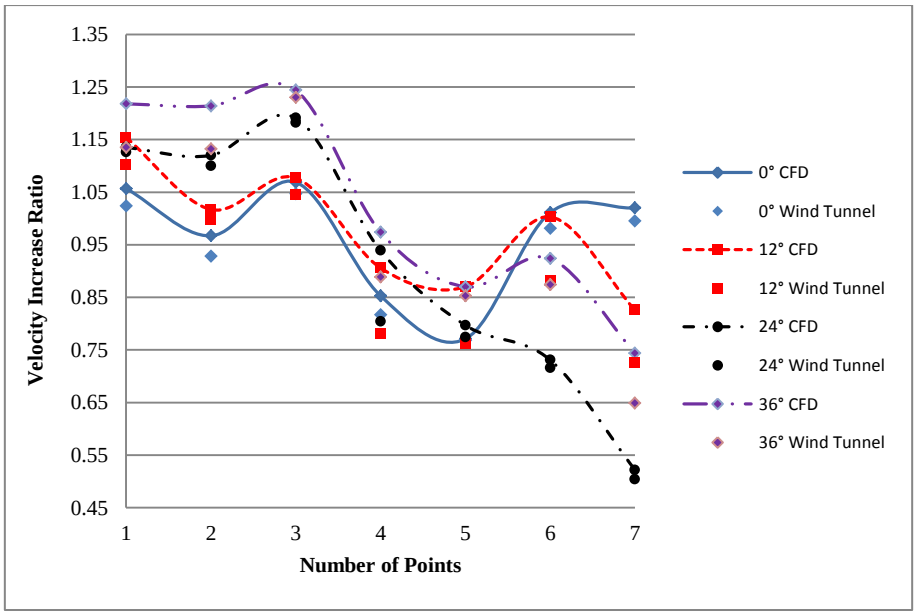


**Fig.5.16. Comparison of Velocity Increasing Ratio at Points**

The acceleration ratios from computational simulation results are also compared with those from the wind tunnel tests, as shown in Fig.5.16. The velocity increasing ratio for each point is average increasing ratios at each specific point of the outlet in different velocities of approaching flow. The values of velocity increase ratio for seven points at different degrees of approaching flow were experimentally validated. The flow velocities at the outlet were determined. It can be seen that, at some points, the increase ratios are extremely low. However, the locations of these extremely low points are vary with directions of the approaching flow. The locations of these poor performance points are determined at the

specific approaching flow direction. The largest value of difference between highest and lowest increase ratio for points happened at $24^{o}$ direction of approaching flow, which would be caused by high intensity of vortices in the direction of approaching flow. The differences between CFD results and wind tunnel results are still small, which are about 2% to 4%. It is evident that there is a good correlation between the experimental and computational results. The present CFD simulation can predict the distribution of the velocity increase ratio successfully. The flow characteristics determined by CFD simulations are reliable.

## 5.4. Summary

In this chapter, the three different models with various numbers of chambers were introduced. The performances of these three models, which are three, four and five chambers models, were investigated by computational fluid dynamic (CFD) method, whose accuracy has been proved in Chapter 4. The five chambers models achieved better performance in accelerating flow velocity and enlarging flow area than the other two models did. A comprehensive analysis of five chamber model was carried out in CFD, and simulation results were validated by the wind tunnel tests. There is a good correlation between simulation results and wind tunnel results. The flow characteristics inside chamber were determined, and the information will be useful for internal dimensions optimisation.

# Chapter 6 – Structural Optimisation of a Chamber

## 6.1. Introduction

In Chapter Four, it was determined that an average velocity increasing ratio was only about 0.95 under different directions of approaching flow. It was observed that the locations of maximum velocity regions could increase the power generating torque of blades, but the average velocity increase ratio still needed to be improved to increase the total amount of wind energy to be captured. Because the flow acceleration behaviour depends on the internal shapes of a chamber, several studies were carried out by using Computational Fluid Dynamic (CFD) method to investigate the different parameters of the internal dimensions on the flow acceleration behaviour.

## 6.2. Effects of Vertical Length on Flow Acceleration

As discussed in Chapter Five, the flow inside chamber had a velocity decreasing stage, and then started to accelerate after an alteration of flow direction. Thus, six models were created with different lengths of vertical path to determine the effects of model height. These models have the same parameters but the different length of vertical path, as shown in red line in Fig.6.1.

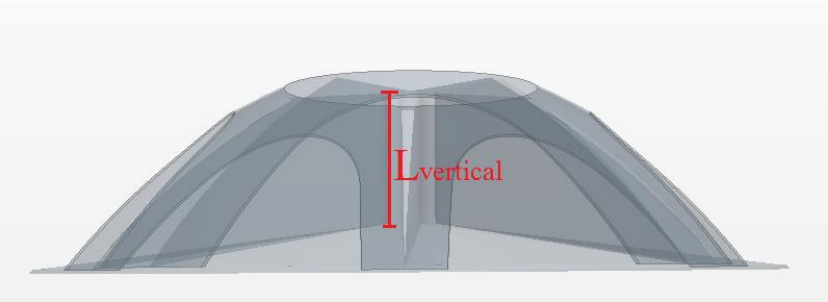


**Fig.6.1. Test model with different length of vertical path**

The 0° of approaching flow is a typical direction, which wind flow can fully fill and go through a chamber. The models were simulated at10m/s velocity of approaching flow and the direction of approaching flow was set as $0^{o}$. The shroud was designed to accelerate approaching flow up to the blades, so that the flow velocity at the shroud outlet was studied. The maximum velocity and average velocity at the shroud outlet of the different models were measured and compared as shown in Fig.6.2.

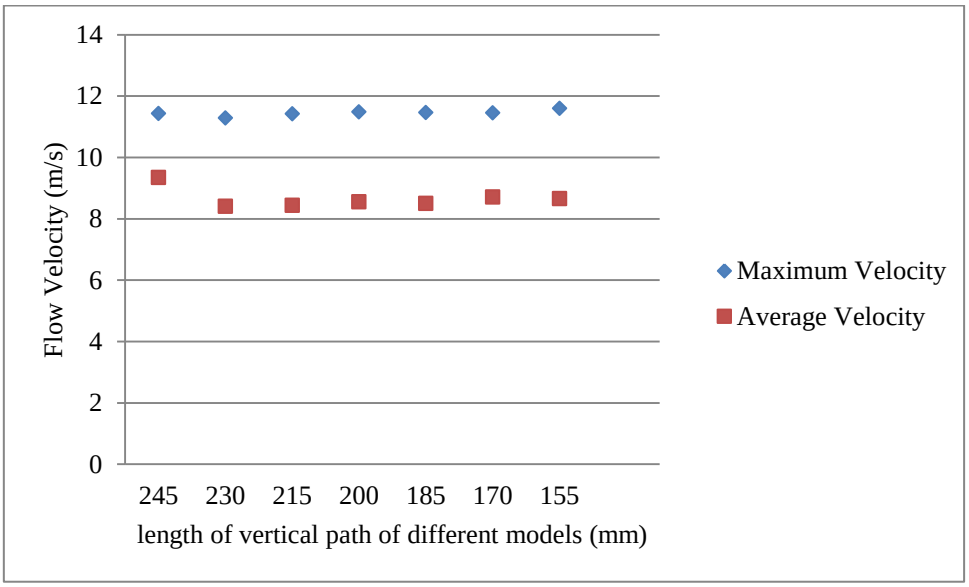


**Fig.6.2. Flow velocities at the shroud outlet versus different models**

It can be seen that the flow velocity of different models with various lengths of the vertical path are similar. The maximum velocity and average velocity of different models are around 11.5m/s and 8.5m/. There are no obvious trends of length effect along the vertical path. In order to get more details of the flow characteristics, the pressure distributions inside chamber were studied. A plane section and a straight line probe were employed to view the pressure distributions inside the chamber. As shown in Fig.6.3, the plane section was placed in the middle of shroud and the straight line probe was located near the central axis of the chamber. The plane section was used to present the pressure distribution inside the chamber, and the

straight line was employed to view the pressure alteration during flow acceleration. The coordinates of 15 points along the straight line can be seen in Appendix H.

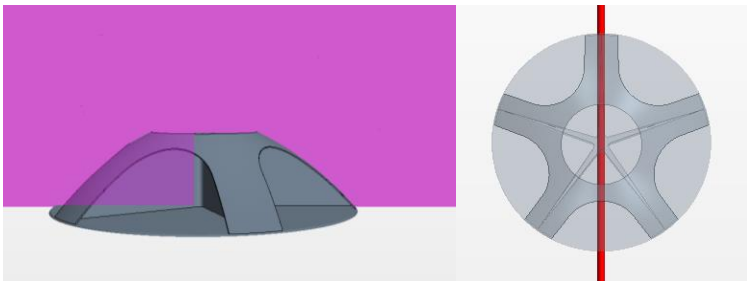

(a) Location of plane section

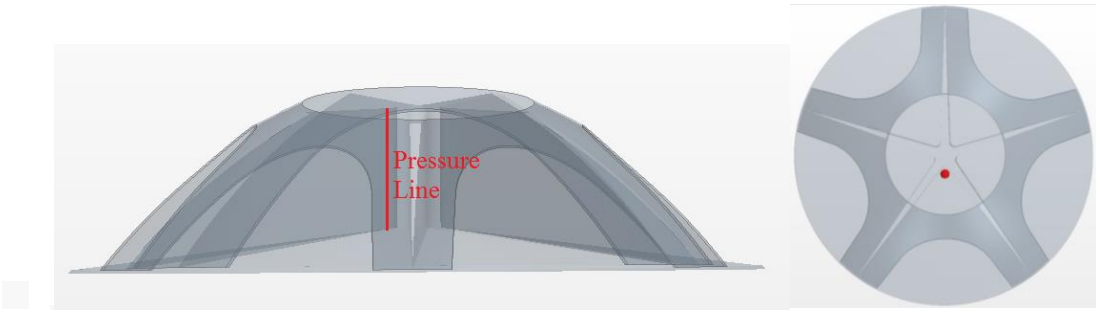


(b) Location of pressure line

**Fig.6.3. Location of a plane section and pressure line**

The pressure alteration can directly reflect the characteristics of flow acceleration. The pressure distributions on the line of different models were shown in Fig.6.4. It appears that the various internal curve models had a similar pressure alteration process. The pressure alteration process can be used to predict flow acceleration behaviour. The low gradient of pressure line means low flow acceleration rate and the high gradient of pressure line means high flow acceleration rate. From Fig.6.4, the flow acceleration process can be divided into three stages. In the first stage, from model bottom to 140mm the model height, the pressure keeps constant with high pressure values which mean that there was no flow acceleration process and the flow velocity was low. The low flow velocity was caused by the drag

generated by wall during flow alteration process. In the second stage, from 140mm to about 225mm of the model height, the pressure started to reduce with a low reduction rate and the pressure dropped from about 55Pa to about 30Pa for various models in 65mm distance for attempts. In this stage, the flow velocity started to increase in a low acceleration ratio. The gradient of pressure drop in this stage is about -384.6Pa/m. Final stage is from about 225mm to the outlet of model about 245mm height. The pressure of various models dropped in a fast ratio from about 30Pa to less than 0Pa in a short distance from 225mm to 250mm.The gradient of pressure drop in this stage is over -1520Pa/m. It was found the last stage is critical to improve the flow acceleration of shroud.

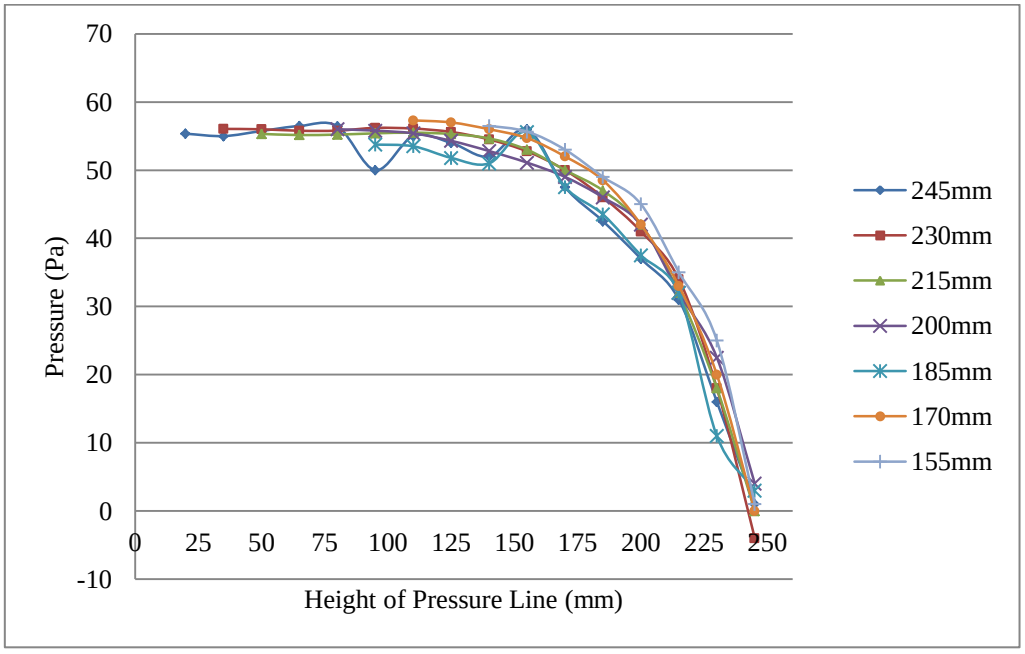


**Fig.6.4. Pressure distribution along the pressure line from the bottom to top**

The region of the flow which achieved significantly acceleration was from 220mm to 245mm height of the model. The region is highlighted in the red rectangle as shown in Fig.6.5. In this region, flow cannot slip out by shroud compressing. Thus, the effect of compression on flow

acceleration is significant in this region. This region is named as flow compression region. It is suggested that increasing the length of this region may improve the flow acceleration of approaching flow.

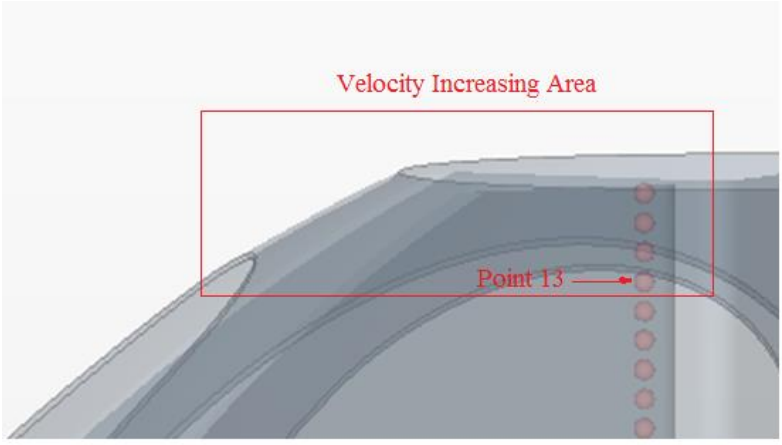


**Fig.6.5. Location of high flow acceleration area**

In order to determine the effects of length of vertical path on flow velocity acceleration, the pressure distributions on the middle plane section of these various models are shown in Fig.6.6. It can be seen that the high pressure region inside a chamber was reduced with a decrease of the vertical length. From Fig.6.6 (a) to Fig.6.6 (g). The flow acceleration process was not affected by the reduction of high pressure region. It also can be seen that the pressure distributions at the velocity accelerating area of different models are nearly the same.

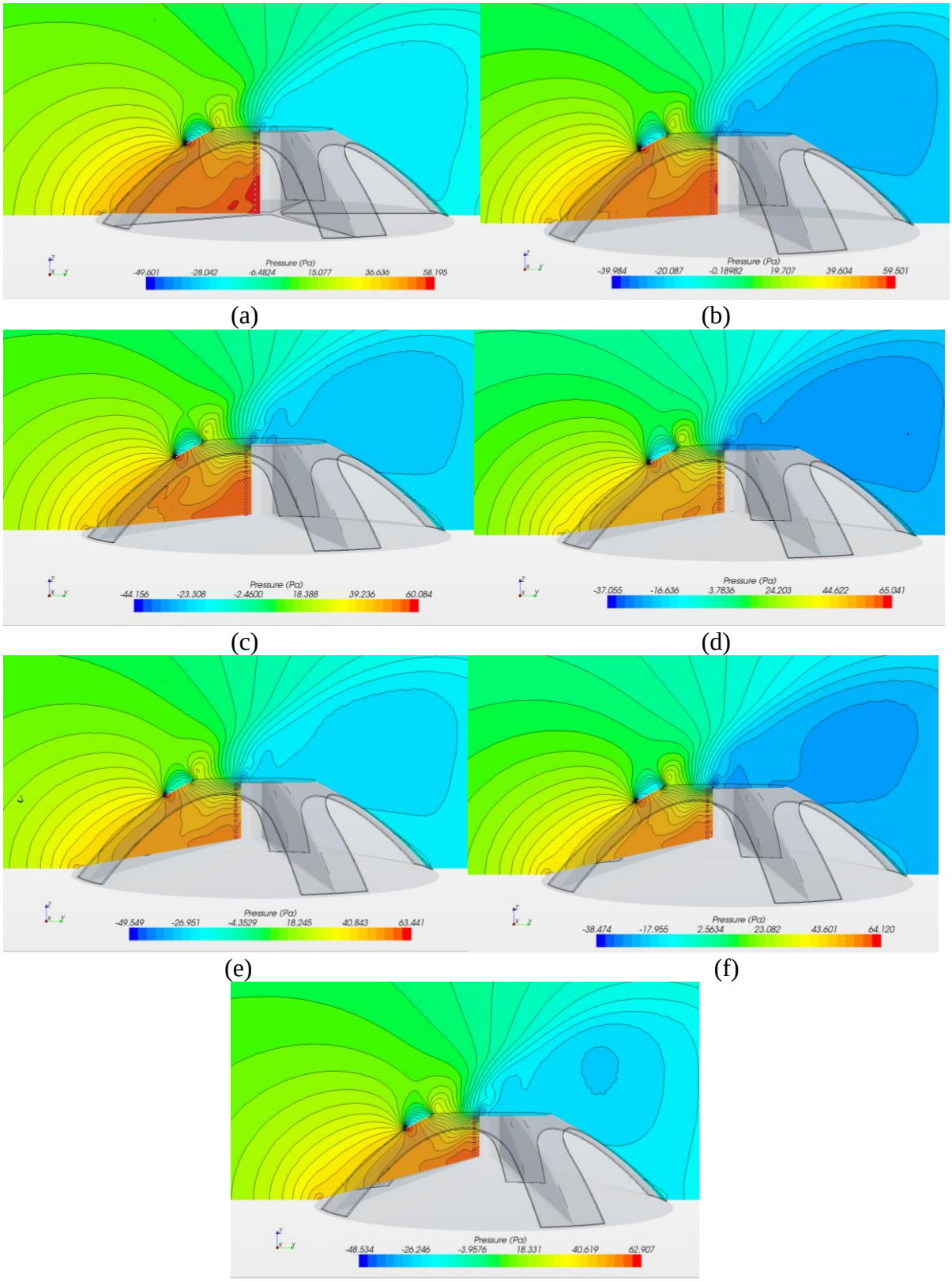


**Fig.6.6. Pressure distributions on plane section (a) 245mm vertical length, (b) 230mm vertical length, (c) 215mm vertical length, (d) 200mm vertical length, (e) 185mm vertical length, (f) 170mm vertical length, (g) 155mm vertical length.**

It can be suggested that the most important parameter of shroud to improve a flow acceleration process is to increase the flow compression region. From both Fig.6.5 and Fig.6.6, it can be predicted that the flow acceleration can be significantly improved by increasing the compression region. Thus, the original model of five chamber mode was divided into three regions, flow capture region, flow direction alteration region and flow acceleration region as shown in Fig.6.7.

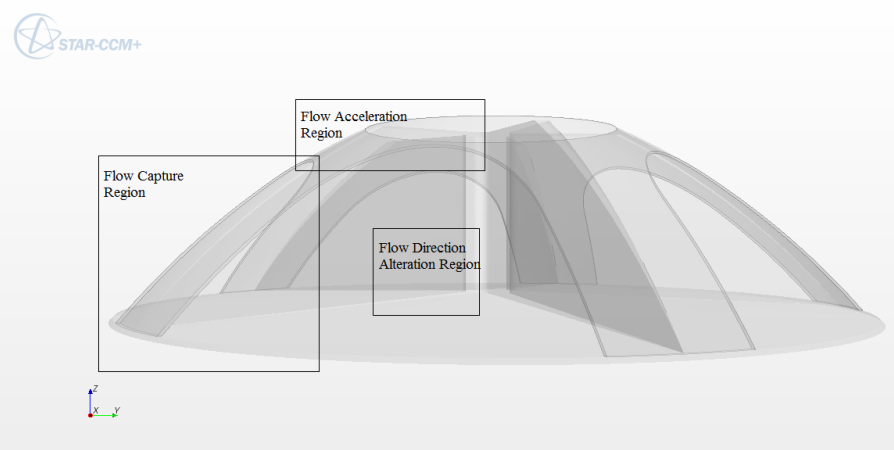


**Fig.6.7. Location of three regions on shroud**

These three regions will be optimised individually. The effects of each parameter of the model on flow acceleration will be studied while keeping the rest of parameters constant. The shroud model was re-designed as shown in Fig.6.8. The height of the model was increased and the complexity of the model was increased with adding some features. The height of flow capture region was increased to capture more flow from higher layer. The long flow acceleration region could gain a high velocity increasing ratio, so that the height of flow acceleration region was increased.

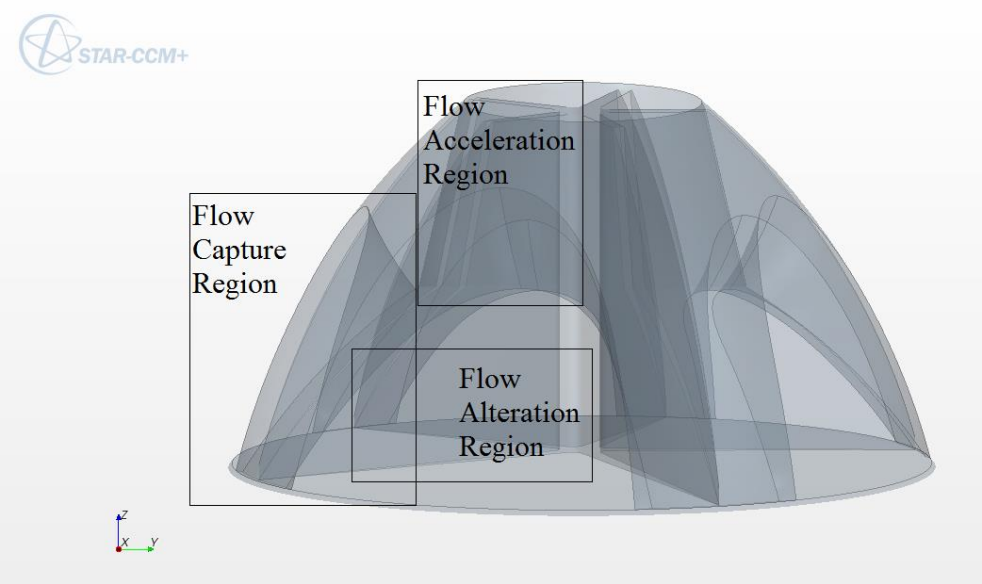


**Fig.6.8. A view of model A**

A new model was named as model A. The major dimensions of model A are shown in Fig.6.9 and the details of model A can be seen in Appendix G. Model A has been generated in 500mm height (H), the diameter of model base ($D_{base}$) is 1000mm and the diameter of model outlet ($D_{outlet}$) is 360mm. The outside curvature of model is created in 1000mm radius (R) with connecting the outlets and the base. There are three important parameters in the flow acceleration region, $D_1$, $D_2$ and L. $D_1$ is the length of upper section of the flow acceleration region, which is 180mm as the radius of shroud outlet. $D_2$ is the length of lower section of the flow acceleration region, which is 240 mm. L is the length of the flow acceleration region, which is 240mm. In the flow capture region, there are four important parameters, r, $h_1$, $h_2$ and b. $h_1$ is the height of internal air gate, which is 240mm. It affects how flow goes into a chamber. For a constant height model, reducing $h_1$ can increase the length (L) of flow acceleration region. The external height of air gate is 360mm, which is marked as $h_2$ in model A. By increasing the height of $h_2$, more flow can be captured. The flow was led through curved surface, which was defined by curve (r), into the chamber. The geometry of r will affect flow direction going into the chamber. The covered broad (b) is used to capture flow

through neighbour into chamber. However, in a specific direction, the wider broad might prevent flow from going into the chamber. The covered broad (b) is 95mm in model A.

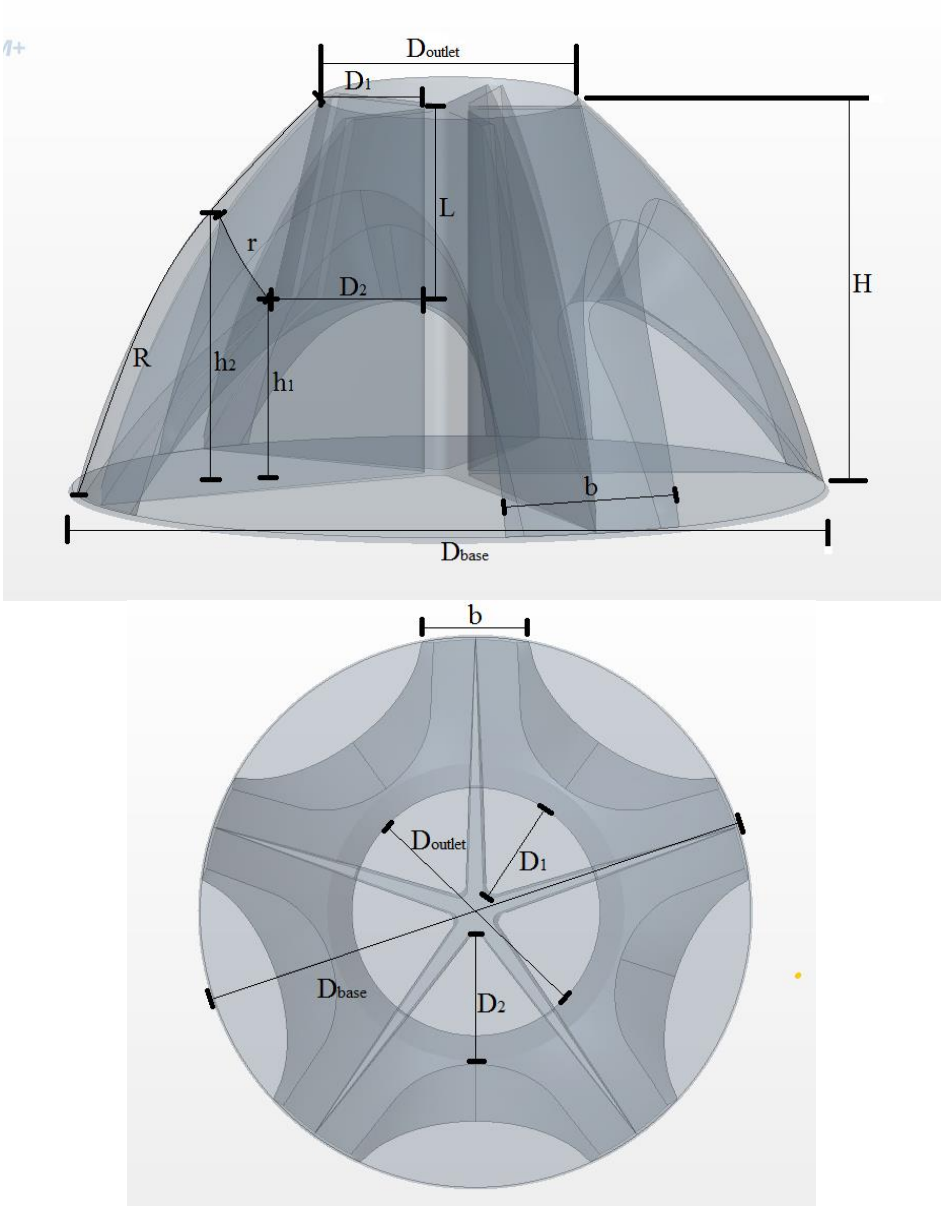


**Fig.6.9. Parameters of model A**

The models with different dimensions will be created and simulated. The effect of every dimension on improving flow concentration will be investigated. The final model will be created by choosing the parameter with the best flow accelerating performance. As the shroud

was designed to concentrate the wind energy, the flow characteristics at the shroud outlet will be determined and compared.

## 6.3. Effects of Acceleration Structures on Flow Characteristics

Three typical structures of flow path as shown in Fig.6.10 have been examined. A nozzle-type model reduces the cross-section, a cylindrical-type model has a constant cross-section and a diffuser-type model expands the ross-section downstream. For both ends of the hollow-structure model, the narrow-end is a sector cross-section of $D_1$ = 180mm and the wide end is $D_2$ = 240mm. The length ratio $L/D_1$=1.4, here, L is the vertical length in flow acceleration region, which is about 252mm. The flow characteristics through these three types of struturces are predicted by Computational Fluid Dynamic (CFD) simulation.

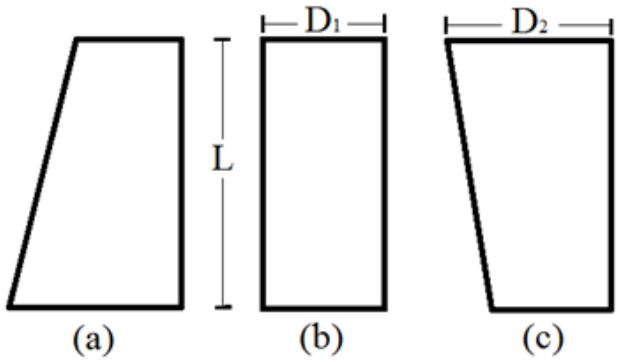


**Fig. 6.10. Three types of hollow structures. (a) nozzle-type model. (b) cylindrical-type model. (c)diffuser-type model.**

As an important factor, the flow velocity at the outlet was firstly studied and compared. The three models with three types of hollow structures were simulated in 10m/s of flow velocity under 0° of approaching flow as shown in Fig.6.11. The maximum velocity and average velocity at the shroud outlet were measured as shown in Fig.6.12.

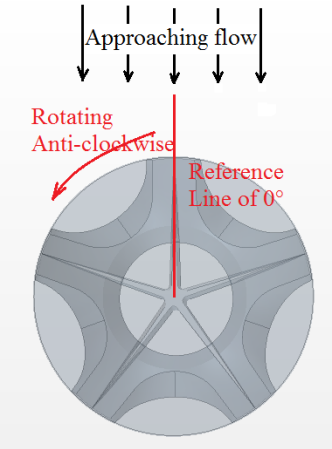


**Fig.6.11. The reference of approaching flow direction**

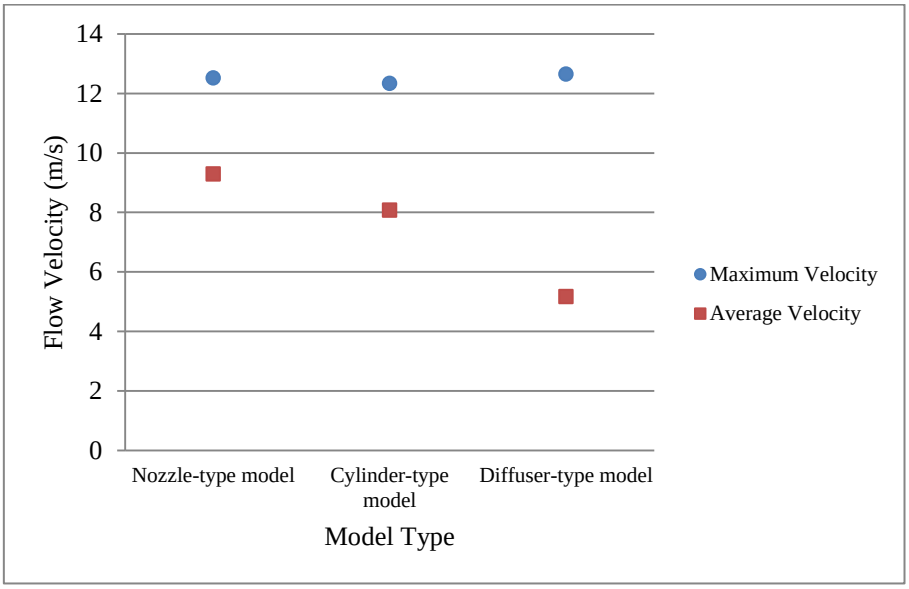


**Fig.6.12. Velocity behaviour at the outlet of different types of models**

From Fig.6.12, it can be seen that there is no significant difference in the maximum velocities from three models with different paths. The maximum velocity from diffuser-type model is slightly higher than that from the other two models. However, the differences between average velocities of these three models are dramatic. The average velocity at the outlet area from nozzle-type model is significantly higher than that from the other two models. This indicates that the nozzle type model is more suitable for the shroud than the others since the

value of average velocity affects the total amount of wind energy that can be transferred. As discussed in Chapter 2, the wind energy is expressed as

$$P = \frac{1}{2}\rho A V^3 \qquad (6.1)$$

where A is flow area, ρ is air density and V is flow velocity.

Given a constant area, the low average flow velocity will make the total wind energy extramely low. The high value of average flow velocity at the outlet of nozzle-type model makes it in comparison with the other two models in high concentration of wind energy. However, the location of maximum velocity is another factor which affects the power output of the wind turbine system. The maximum velocity locations of the three models are shown in Fig.6.13.

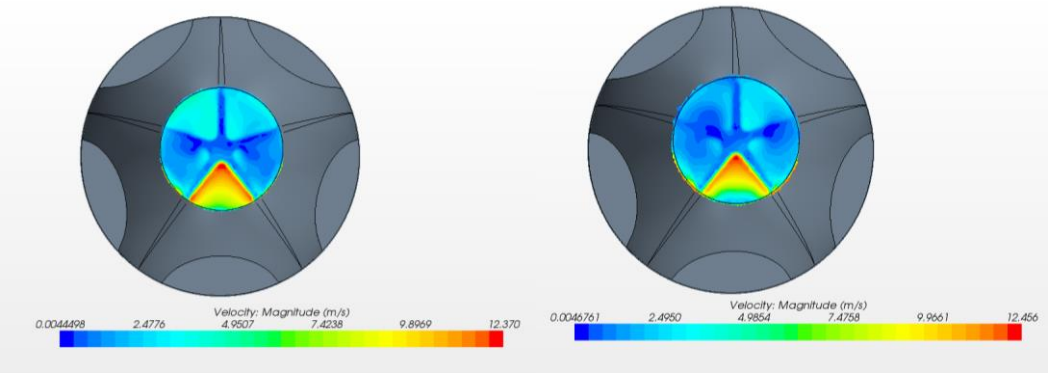


(a) (b)

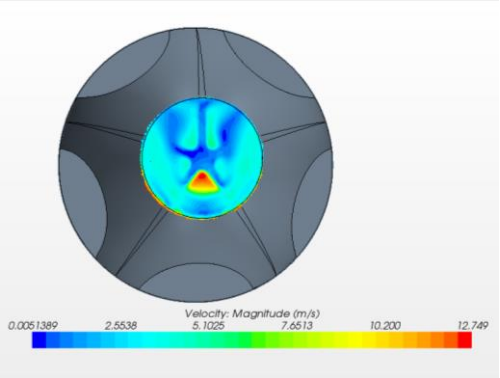


(c)

**Fig.6.13. Velocity distribution at the chamber outlet. (a) Velocity distribution from nozzel-type model. (b) Velocity distribution from cylinder-type model. (c) Velocity distirbution from Diffuser-type model**

From Fig.6.13, it can be seen that there is a high velocity region near the central area of the shroud outlet for all three models. The distributions of this high velocity regions on turbine blades were not symmetry, so that the steady state of blades could be easily broken, which can improve the starting ability of the wind turbine turbine. This is the improvement of all three types of model. However, it was noticed that there were not high velocity regions located at the blade tips. The high velocity at blade tips can provide more torque to increase power output of the novel wind turbine. The Diffuser-type model had worst distribution of high velocity region in the three types of models because there is no high velocity region near edges of the outlet. Nozzle-type model and cylinder-type model have high velocity regions along edges of outlet. Thus, the nozzle-type model achieve best flow characteristic of maximum velocity locations in all three models.

In order to visulise the process of flow velocity alteration inside a chamer, a pressure line was chosen and pressure along the pressure line inside a chamber as shown in Fig.6.14. The diffuser-type model achieved the lowest pressure at the outlet, which means the highest maximum velocity of these three models as disccused before. It was also found that the diffuser-type model had higher gradient of pressure reduction than other two models, and this means the diffuser-type model achieved faster flow acceleration process than the other two models. The total amount of wind energy depends on the value of average velocity at the outlet, therefore the diffuser-type model will not be considered due to its low average velocity at the outlet. It was suggested that the nozzle structure is most effective for the novel wind turbine system to accelerate the wind flow through the shroud

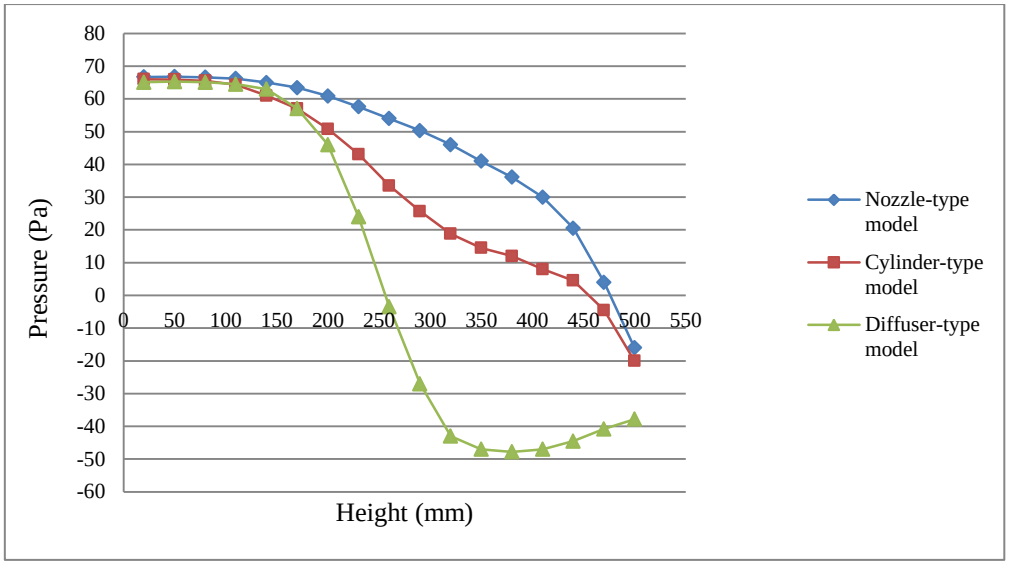


**Fig.6.14. Pressure distribution along pressure line**

Fig.6.15 shows the velocities in the middle section. It can be found that the flow acceleration process of diffuser-type model and cylinder-type model was faster than that of nozzle-type model. They both gained a velocity increase after the flow was led to the vertical direction. The nozzle-type model had a longer acceration process and achieved maximum velocity near the outlet layer. However, the acceleration process of nozzle-type model continued until the flow left the chamber. With this feature, it can be suggested that if the length (L) of the nozzle model was increased, the maximum velocity and average velocity could be increased. However, the diffuser-type model had a velocity decreasing process near the outlet and this would cause the velocity continuely to decrease if the length (L) was increased. The most important is the location of maximum velocity at the outlet layer. Therefore, it is confirmed that the nozzle structure is most effective for the novel wind turbine system to accelerate the wind flow through the shroud.

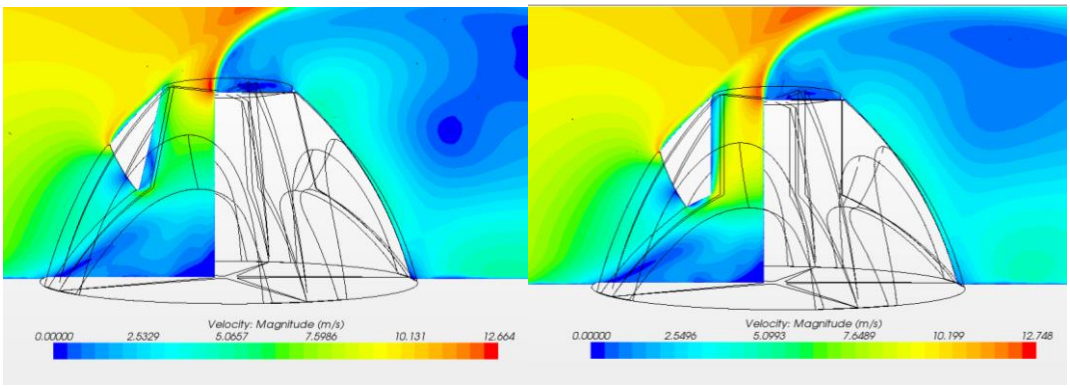


(a) (b)

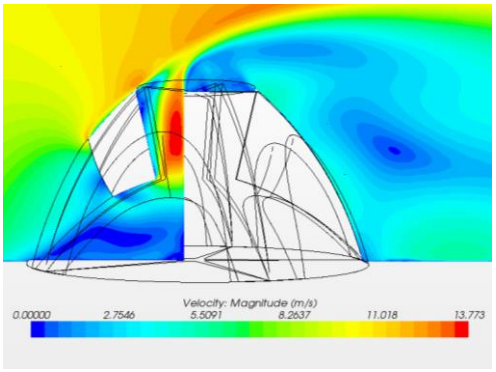


(c)

**Fig.6.15. Velocity distribution along middle section and outlet of chamber. (a) Velocity distribution of nozzel-type model. (b) Velocity distribution of cylinder-type model. (c) Velocity distirbution of Diffuser-type model**

In order to achieve further improvements in flow acceleration, the various parameters of the nozzle structure, as shown in Fig.6.16, were studied and compared. The length (L) and outlet radium ($D_1$) of nozzle structure were kept constant. The models with different $D_2$ were created and simulated. The ratio of $D_2$ and $D_1$ was expressed as α, which is 1.33 for model A. The velocity characteristics at the outlet of five models with various α, which are 1.11, 1.22, 1.33, 1.44 and 1.55, were measured and compared. The models were analysed in $0^o$ of approaching flow at which model A gained its worst flow acceleration. If the flow characteristics of models can be improved in this direction of flow, the flow characteristics in other directions may be improved as well. By doing this, the time of simulation can be

siginificantly reduced. The comparison of maximum velocity and average velocity is shown in Fig.6.17.

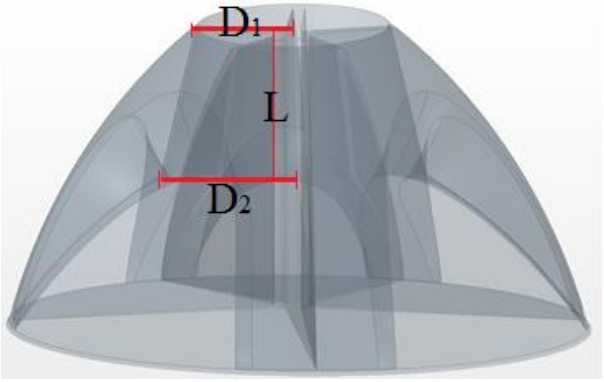


**Fig.6.16. The sketch of nozzle type model**

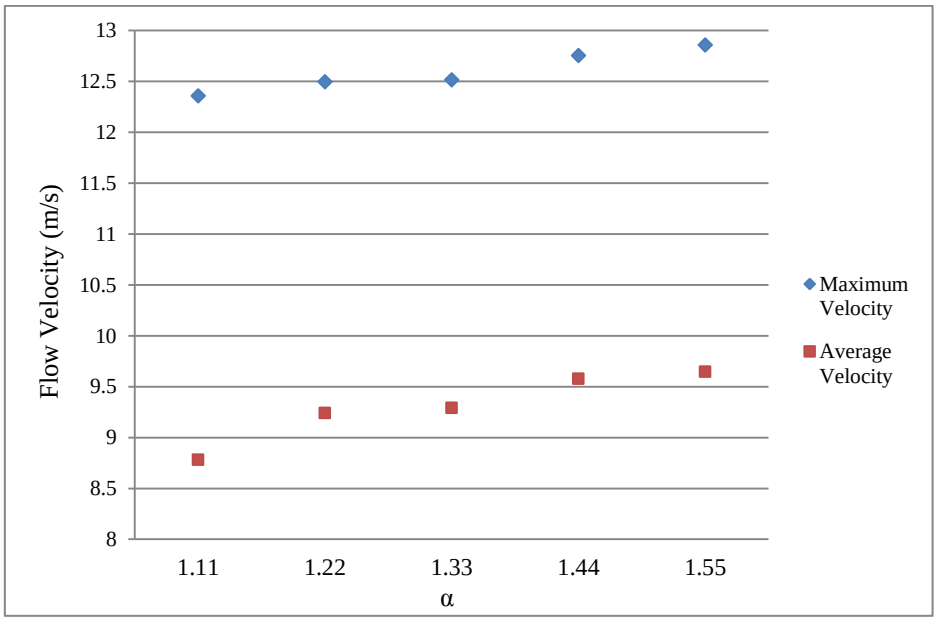


**Fig.6.17. Maximum velocity and average velocity of various nozzle structure**

As shown in Fig.6.17, it is found that the flow characteristics at the outlet were improved in both maximum velocity and average velocity with increasing ratio α. Thus, the large ratio α would be chosen to improve flow acceleration of the shroud. However, the ratio α was limited by model diameter $D_{base}$. As to the original nozzle type model, which $D_{base}$ is 1000mm, the largest ratio α can be chosen is 1.55. The improved model (α=1.55) was tested

and compared with original nozzle type model (α=1.33) in various directions of approaching flow to see if the shroud should be able to work in different directions of approaching flow.

The improved model (α=1.55) and original nozzle type model (α=1.33) were simulated in different directions of approaching flow. The velocity of approaching flow is 10m/s. Maximum velocity and average velocity at the shroud outlet were measured and comparied as shown in Fig.6.18.

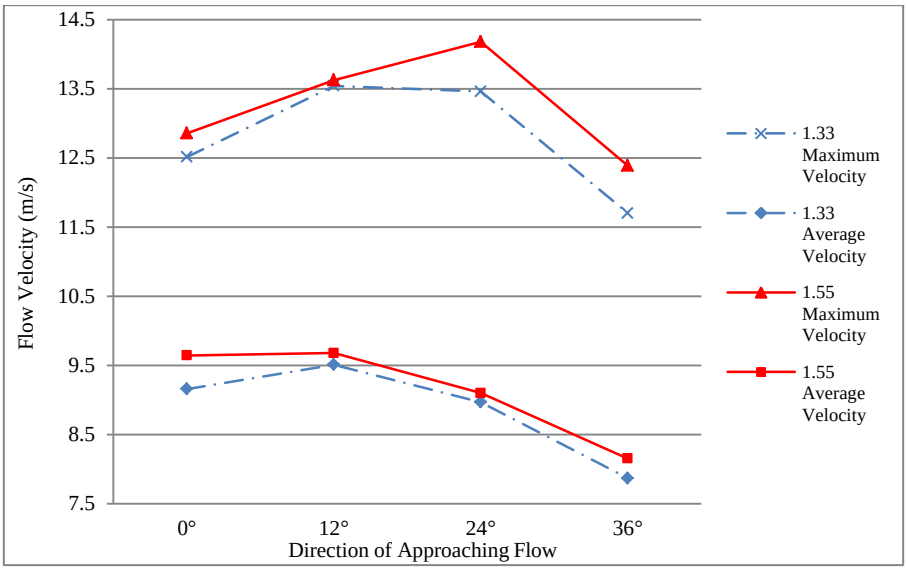


**Fig.6.18. Flow characteristics at the outlet of different shrouds in various directions of approaching flow**

It can be seen that the maximum velocity and average velocity from improved model (α=1.55) are higher than those from the original nozzle type model (α=1.33) in various directions of approaching flow. Especially in 24° and 36° of approaching flow, maximum velocity and average velocity were increased about 7.2% and 3.85%, respectively, compared with the original nozzle type model (α=1.33).

It was predicted that increasing the length (L), which is length of flow acceleration refer to Fig.6.17, of flow acceleration region will improve the performance of flow acceleration of the shroud. Thus, different nozzle-type models with various length, 170mm, 190mm, 210mm, 230mm and 250mm were created and simulated. The maximum velocity and average velocity

at the outlet of different models were presented as shown in Fig.6.19. It can be seen that maximum velocity and average velocity were increased by increasing the length (L) of flow acceleration region. Velocity acceleration was proportional to the length (L). The flow accelerating ratio of flow acceleration region can be improved by increasing the length (L). The length (L) can not be infinitely increased so that it will be 250mm for the final model.

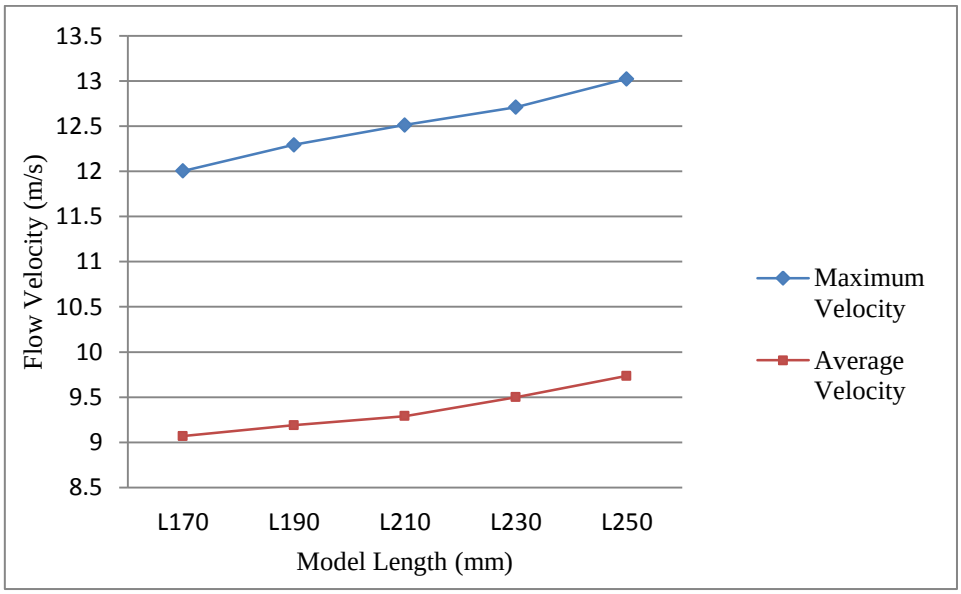


**Fig.6.19. Maximum velocity of various height models**

## 6.4. Concept of Flange Structure and its Function

It was reported that the wind speed could be increased by adding a ring-type flange at the exit periphery to the diffuser body (Abe & Ohya, 2004; Ohya, et al., 2008), Thus, a flange structure was implemented on the nozzle-type shroud of the novel wind turbine to improve the flow acceleration. The middle block section of the shroud was reduced to create a flange part inside shroud (as shown in Fig.6.20). For various models, the shroud height (H) was kept constant and flange heights (h) were added as 50mm, 100m, 125mm, 150mm, 175mm, 200mm, 250mm and 300mm respectively, by reducing the height of middle blockage section ($H_m$). These models were simulated in CFD, and the flow characteristics at the outlet of these models were investigated. Sketches of shrouds with flange were shown in Fig.6.20.

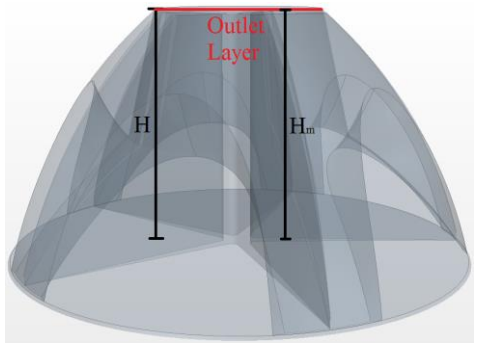


(a)

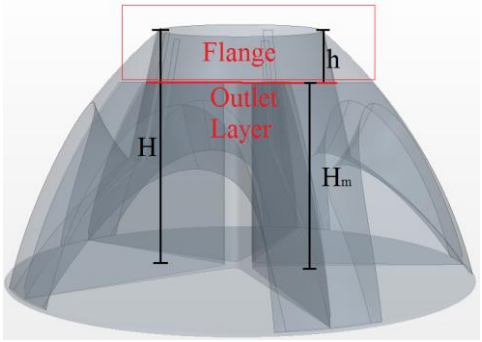


(b)

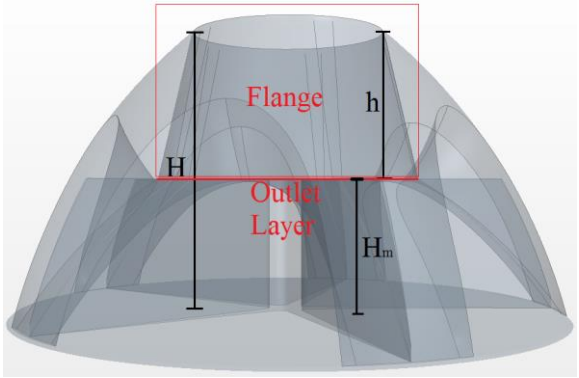


(c)

**Fig.6.20. Sketch of models with different height of flange (a. model without flange, b. model with 100mm of flange, c. model with 260mm flange)**

The maximum velocity and average velocity at the outlet layer of different models were measured and compared as shown in Fig.6.21.

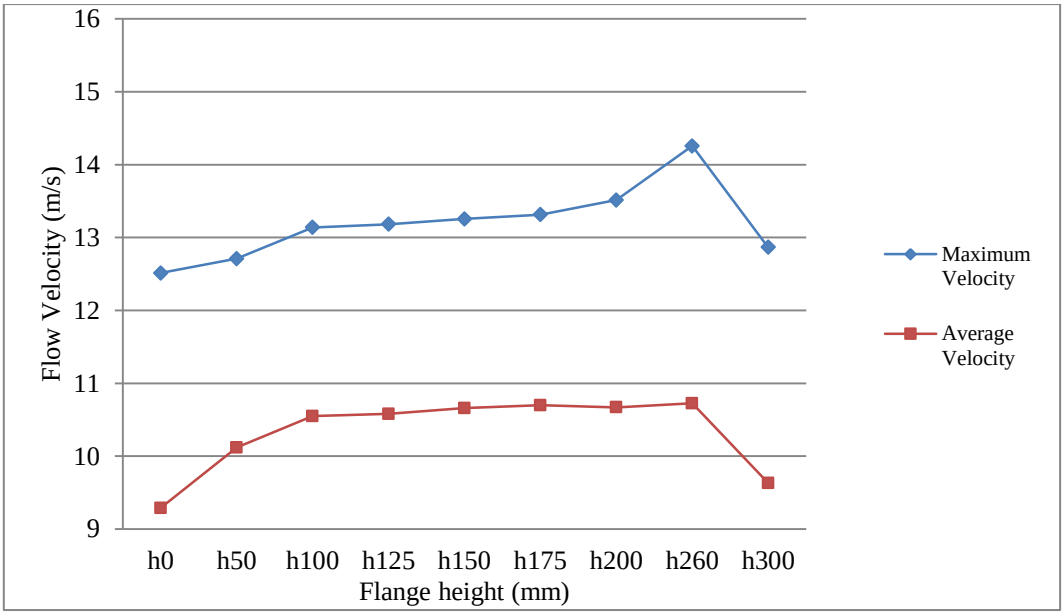


**Fig.6.21. Velocity performance at outlet of different flange height models**

The flow characteristics at the outlet layer of these models with different flange heights (h) were shown as Fig.6.21. It can be seen that a flange could improve the values of shroud in both maximum velocity and average velocity. They increased with an increase of flange heights (h). There is a significant improvement from non-flange (h0) to 100mm of flange height, which is about 6.3% increase in maximum velocity and 12.6% increase in average velocity. It was suggested that the flow acceleration of shroud could be improved by implementing a flange, especially the average velocity could be increased significantly. Furthermore, the outlet area can be enlarged due to the implementation of a flange as shown in Fig.6.20. For a model with 100m flange height, the outlet area increased about 1.27 times of the outlet area without the flange. With an increase of both flow velocity and cross-section area increase, the total wind power captured by 100mm flange height model can be increased about 1.81 times of that from the model without a flange. The pressure distributions on the middle axis for various flange heights (h) were shown in Fig.6.22. The gradients of the models with flange are higher than non-flange model. This means that the flange structure gave faster flow acceleration response. Due to limitation of geometry, the maximum height of

a flange is 300mm. The height of a flange could be 260mm in final model, which can provide better flow acceleration than that of other models.

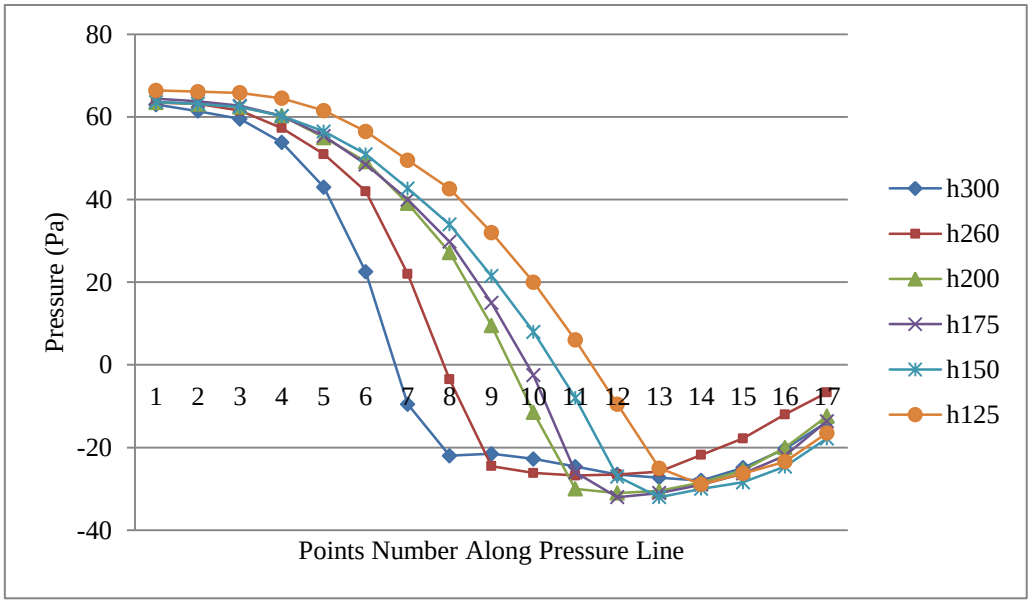


**Fig.6.22. Pressure distributions on line of different flange heights**

In order to determine what may affect the improvement of flow acceleration, the pressure distribution along the middle section of model was extracted from the CFD simulation. The pressure distribution of the model with 100mm height of flange was shown in Fig.6.23. It can be seen that a low pressure region was generated above the outlet layer of the shroud. The low pressure region increased the pressure difference between the inlet and the outlet of shroud. With this great pressure difference, more mass flow can be inhaled into the chamber. This is the reason that caused a significant increase of the average velocity. Owing to this effect, the flow coming into the chamber can be effectively concentrated and accelerated. The blades will be placed near the bottom of the nozzle structure, where the diameter of the nozzle structure is increased. Thus, it can be seen that the blade swept area was increased with applying a flange structure. Due to the increase both in average velocity and flow area, the total amount of wind energy coming through the shroud can be significantly increased.

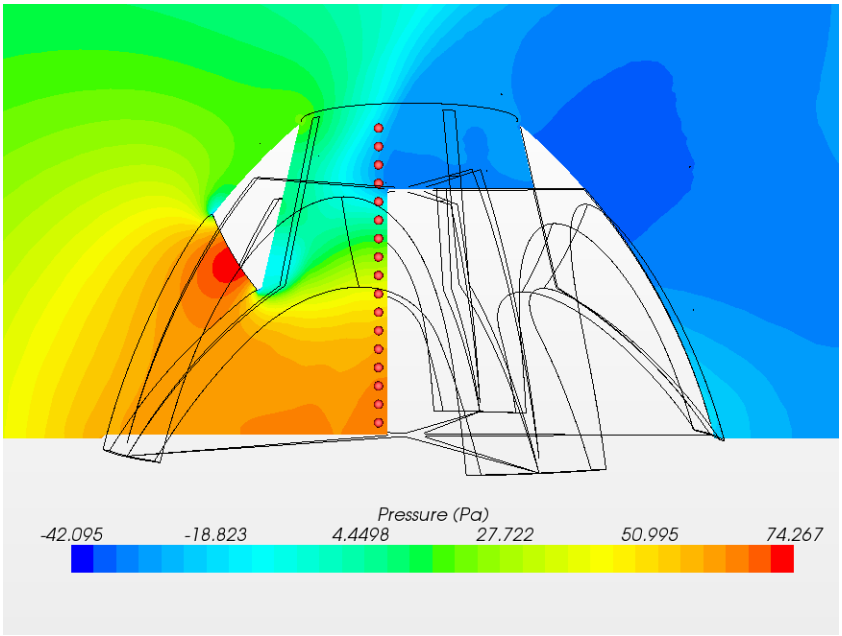


**Fig.6.23. Pressure distribution inside chamber**

## 6.5. Effects of the Shroud Board on Flow Characteristics

The original model was simulated in different directions of approaching flow. Due to the symmetry structure, the model was studied in different directions of approaching flow, $0^o$, $12^o$, $24^o$ and $36^o$ (the reference 0° of flow direction was shown in Fig.6.11). These four different directions are typical and can be used to predict any conditions of approaching flow directions. As shown in Fig.6.18, it was found that the worst flow behaviour at the outlet happened at $36^o$ of approaching flow. It was found that the broad width (b) is the reason to cause this. In model A, the broad width (b) is 190mm (Details can be seen in Appendix J). In fact, the broad is important to the shroud. It is used to stop flow slip out from two sides of model as shown in Fig.6.24, so that the shroud could capture more mass flow.

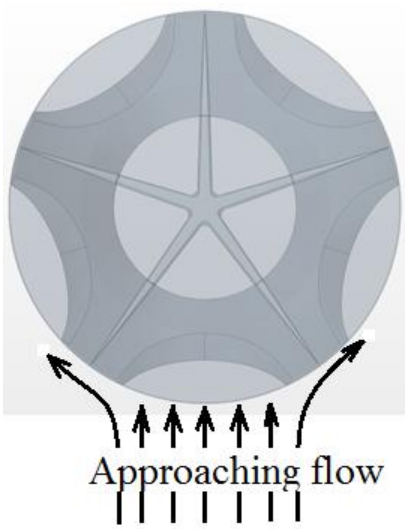


**Fig.6.24. An image of flow approaching shroud**

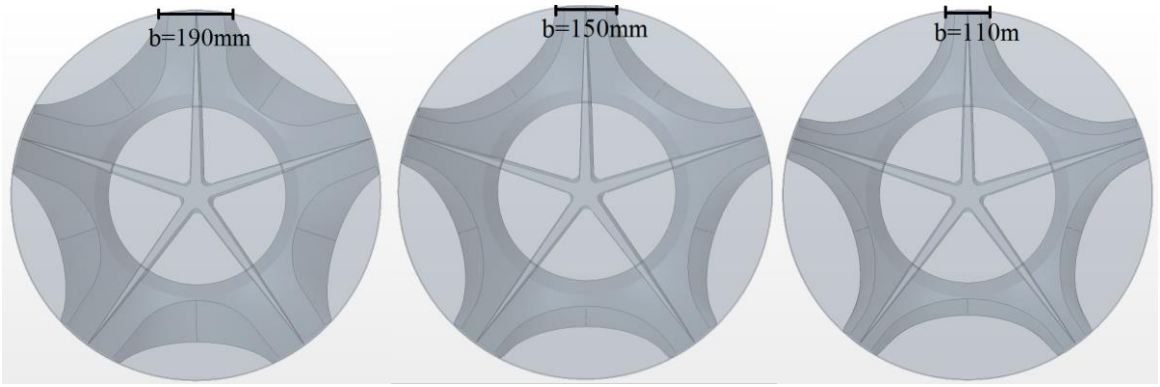


**Fig.6.25. Models with different widths of broad**

The sketches of models with different broad widths can be seen in Fig.6.25. The models with different broad width (b), 190mm, 150mm, 110mm and 90mm, were simulated and analysed in different directions of approaching flow at 10m/s. The maximum velocity and average velocity at the outlet were measured and compared separately, as shown in Fig.6.26 and Fig.6.27.

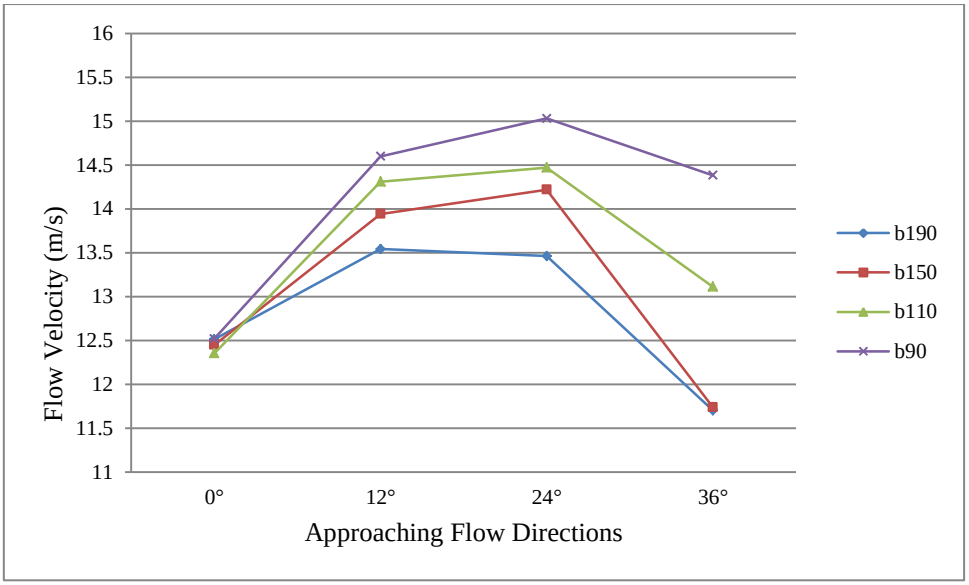


**Fig.6.26. Maximum velocity of different wide broads**

Fig.6.26 shows the maximum velocity at the outlet of the four models with various broad widths in different directions of approaching flow. It can be seen that at $0^o$ of approaching flow, the flow concentration of different broad models is similar. The maximum velocity increased about 1.25 times as approaching flow. However, the maximum velocities of these models are various in other directions of approaching flow. The differences of the maximum velocity between four models reached the highest value (26%) at 36° of approaching flow. This is because narrower broad can capture more mass flow. The results of flow compressing are improved, which increase flow acceleration ratio, so that the maximum velocity is significantly increased of the 90mm broad model.

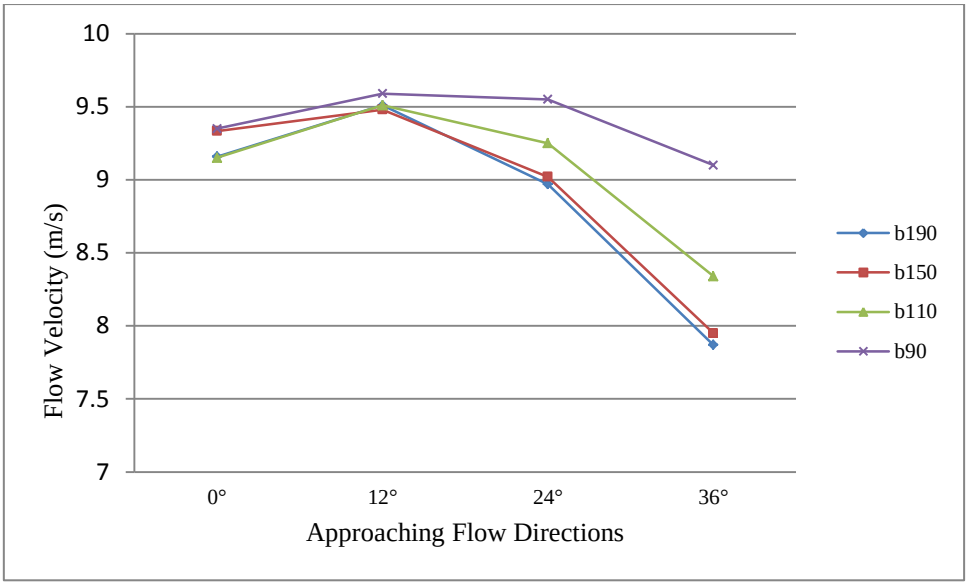


**Fig.6.27. Average velocity of different wide broads**

Fig.6.27 shows the average velocity at the outlet of the models with different broad widths in various directions of approaching flow. There are slight differences of average velocity between four models in $0^o$ and $12^o$ of approaching flow. However, the difference of the average velocities among four models reached about 5.8% and 12.3%, respectively, in $24^o$ and $36^o$ of approaching flow.

According to Fig.6.26 and Fig.6.27, it was found that the flow acceleration was affected by the broad width due to an impact on mass flow capture. At $0^o$ of approaching flow, maximum velocities and average velocities of different models are similar since flow could go through a chamber smoothly. However, in other directions of approaching flow, some mass flows were blocked by the broad, so that the model with wider broad got lower flow acceleration. The worst conditions happened at $36^o$ of approaching flow. The coming flow was blocked by front broad and slipped out from two sides of shroud. With a wider broad, the more flow will slip out so that the mass flow going through the chamber is reduced. Due to a reduction of mass flow, the total amount of wind energy will be reduced. Therefore, it is recommended that the final model will have a 90mm board width.

## 6.6. Effects of Flow Capture Region on Flow Characteristics

The major parameters of the flow capture region can be seen in Fig.6.28. The geometry of flow capture region relied on three parameters, $H_{outside}$, $H_{inside}$ and $r_{lead}$. The amount of mass flow that goes into a chamber depends on the area which is controlled by the height of $H_{outside}$ as shown in Fig.6.28. However, changing one parameter in this region will affect the other parameters. An increase of $H_{outside}$ will reduce angle α. Four models with different heights of $H_{outside}$ were created, and $H_{inside}$ was kept constant. The models were simulation in CFD and the flow characteristics at the outlet were determined as shown in Fig.6.29.

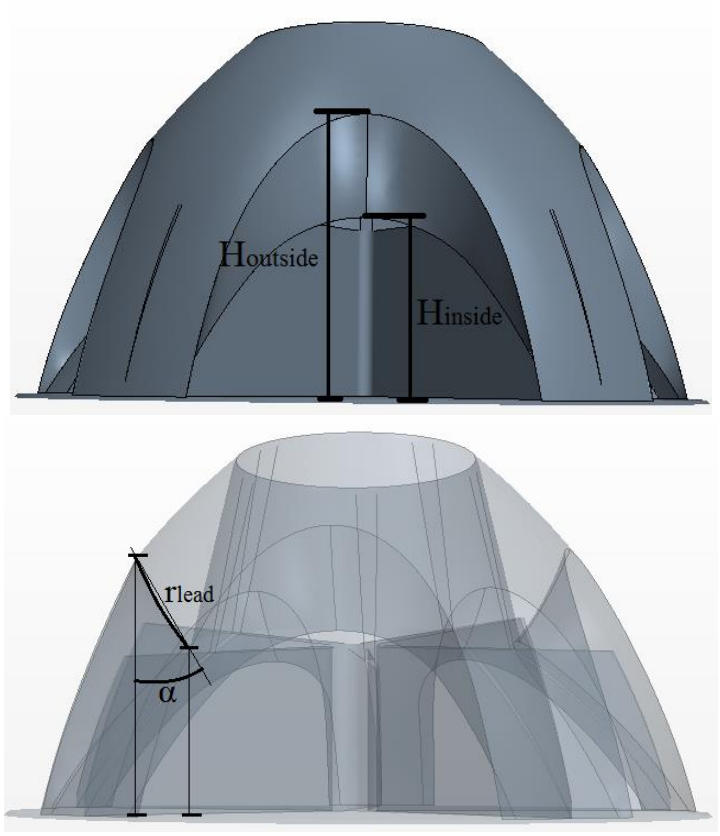


**Fig.6.28. Major dimensions of flow capture region**

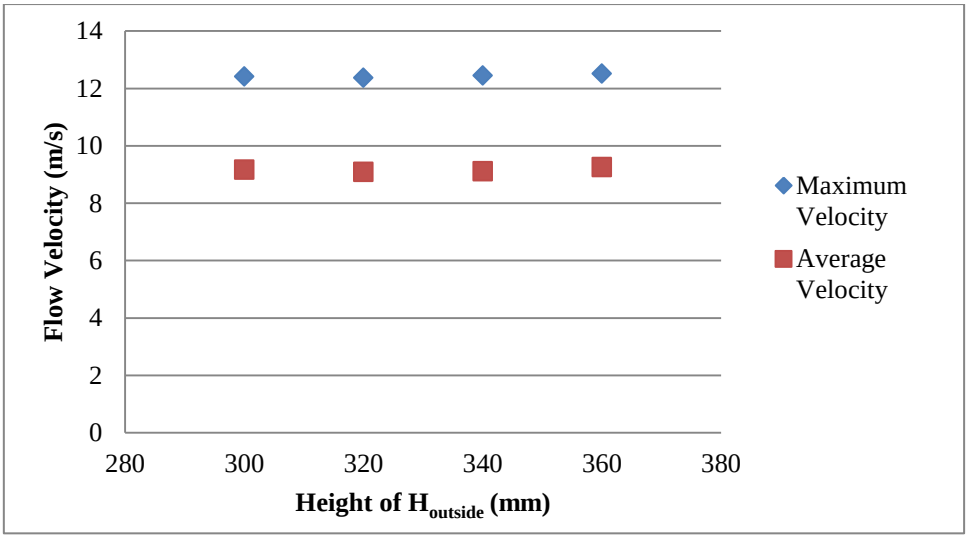


**Fig.6.29. Flow velocity at outlet of models with various $H_{outlet}$**

It can be seen that the flow characteristics at the outlet of different models are similar. The differences of maximum velocity between models with different $H_{outlet}$ are less 1%. The differences of average velocity between models with different $H_{outlet}$ are about 1%. Thus, it is considered that the slight differences may be caused by the errors in simulation. Thus, it was suggested that increasing height of $H_{outside}$ will not give significant improvement in flow acceleration.

In order to determine the effects of the curve r, several models were created as shown in Fig.6.30. The value of r is the radius of the curve and the direction of the curve is recorded as positive. The models were simulated and flow characteristics at the outlet were determined as shown in Fig.6.31. It can be seen that the difference of maximum velocity and average velocity between these models are not significant. The model with r=-300 curvature achieved slight improvement in both maximum velocity and average velocity. The improvements are about 3% and 1.5% for maximum velocity and average velocity, respectively. The reason that caused the increasing of flow velocities may be due to simulation errors, but the r in final model will still be -300mm which means the radius of curve is 300m and the direction is inward (marked as red).

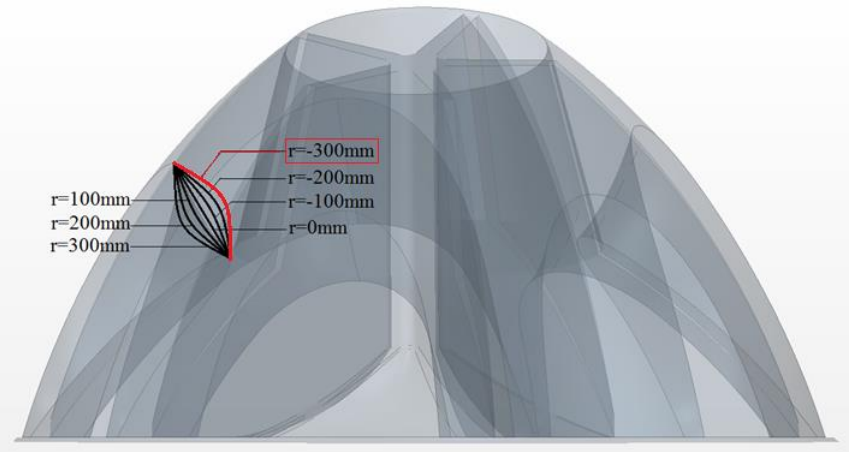


**Fig.6.30. Different dimensions of curvature r**

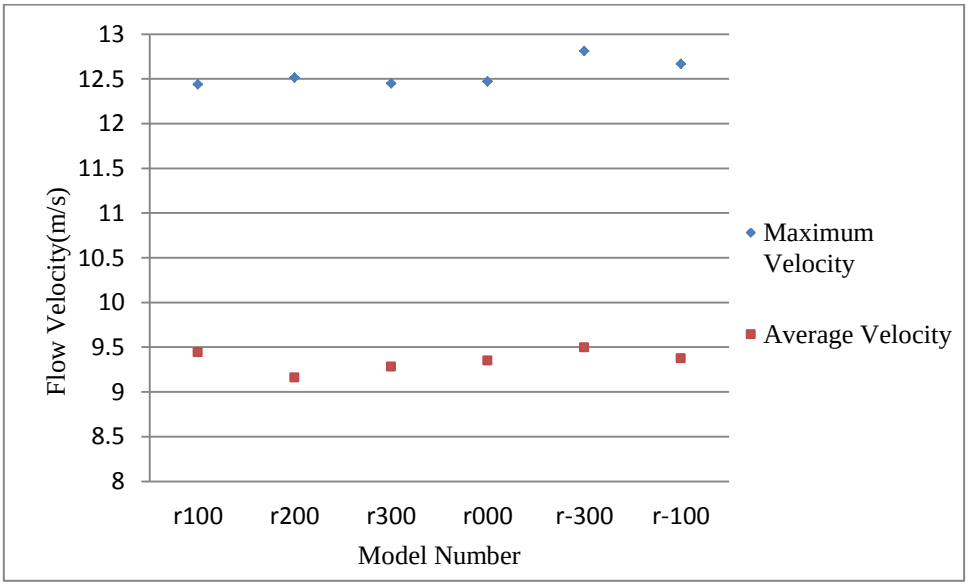


**Fig.6.31. various structures of curve $r_{lead}$**

## 6.7. Effects of Flow Alteration Region on Flow Acceleration

The flow going into chamber was led from horizontal to vertical by the bottom curve as shown in Fig.6.32. Two parameters were used to control the geometry of bottom surface, which are distance before leading flow to vertical (L) and height of leading curve ($H_{curve}$). Different parameters of L and $H_{curve}$ were studied.

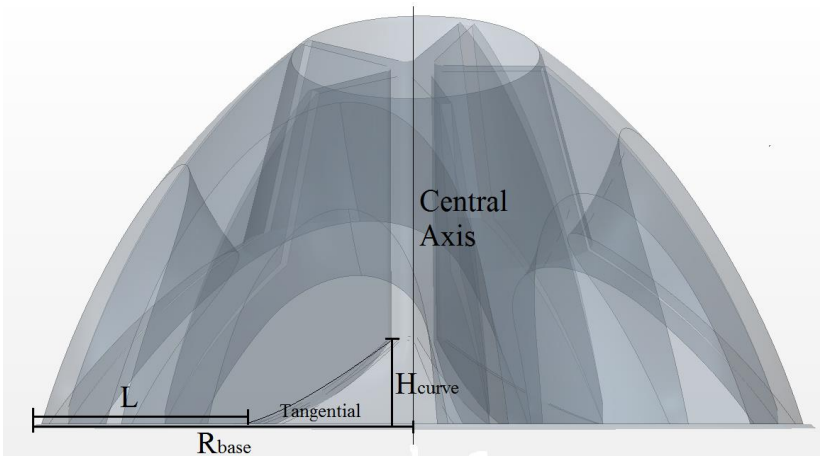


**Fig.6.32. Two dimensions of flow alteration region**

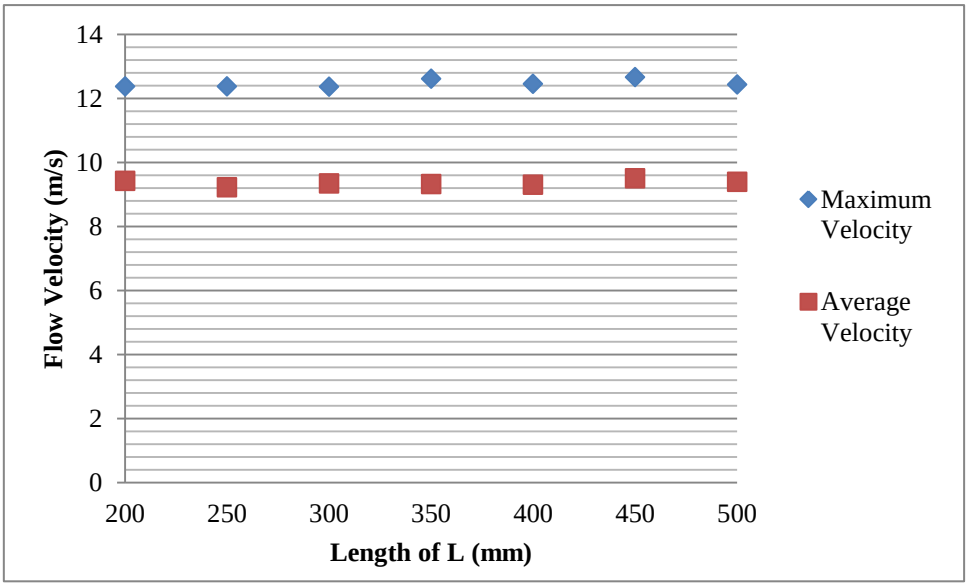


**Fig.6.33. Flow characteristics of different Leading Length (L)**

Models with 100mm height of curve ($H_{curve}$) and different leading Lengths (L) were created, and their flow characteristics at the outlet were predicted under 0° of approaching flow with 10m/s velocity. Both maximum velocity and average velocity of the different models are presented in Fig.6.33. The differences of maximum velocity and average velocity between various models are about 2% and 1%, respectively. It appears that values of differences are very small, which may not be caused by the differences of geometry but caused by simulations accuracy. Thus, it was suggested that the bottom curve will not have a significant

effects on flow acceleration. The pressure distributions along central axis inside the chamber were presented in Fig.6.34. It can be seen that the distributions of pressure for different models are similar. It is an other evidence to prove that the flow acceleration is not affected by the dimension of leading length (L).

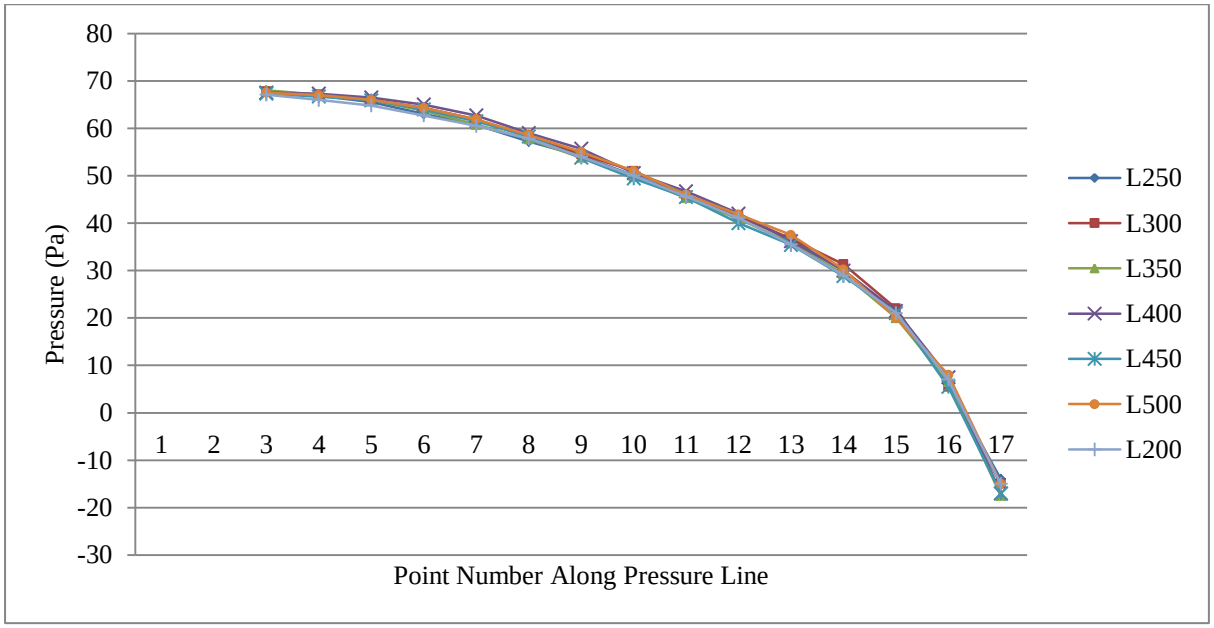


**Fig.6.34. Pressure distribution along pressure line**

As mentioned, the bottom surface is affected by leading length (L) and height of curve ($H_{curve}$). Thus, the models with 350mm of leading length (L) and different heights of curve ($H_{curve}$) were created and simulated. The average and maximum velocities at the outlet of shroud were measured and compared as shown in Fig.6.35.

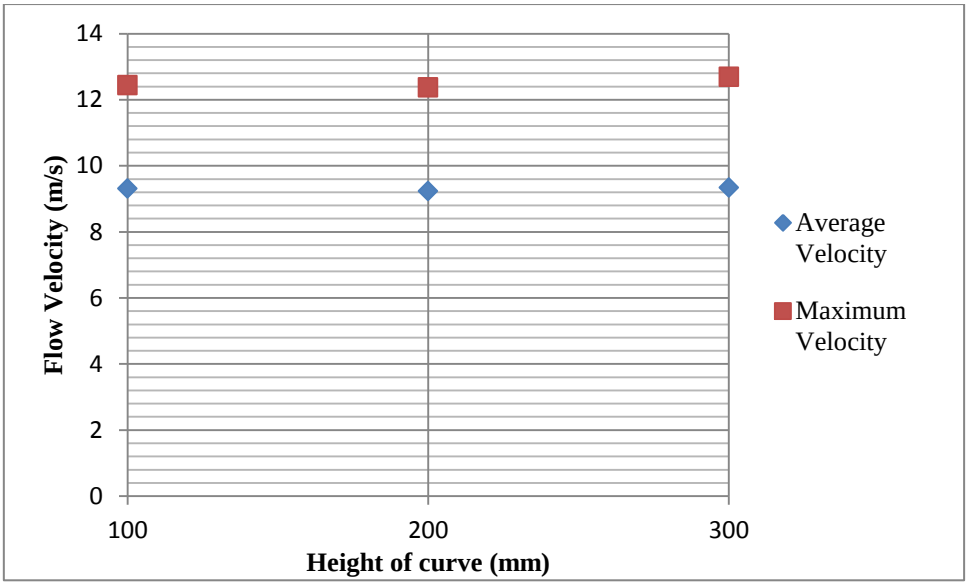


**Fig.6.35. Flow characteristics of different height of curve ($H_{curve}$)**

From Fig.6.35, it can be seen that flow characteristics of different models are similar. The small difference may be caused by the accuracy of simulation, but no the effect of geometry. It can be suggested that the geometry of bottom surface may not bring significant improvement on flow acceleration.

## 6.8. Flow Characteristics of the Final Model

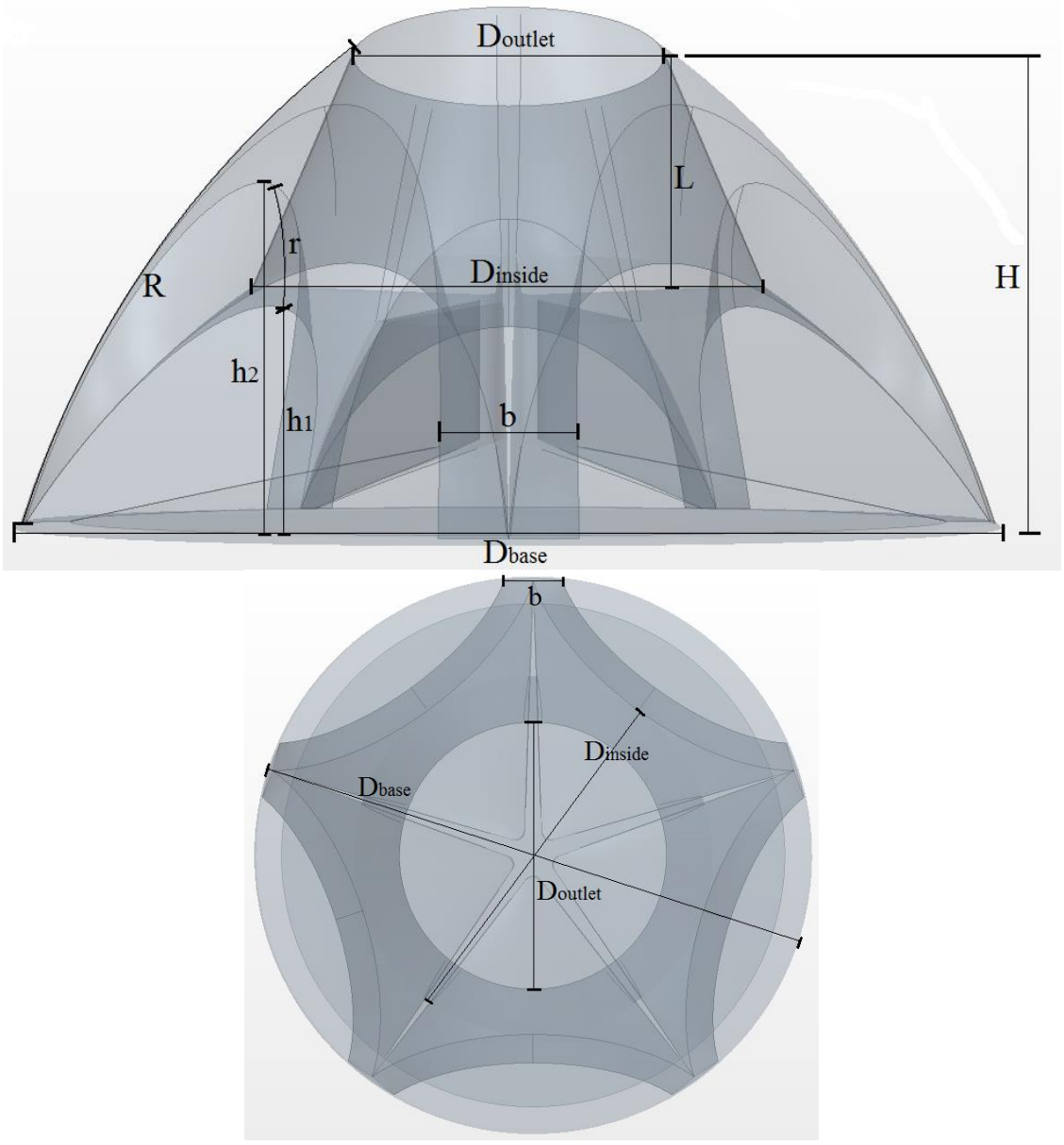


**Fig.6.36. Dimensions of final model**

A final model was created in the dimensions that determined in the previous sections. The dimensions were selected due to the performance of flow acceleration. The model was created in 500mm height (H) with a 260mm flange (L). The nozzle ratio was set as 1.55, which had $D_{outlet}$ =180mm and $D_{inside}$ = 560mm. The covered broad (b) now has a width of

90mm. The dimensions of final model were shown as Fig.6.36. The engineering drawing of the final model can be seen in Appendix L.

The final model was simulated in various directions of free stream flow with 10m/s velocity. The flow characteristics at $D_{inside}$ were measured and compared with those of model A as shown in Fig.6.36.

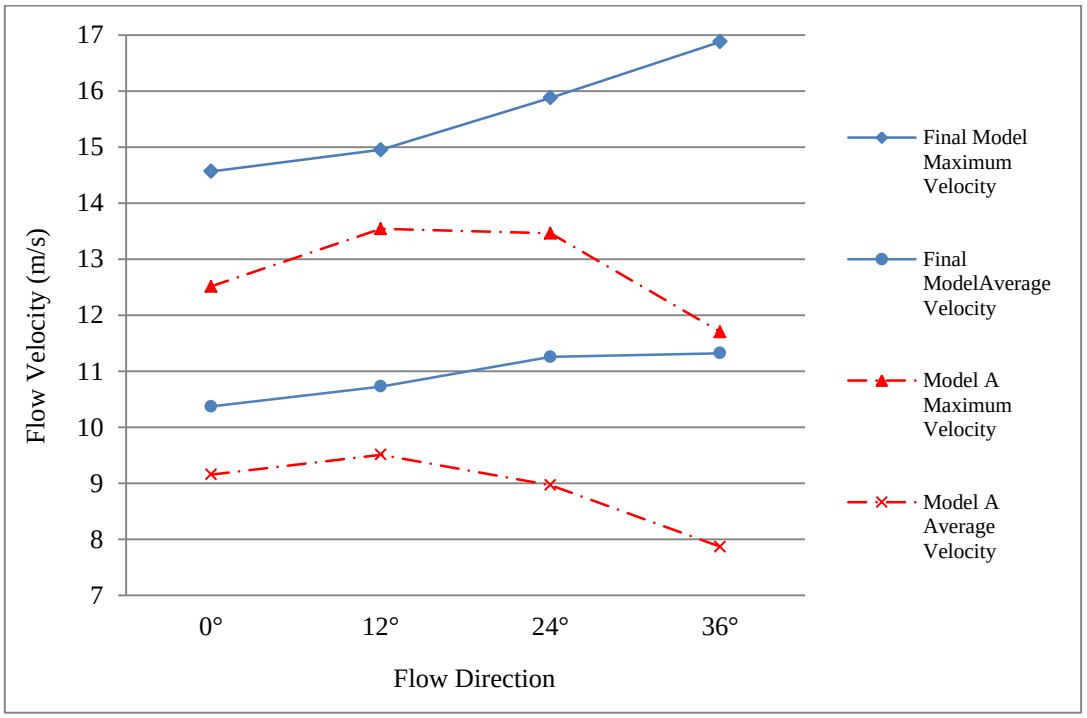


**Fig.6.37. Flow characteristics at the outlet of shroud in different directions of approaching flow**

From Fig.6.37, it can be found that final model has achieved significant improvements in both maximum velocity and average velocity. The maximum velocity increase was about 20.53%, 14.1%, 24.19% and 51.78% at $0^o$, $12^o$, $24^o$ and $36^o$ of approaching flow, respectively. The locations of high velocity regions at the outlet of these two models are same so that the potential of power output of the final model can be significantly increased. In particular, in $36^o$ of approaching flow, the maximum velocity increased to 16.88m/s in 10m/s inlet flow, which is about 51.78% increase compared with model A. The average velocity accelerating

was increased about 12.12%, 12.17%, 22.85% and 34.51% in $0^o$, $12^o$, $24^o$ and $36^o$ of approaching flow, respectively. The model performance in $36^o$ of approaching flow was the worst compared with the other directions of approaching for model A. However, the performance had been significantly increased by reducing the board width. The nozzle structure of final model is 1.55 so that the flow area of the novel wind turbine system has been increased to 2.4 times as the flow area of model A. With a total of improvement in velocity and area, the power output of the final model could be increased about 4 times compared with that of model A. The final model has achieved maximum 1.69 times velocity improvement of approaching flow, which implies 4.8 times wind energy concentrated for a specific area of the shroud outlet.

## 6.9. Summary

This chapter has addressed the optimisation outcomes for a shroud chamber. A comprehensive analysis of internal flow inside a chamber has been carried out, and the essential parameters to improve the acceleration factor have been determined. The shroud was divided into three regions, flow capture region, flow alteration region and flow acceleration region. Each region was studied and optimised. A final model has been created with the parameters determined from the optimisation studies. The final model was simulated under different directions of approaching flow. It is evident that the final model can achieve improvements in accelerating flow velocity and enlarging flow area. Compared with flow characteristics of model A, the maximum velocity and average velocity of final model have been increased about 20% in various directions of approaching flow, and flow area increased about 140%.

# Chapter 7 – Concepts of Blades

This chapter introduces the development of blades for the novel wind turbine and discuss the improvements of the shroud by implementing a guide vane.

## 7.1. Introduction

Due to the shroud part of the novel shroud wind turbine, the flow from any directions can be unified to the vertical directions with flow speed acceleration. Thus, the requirements of blades can be significantly reduced by the simplified flow conditions. The blade design of novel shroud wind turbine is focused on the power output. It was reported that the application of impulse turbines is suitable for the novel shroud wind turbine (Ying, Chen, & Xu, 2012). Because the impulse turbine can achieve higher power output than that of conventional wind turbine in a wide velocity range (Setoguchi, Santhakumar, Maeda, Takao, & Kaneko, 2001). The concept of impulse turbine was first carried out by Sctoguchi for Wells turbine (Kaneko, Setoguchi, & Raghunathan, 1992). At beginning, the performances of impulse turbine were not good. Several disadvantages, especially narrow range of flow, poor starting ability, high speed operation and high noise, were reported (Setoguchi, Kaneko, Maeda, Kim, & Inoue, 1993). However, the self-pitch controlled guide vanes were used to overcome these drawbacks, so that the power output of an impulse turbine were significantly improved (Setoguchi, Kaneko, Taniyama, Maeda, & Inoue, 1996). With the guide vanes, the impulse turbine can work in a good starting capability and low operating speeds of wind flow. The typical structure of fixed guide vane impulse turbine is shown in Fig.7.1. The directions of approaching flow can be controlled and accelerated through the guide vanes. The flow that coming to the blades can advantage of direction of angle of attack and the efficiency of blades can be improved. The impulse turbine is a good option for the novel shroud wind

turbine due to its high performance and low manufacture cost (Thakker, Sheahan, Frawley, & Khaleeq, 2002). The most important reason that implement impulse turbine on the novel wind turbine is the similar flow conditions inside the shroud of novel wind turbine. The technologies of impulse wind turbine have developed for decades. The implementation of impulse turbine can significantly reduce the time to develop turbine blade for the novel wind turbine.

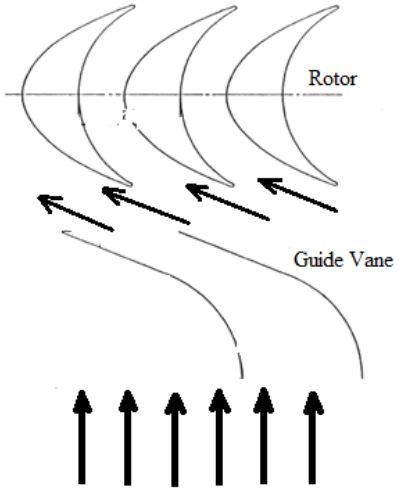


**Fig.7.1. Fixed guide vane impulse turbine**

## 7.2. Flow Characteristics after a Guide Vane

A guide vane can be implemented inside a shroud to modify the flow direction and accelerate the flow velocity. The flow inside the novel wind turbine shroud is unsteady and high turbulence can be generated at some regions near the shroud outlet. Thus, the flow pattern can be optimised by a guide vane to achieve a steady flow. In this thesis, the flow characteristics after guide vanes were studied. The guide vane used in the novel wind turbine shroud is to make this incoming flow steadier before attacking the blades. The studied geometry of guide vane was based on the work carried out by Ying (Ying, et al., 2012). In his study, the power coefficient of the novel shroud wind turbine was predicted, but the details of flow conditions through guide vane were not studied. Thus, the performances of the shroud

with guide vane were analysed by CFD simulations. Due to symmetry structure, the model was simulated under 0°, 12°, 24° and 36° directions of approaching flow. In the CFD simulations, 5 million mesh cells were built and a steady-state Reynolds Averaged Navier-Stoke method was applied. The turbulent model was set as k-omega model.

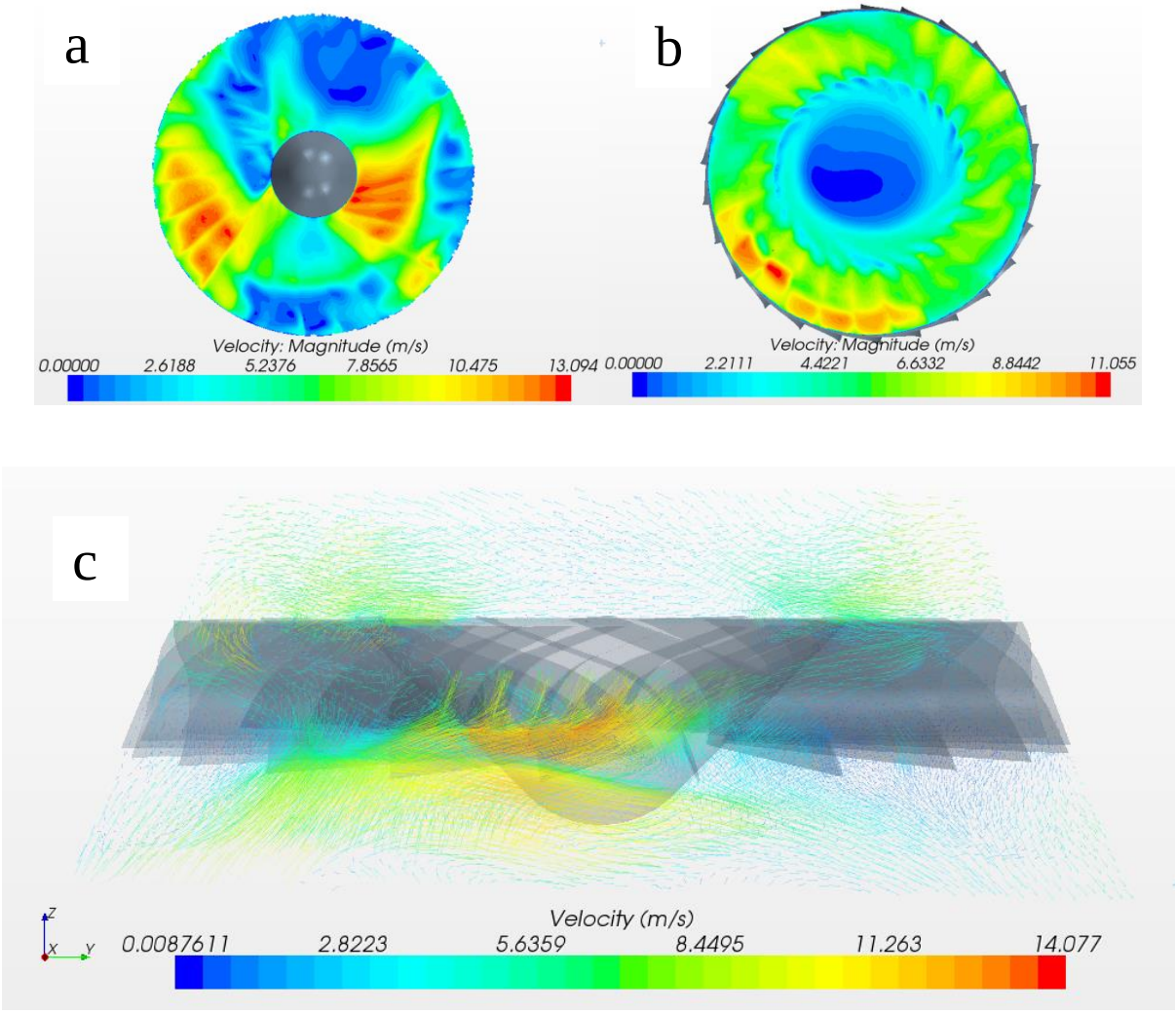


**Fig.7.2. Flow characteristics with guide vane under 0° of approaching flow**

The flow characteristics after through guide vane, which include velocities and directions, can be clearly seen from Fig.7.2. It can be seen that there are vortices at the outlet layer before flow entered the guide vane (Fig.7.2.a). The vortex was disappeared after the flow gone through the guide vane (Fig.7.2.b). The flow became steady and flow directions were controllable by the guide vane structure. The flow reached the same angle of attack as that

guide vane led (Fig.7.2.c). During the process of flow through the guide vane, it was noticed that there was energy loss, which would reduce power output of the novel wind turbine. The high velocity regions were optimised, and the locations of high velocity region were more concentrated near the blade tips than the locations of high velocity region without guide vanes. However, the maximum velocity was reduced by implementing a guide vane. This was caused by the entrance of guide vane that the angle at guide vane entrance was not optimised to meet the flow features at the shroud outlet. A model with guide vanes was analysed under various directions of approaching flow. It was found out that the flow directions after guide vane could be efficiently modified under different directions of approaching flow. The flow directions were controlled by guide vane and high velocity regions were modified near to the blade tips by guide vane.

## 7.3. Power Coefficient of the Novel Wind Turbine

A model of the novel wind turbine, which consists of a shroud with guide vanes and impulse turbine blades, was created in CATIA and simulated in computational fluid dynamic software. The impulse turbine consists of 30 blades and the number of guide vanes was 26 (Ying, et al., 2012). The final model of shroud was used for simulations. The domain was created big enough to avoid blockage effect of wall, which was 2m × 3.5m × 4m. Total 6 million of hexahedral mesh cells were used for simulation. A steady-state RANS method was applied and k-omega SST turbulence model was employed. The model was simulated in 10m/s of approaching flow. The rotational speed of the blades was set as 1000rpm. The power coefficient of the turbine blades was calculated by using equation 7.1.

$$C_p = \frac{T\omega}{0.5\rho U^3 A} = \frac{2\pi T \frac{n}{60}}{0.5\rho U^3 A} \qquad (7.1)$$

where, $T$ is the torque generated by blades, $\rho$ is the density of air, $U$ is the average velocity of flow at shroud outlet and $A$ is the area of flow goes through the shroud outlet.

The results were shown in Fig.7.3. The power coefficient of the novel wind turbine in different directions (0°, 12°, 24° and 36°) of approaching flow was determined.

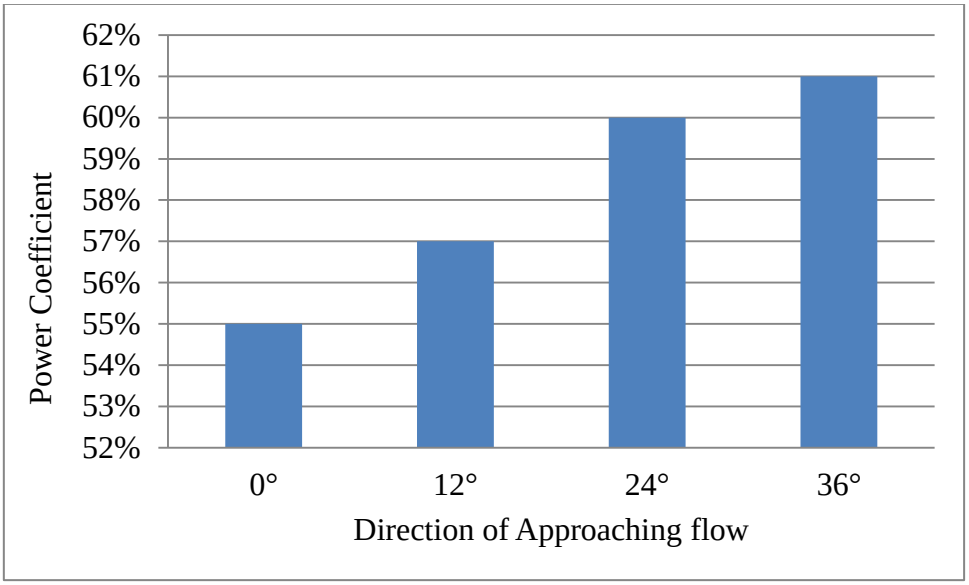


**Fig.7.3. Power coefficient of a novel wind turbine system in different directions of approaching flow**

From Fig.7.3, it can be seen that the power coefficient of the novel wind turbine is various in different directions of approaching flow. The lowest power efficient is about 55% in 0° of approaching flow and the highest power efficient is about 61% in 36° of approaching flow.

## 7.4. Summary

This chapter has conducted a brief discussion about impulse turbine. The structure features and developments of impulse wind turbine were studied. The impulse turbine was used for wave energy generation (Setoguchi, et al., 2001), which has similar working conditions to the novel shroud wind turbine. Thus, it is suggested that the impulse turbine is suitable to be implemented on the novel wind turbine due to its high power coefficient and low

manufacture cost. A guide vane structure was implemented on the shroud to improve the performance of the shroud. The flow characteristics before and through the guide vanes have been studied. The flow direction is fully controlled by the guide vanes so that it can be predicted that the guide vane can make the flow achieve an advantage of angle of attack to the blade.

# Chapter 8 – Discussion of the Novel Wind Turbine

This chapter will discuss the suitability of the novel wind turbine to be used in urban areas and address the geometry improvements of the shroud. The highlights of the novel wind turbine will be discussed.

## 8.1. Highlights of the Novel Wind Turbine

The novel wind turbine is an innovation of urban wind turbines and has been specifically designed for urban areas. The requirements of an urban wind turbine to be widespread have been studied and the drawbacks of existing urban wind turbines have been discussed. The novel wind turbine has been designed to fill the gap of utilising wind energy in urban areas. The suitability of the novel wind turbine to be used in urban areas has been investigated. The details of the novel shroud wind turbine are addressed as following,

- **Manufacture.** The manufacture cost of the novel wind turbine can be lower than conventional wind turbines. The high manufacturing cost of the conventional wind turbine is due to the complexity of turbine blades. The complexity of turbine blades is caused by uncontrollable flow conditions. In order to achieve good power output under variable flow conditions, the blades in conventional wind turbine have to be complicated. The blades of conventional wind turbines required twisted blades or yaw mechanic to achieve high power output, so that the costs of its manufacture were increased. The shroud of novel wind turbine was designed to unify various directions of approaching flow to the fixed outlet. The flow approaching blades can be simplified. It was proved that the complex flow conditions in urban areas have been modified by the shroud and the flow characteristics inside shroud were suitable to be implemented the impulse

turbine. The impulse turbine can achieve good power output with simple blade structure which may cost much less to be manufactured.

- **Urban Flows.** The flow conditions are complex due to the terrains in the urban areas. The most serious problem, which reduces the performance of an urban wind turbine, is the frequently changing flow directions. The novel shroud wind turbine has been designed to collect wind flows from any directions and guide flows to the vertical outlet. Thus, the problem of frequently changing directions of flow can be solved.
- **Maintenance.** The high maintenance cost of the conventional wind turbines is caused by the high location of wind turbine generators and gearboxes, which increases the work load difficulty for maintenance. However, the generator of this novel wind turbine will be placed inside a shroud. The novel shroud wind turbine is easy to access for maintenance. Also, the generator and other components are protected by the shroud. The maintenance loads can be reduced so that the maintenance cost will be reduced significantly.
- **Safety.** The urban wind turbines are used in a densely population area. Thus, the safety is an important issue needed to be considered. With a high rotating speed, the wind turbine blades are easy to be damaged and to hurt the people around. The blades of this novel wind turbine are protected by the shroud. The blades cannot be easily damaged. If the blade was damaged, the shroud can keep blades inside and will not cause danger to the people around. The safety of the novel shroud is high.
- **Integration.** The structure of an urban wind turbine needs to have a good integration with urban environments. This novel wind turbine has been designed as an independent system. Thus, it can be placed on the top of roof to achieve a good integration with a building.

- **Power output per unit area.** The energy generation per unit area is important for wind turbines used in the urban areas due to limited spaces in the urban areas. The concentration of wind energy is an efficient way to increase the power output per unit area. This novel wind turbine has been designed with a flow guide chamber. The wind flow can be captured and concentrated by the chamber around the shroud and can be led through the chamber. During this process, the flow acceleration is achieved due to the specific structure of a chamber. More energy can be captured by the novel wind turbine shroud and the power coefficient of the novel wind turbine is higher than that of conventional wind turbines. The wind energy concentration and high power coefficient lead a high power output per unit area of the novel wind turbine than that of conventional wind turbine.
- **Noise.** The level of noise should be low when a wind turbine is used in urban areas. The noise is mainly caused by the high tip speed of turbine blades. The noise generation of the novel wind turbine blades have not been studied in this thesis. However, it was proved that the vortices generated from the blade tips can be considerably suppressed through interference with the boundary layer within a diffuser shroud (Göçmen & Özerdem, 2012). Thus, the aerodynamic noise of novel wind turbine can be reduced substantially.

According to the structure features of the novel wind turbine, it can be seen that the novel shroud wind turbine is a remarkable design for the urban wind turbines. Based on this study, the novel shroud wind turbine has met all requirements of urban wind turbines and can achieve potential of high power output due to the concentration of wind energy. The design purposes of the novel shroud wind turbine have been achieved.

## 8.2. Developments of a Shroud

The innovation of the novel wind turbine can fill the gaps utilising wind energy in urban areas. It can satisfy the requirements of an urban wind turbine. In this thesis, a comprehensive study about nozzle structure has been carried out. The flow characteristics of original shroud, a four chamber model, were investigated. Then, many improving approaches have been used. Because wind energy is proportional to flow area and cubed with flow velocity, the improvements were carried out in two aspects, increasing the area of flow passing through and accelerating the velocity of approaching flow. Two staged improving models are five chambers model and the final model. The sketches of these two models and four chambers model are shown in Fig.8.1. The details of these models can be seen in Appendix I, Appendix K and Appendix L. The base diameter ($D_{base}$) of these three models is same, which is 1000mm. The outlet diameter ($D_{outlet}$) of these three models is 200mm. The difference between final model and the other two models is the location of blades. In four chambers model and five chambers model, the blades will be located at shroud outlet which limits the swap area of blades to $A_{outlet} = \frac{1}{8}\pi D_{outlet}^2$. In the final model, the blades will be located inside the chamber and the swap area of blades can be increased due to the diffuser structure of the chamber.

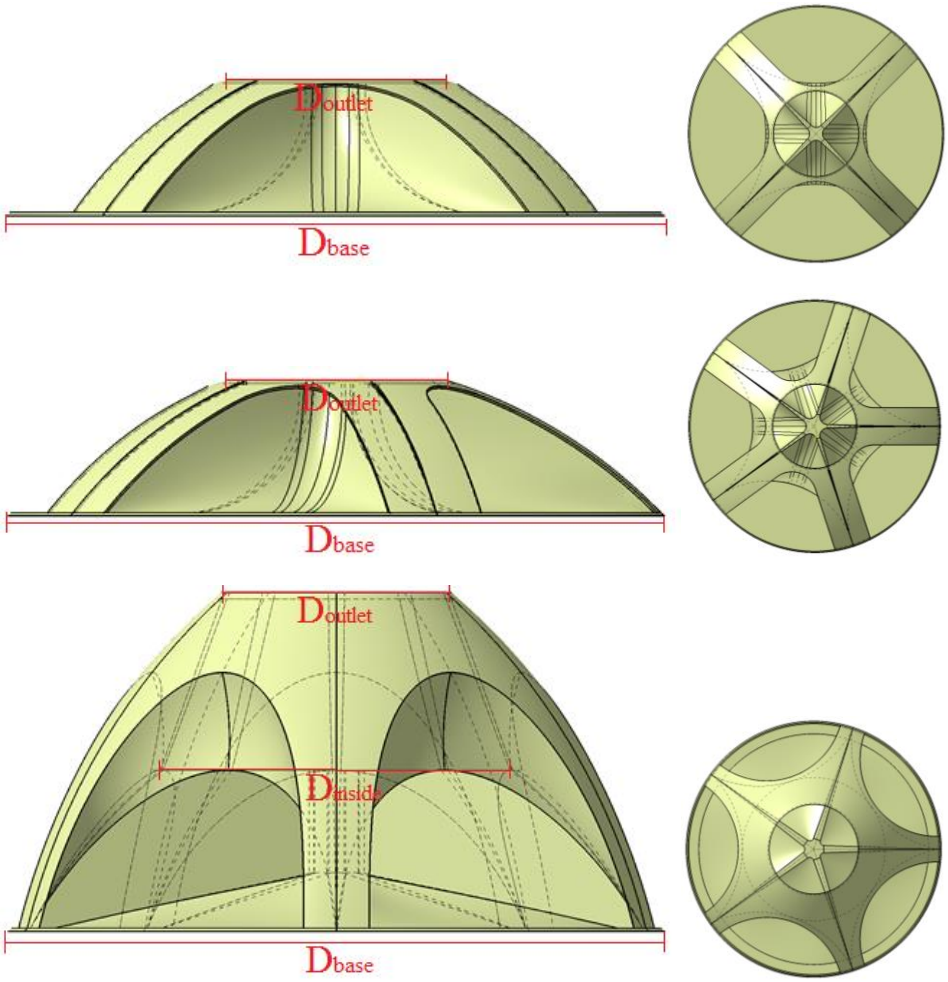


**Fig.8.1. Sketch of model in different stages**

In the first stage, the number of shroud chambers was increased from four to five. The reason is that the area of flow through the shroud outlet can be increased while the flow velocity can be kept the same. According to the simulation results, it has been found that the area that flow goes through is various under different directions of approaching flow. The various conditions of four chamber model and five chamber model are shown in Fig.8.2.

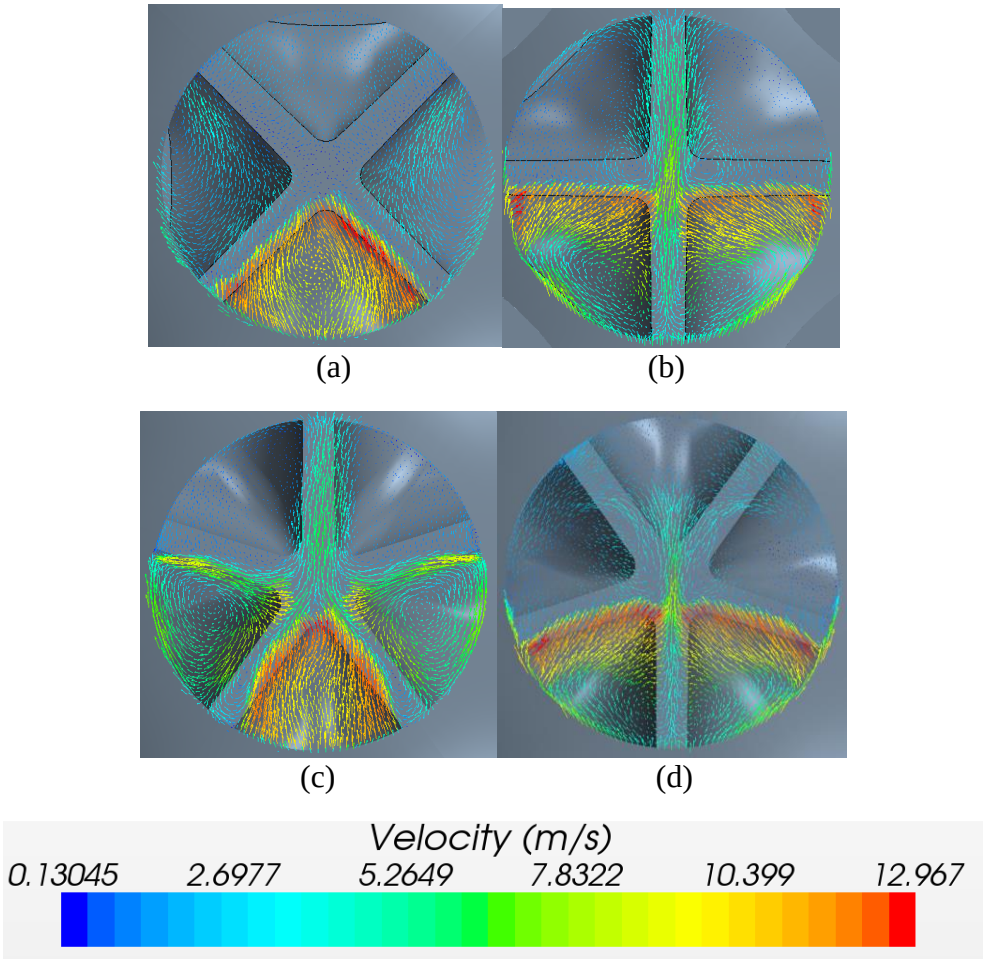


**Fig.8.2. Vector plots of flow at outlet of shroud under various directions of approaching flow (10m/s) (a). 0° of approaching flow through four chamber shroud. (b) 45° of approaching flow through four chamber shroud. (c). 0° of approaching flow through five chamber shroud. (d). 36° of approaching flow through five chamber shroud**

From Fig.8.2, it can be seen that the areas of flow through a shroud are different between four chamber model and five chamber model. Flow may go through one or two chambers of four chamber model and go through two or three chambers when flow goes through the five chambers model. Due to the same diameter of outlet, the total outlet area of the shroud is the same. As proved in Section 5.2, the flow acceleration of four chamber model and that of five chamber model are similar. Therefore, the five chamber model can apply more mass flow than four chamber model can. The total amount of wind energy will be increased due to an enlarge flow area.

In the second stage, both the flow accelerating ratios and flow area have been increased. A single chamber has been modified to a diffuser which can achieve a better flow acceleration. It has been deserved that the average and maximum velocity increasing ratios of the final model were about 1.1 and 1.55, respectively. The final model had the much better flow velocity increasing ratios than that of the original four chamber model, which are 0.95 of average velocity increasing ratio and 1.25 of maximum velocity increasing ratio. The increase of velocity acceleration is about 15.8% of average velocity increasing ratio and 24% of maximum velocity increasing ratio respectively. It should be noticed that wind energy behaves as a cube of flow velocity. Thus, a slight acceleration of flow velocity can bring a significant increase of wind energy. The flow area also has been enlarged due to an introduction of the diffuser structure. The diameter of these three models is the same, which is $D_{outlet}$. However, the blades can be placed inside the shroud of the final model, which will be located at $D_{inside}$ (as shown in Fig.8.1). According to work carried out in Section 6.3, the $D_{inside}$ is equal to 1.55 times of $D_{outlet}$ of the shroud. Thus, the flow area can be increased to 2.4 times as $A_{outlet}$. A comprehensive comparison between these three models was addressed. It was assumed that the outlet area is $A_{outlet}$ and the air density is ρ, and for the four chamber model the velocity at shroud outlet is $U_{max.}$The power output of four chamber model can be determined as P. With accelerating flow velocity and enlarging flow area, the improvements of shroud at different stage can be seen in Table 8-1.

| | Velocity at Outlet | Flow Area | Wind Energy |
|---|---|---|---|
| **Four Chamber Model** | U | $A_{outlet}$ | P |
| **Five Chamber Model** | U | $1.2A_{outlet}$ | 1.2P |
| **Final Model** | 1.24U | $2.4\times1.2A_{outlet}$ | 3.6P |

**Table 8-1. Improvements of shrouds at different stages**

According to Table 8-1, the improvement of the shroud in every stage can be seen. In the design of four chamber model, the main target was to meet the requirements of urban wind turbines. However, the velocity acceleration has been achieved as well. The five chambers model was created to improve the area of the outlet. The flow areas can increase 20% after the change, which means that the potential of wind energy generation increased 1.2 times as four chamber model can. The structure of the final model has achieved a significant improvement in accelerating flow velocity and enlarging flow area, compared with four chamber model. The shroud was designed to concentrate wind energy so that the total wind energy through the shroud outlet is essential. It can be seen that wind energy concentration of the final model has reached 3.6 times as four chamber model by increasing flow acceleration ratio and enlarging flow area.

## 8.3. Power Coefficient of Novel Wind Turbine

The impulse turbine (Ying, et al., 2012) has been implemented on the novel wind turbine. Power coefficient is an essential factor to adjust the performance of a wind turbine. Thus, several simulations have been carried out to determine the performance of the whole system. The blades were placed inside chamber and a guide vane was implemented. The model of the The model was simulated under 10m/s of approaching flow under four directions, 0°,12°,24°and 36°. The rotational speed of rotor was kept as 1000 rpm in all simulations. The power coefficient of different directions of approaching flows have been determined and compared with conventional wind turbines.

| | Actual Power Coefficient | Maximum Power Coefficient |
|---|---|---|
| The novel shroud wind turbine | 55%~61% | |
| HAWTs | 40%~50% | 59% |
| VAWTs | 20%~30% | 70% |

**Table 8-2. Comparison of power efficiency between the novel wind turbine and conventional wind turbine**

From Table 8-2, it can be seen that the novel shroud wind turbine has achieved better power coefficient than HAWTs and VAWTs. The power coefficient of the novel shroud wind turbine has reached 55%~61% in various directions of approaching flow. The power coefficients of the novel shroud wind turbine have already exceeded this type of the conventional wind turbines. It should be noticed that optimisation work of flow acceleration of the shroud can be further carried out. The novel wind turbine has a great potential to be used in urban areas.

## 8.4. Summary

This chapter addressed the design and optimisation work carried out in this study. The development of the novel shroud wind turbine was detailed. A discussion was carried out to prove the innovation of the novel shroud wind turbine. The novel shroud wind turbine was designed to meet the requirements of urban wind turbine working in urban areas, and it was proved that the design purpose has achieved. The shroud of the novel wind turbine is an essential part of the whole system. Thus, the structural optimisation of the shroud was the main focus, and the performance of wind energy concentration of final model was significantly increased. The final model has achieved 2.6 times more increase of power generation than the original four chamber model. The power coefficient of the whole wind

turbine system was predicted. The power coefficient of blades with the final shroud model achieved 55%~61%, which is higher than power coefficient of the conventional wind turbines. Also, some improvements can be carried out, such as guide vane optimisation. The design of the novel shroud wind turbine is a success.

# Chapter 9 – Conclusions and Future Work

## 9.1. Findings and Contributions

This research has focused on the innovation of an urban wind turbine and analysed the aerodynamic performance of the novel wind turbine. In this research, a novel wind turbine has been specifically designed for urban areas and the performance of the novel wind turbine has been analysed using CFD simulation and wind tunnel test. The findings of this thesis can be drawn as follows:

- A novel urban wind turbine has been designed to fill the gap of widely application of wind turbine in urban areas. Implementing of urban wind turbines is an efficient way to reduce $CO_2$ emission level and solve energy shortage. The power output of the conventional urban wind turbines is limited by urban flow characteristics which include low speed and frequently changing direction of flow. Several requirements should be satisfied for an urban wind turbine, which include manufacturing, maintenance, noise, safety, integration and power output. In this thesis, a novel wind turbine has been designed to satisfy all the requirements of an urban wind turbine. The novel wind turbine consists of two parts, shroud and blades. The shroud is used to accelerate flow velocity and unify the flow direction, which is critical to the novel wind turbine. The shroud was examined in CFD simulation and wind tunnel test. The suitability of installing the novel wind turbine in urban areas has been proved. Some of the results have been published as shown in Appendix A.

-

- The geometry of shroud was optimised and the wind energy concentration of the shroud has been improved. The shroud is a critical part of the novel wind turbine. It is not only designed to achieve integration with urban environments and better safety, but it is also used for concentrating wind energy. The wind energy is proportional to the flow area and cube of the flow velocity. Thus, increasing flow area or accelerating flow can improve the concentration of wind energy. In this thesis, different geometries of the shroud were created and investigated in CFD simulations. The flow area has been increased and flow acceleration factor has been improved. The energy concentration of the shroud has been significantly improved.

- The dimensions of an improved shroud, the final model, have been identified. The effects of major parameters of the shroud on flow acceleration have been studied. In this thesis, the shroud was divided into three regions, flow capture region, flow alteration region and flow acceleration region. The investigation of effects of parameters on flow acceleration was carried out individually by each parameter. The heights of shroud, ratios of nozzle and widths of broad have significant effects on flow acceleration. The results reflected the potential and directions to improve the shroud in future development.

- The turbine blades of the novel wind turbine were recommended and a guide vane can be implemented on shroud to control the attacking directions of flow. The turbine blades are essential to the power output of a wind turbine system, and the efficiency of blades is significantly affected by the direction of attacking flow. In this thesis, impulse turbine is recommended as a good option to achieve high power output of the novel wind turbine and a guide vane can be implemented to fully control the

directions of attacking flow. A guide vane is implemented on final model of shroud, and the flow direction was controlled by guide vane. The results are instructive for further development of the novel wind turbine.

## 9.2. Future Work

Further research can be focused on determining power output of the novel wind turbine and testing the novel wind turbine in real wind flow.

- The shroud of the novel wind turbine can be tested in real wind condition. In wind tunnel tests, the various directions of approaching flow were achieved by rotating model. In reality, the flow velocity and direction may change rapidly. Thus, the novel wind turbine needs to be tested in real wind condition in future.

- The further optimisation works of shroud can be carried out. Within the limited time, only the major parameters that can improve the performance of flow acceleration by the shroud were optimised. Several parameters that caused little differences between the performances of flow acceleration were noticed. It was recommended that the differences may be caused by the errors in CFD simulations due to limitation of time and computer capability. In future, finer mesh can be used to improve the accuracy of simulation results to determine the further improvements that can be achieved by optimising parameters of the shroud.

- The power outputs of the novel wind turbine need to be determined. In this research, the developments of the novel wind turbine were focused on the shroud. Even if the blades of the novel wind turbine were studied, the power outputs of the novel wind turbine were not determined. In future, the works to determine power output of the

novel wind turbine can be carried out by using geometries of shroud and impulse turbines.

# References

**Abe, K., Nishida, M., Sakurai, A., Ohya, Y., Kihara, H., Wada, E., & Sato, K.** (2005). Experimental and numerical investigations of flow fields behind a small wind turbine with a flanged diffuser. *Journal of wind engineering and industrial aerodynamics, 93*(12), 951-970.

**Abe, K., & Ohya, Y. (2004).** An investigation of flow fields around flanged diffusers using CFD. *Journal of wind engineering and industrial aerodynamics, 92*(3), 315-330.

**Akwa, J. V., Vielmo, H. A., & Petry, A. P. (2012).** A review on the performance of Savonius wind turbines. *Renewable and Sustainable Energy Reviews, 16*(5), 3054-3064.

**Alexander, A. (1978).** Wind tunnel corrections for Savonius rotors. *NASA STI/Recon Technical Report A, 79*, 40127.

**Anderson, D., Whale, J., Livingston, P., & Chan, D. (2008).** Rooftop Wind Resource Assessment using a Three-Dimensional Ultrasonic Anemometer.

**Avva, R. K., Smith, C. E., & Singhal, A. K. (1990).** *Comparative study of high and low Reynolds number versions of k-epsilon models.* Paper presented at the AIAA, Aerospace Sciences Meeting.

**Baik, J. J., Park, R. S., Chun, H. Y., & Kim, J. J. (2000).** A laboratory model of urban street-canyon flows. *Journal of applied meteorology, 39*(9), 1592-1600.

**Barlow, J. B., Rae, W. H., & Pope, A. (1999).** Low-speed wind tunnel testing.

**Bertin, J. J., & Smith, M. L. (1989).** *Aerodynamics for engineers* (Vol. 1): Prentice Hall Englewood Cliffs.

**Betz, A. (1926).** Windenergie und ihre Ausnutzung durch WindmühlenVandenhoeck und Ruprecht. *Göttingen, Germany*.

**Blackmore, P. (2010).** Building-mounted micro-wind turbines on high-rise and commercial buildings: Watford: BRE.

**Blazek, J. (2001).** *Computational fluid dynamics: principles and applications*: Elsevier Science.

**Bradshaw, P., & Pankhurst, R. (1964).** The design of low-speed wind tunnels. *Progress in Aerospace Sciences, 5*, 1-69.

**Britain, G. (2005).** *Wind Power in the UK: A Guide to the key issues surrounding onshore wind power development in the UK*: The Commission.

**Burton, T., Sharpe, D., Jenkins, N., & Bossanyi, E. (2002).** Wind‐Turbine Performance. *Wind Energy Handbook*, 173-207.

**Campbell, D., Stankovic, S., Graham, M., Parkin, P., van Duijvendijk, M., de Gruiter, T., . . . Blanch, M. (2001).** Wind Energy For The Built Environment (Project Web)". *Imperial College, Mecal Applied Mechanice and the University of Stuttgart. London*.

**Carle, A., & Fagan, M. (1996).** Improving derivative performance for CFD by using simplified recurrences. *Berz et al*, 343-352.

**Carlin, P. W., Laxson, A. S., & Muljadi, E. (2001).** *The history and state of the art of variable-speed wind turbine technology*: National Renewable Energy Laboratory.

**Chappell, M., & Enterprises, M.** Wind Energy Basics.

**Cignoni, P., Montani, C., & Scopigno, R. (1998).** A comparison of mesh simplification algorithms. *Computers & Graphics, 22*(1), 37-54.

**Dannecker, R. K. W., & Grant, A. D. (2002).** Investigations of a building‐integrated ducted wind turbine module. *Wind Energy, 5*(1), 53-71.

**Dayan, E. (2006).** Wind energy in buildings: Power generation from wind in the urban environment-where it is needed most. *Refocus, 7*(2), 33-38.

**de Carmoy, G. (1978).** The USA faces the energy challenge. *Energy policy, 6*(1), 36-52.

**Eggleston, D. M., & Stoddard, F. (1987).** Wind turbine engineering design.

**Eriksson, S., Bernhoff, H., & Leijon, M. (2008).** Evaluation of different turbine concepts for wind power. *Renewable and Sustainable Energy Reviews, 12*(5), 1419-1434.

**Flavin, C. (2008).** Building a low-carbon economy. *State of the World*, 75-90.

**Fleming, P., & Probert, S. (1984).** The evolution of wind-turbines: An historical review. *Applied energy, 18*(3), 163-177.

**Fujisawa, N. (1992).** On the torque mechanism of Savonius rotors. *Journal of wind engineering and industrial aerodynamics, 40*(3), 277-292.

**Gasch, R., & Twele, J. (2007).** Windkraftanlagen Grundlagen. *Entwurf, Planung und Betrieb, Teubner, Wiesbaden*.

**Ghosh, T. K., & Prelas, M. A. (2011).** Wind Energy. *Energy Resources and Systems*, 1-77.

**Gilbert, B., Oman, R., & Foreman, K. (1978).** Fluid dynamics of diffuser-augmented wind turbines. *J. Energy;(United States), 2*(6).

**Glauert, H. (1935).** Airplane propellers. *Aerodynamic theory, 4*, 169-360.

**Göçmen, T., & Özerdem, B. (2012).** Airfoil optimization for noise emission problem and aerodynamic performance criterion on small scale wind turbines. *Energy*.

**Gorelov, D., & Krivospitsky, V. (2008).** Prospects for development of wind turbines with orthogonal rotor. *Thermophysics and Aeromechanics, 15*(1), 153-157.

**Grant, A. (1994).** Development of a ducted wind energy converter. *Wind Engineering, 18*(6), 297-304.

*Urban wind energy conversion: The potential of ducted turbines,* 1157-1163 (2008).

**Grimmond, C., & Oke, T. R. (1999).** Aerodynamic properties of urban areas derived from analysis of surface form. *Journal of Applied Meteorology, 38*(9), 1262-1292.

**Guide, U. (2009).** Star-CCM+ version 4.04. 011: CD-ADAPCO.

**Gunnell, D., Platt, S., & Hawton, K. (2009).** The economic crisis and suicide. *BMJ, 338*.

**Hau, E. (2010).** Wind Turbines: Fundamentals, Technologies, Application, Economics Author: Erich Hau, Horst Von Renouard, Publisher: Spring.

**Hau, E., & Platz, H. (2008).** Wind Turbines-Fundamentals, Technologies, Application, Economics.

**Howell, R., Qin, N., Edwards, J., & Durrani, N. (2010).** Wind tunnel and numerical study of a small vertical axis wind turbine. *Renewable Energy, 35*(2), 412-422.

**Igra, O. (1981).** Research and development for shrouded wind turbines. *Energy Conversion and Management, 21*(1), 13-48.

**Islam Abohela, N. H., Steven Dudek. (2013).** Effect of roof shape, wind direction, building height and urban configuration on the energy yield and positioning of roof mounted wind turbines. *Renewable Energy, 50*, 1106-1118.

**Islam, M., Mekhilef, S., & Saidur, R. (2013).** Progress and recent trends of wind energy technology. *Renewable and Sustainable Energy Reviews, 21*, 456-468.

**Islam, M., Ting, D. S. K., & Fartaj, A. (2008).** Aerodynamic models for Darrieus-type straight-bladed vertical axis wind turbines. *Renewable and Sustainable Energy Reviews, 12*(4), 1087-1109.

**Johnson, A. A., & Tezduyar, T. E. (1999).** Advanced mesh generation and update methods for 3D flow simulations. *Computational Mechanics, 23*(2), 130-143.

J**oselin Herbert, G., Iniyan, S., Sreevalsan, E., & Rajapandian, S. (2007).** A review of wind energy technologies. *Renewable and Sustainable Energy Reviews, 11*(6), 1117-1145.

**Kaneko, K., Setoguchi, T., & Raghunathan, S. (1992).** Self-rectifying turbines for wave energy conversion. *International Journal of Offshore and Polar Engineering, 2*(3).

**Kato, S., Murakami, S., Takahashi, T., & Gyobu, T. (1997).** Chained analysis of wind tunnel test and CFD on cross ventilation of large-scale market building. *Journal of wind engineering and industrial aerodynamics, 67*, 573-587.

**Kirke, B. K. (1998).** *Evaluation of self-starting vertical axis wind turbines for stand-alone applications.*

**Kissel, J. M., & Krauter, S. C. W. (2006).** Adaptations of renewable energy policies to unstable macroeconomic situations—Case study: Wind power in Brazil. *Energy policy, 34*(18), 3591-3598.

**Klopfenstein Jr, R. (1998).** Air velocity and flow measurement using a Pitot tube. *ISA transactions, 37*(4), 257-263.

**Kumar, S., Gupta, R., & Banerjee, S. (1998).** An experimental investigation of the characteristics of free-surface turbulence in channel flow. *Physics of fluids, 10*, 437.

**Kyozuka, Y. (2008).** An experimental study on the Darrieus-Savonius turbine for the tidal current power generation. *Journal of Fluid Science and Technology, 3*(3), 439-449.

**Lanzafame, R., & Messina, M. (2007).** Fluid dynamics wind turbine design: Critical analysis, optimization and application of BEM theory. *Renewable Energy, 32*(14), 2291-2305.

**Ledo, L., Kosasih, P., & Cooper, P. (2011).** Roof mounting site analysis for micro-wind turbines. *Renewable Energy, 36*(5), 1379-1391.

**Lee, B. (1975).** The effect of turbulence on the surface pressure field of a square prism. *J. Fluid Mech, 69*(2), 263-282.

**Makkawi, A., Celik, A., & Muneer, T. (2009).** Evaluation of micro-wind turbine aerodynamics, wind speed sampling interval and its spatial variation. *Building Services Engineering Research and Technology, 30*(1), 7-14.

**Maskell, E. (1963).** A theory of the blockage effects on bluff bodies and stalled wings in a closed wind tunnel: DTIC Document.

**Matsushima, T., Takagi, S., & Muroyama, S. (2006).** Characteristics of a highly efficient propeller type small wind turbine with a diffuser. *Renewable Energy, 31*(9), 1343-1354.

**Menet, J. L. (2004).** A double-step Savonius rotor for local production of electricity: a design study. *Renewable Energy, 29*(11), 1843-1862.

**Mertens, S. (2002).** Wind energy in urban areas: Concentrator effects for wind turbines close to buildings. *Refocus, 3*(2), 22-24.

**Miley, S. J., & Texas, A. (1982).** *A catalog of low Reynolds number airfoil data for wind turbine applications*: NTIS.

**Miller, R. (1988).** Islamic technology: an illustrated history. *Medical History, 32*(4), 466.

**Miller, R. W. (1983).** Flow measurement engineering handbook.

**Mittal, R., Sandhu, K., & Jain, D. (2010).** An Overview of Some Important Issues Related to Wind Energy Conversion System (WECS). *International Journal of Environmental Science and Development, 1*(4), 351-362.

**Mohammadi, B., & Pironneau, O. (1993).** *Analysis of the k-epsilon turbulence model*: Wiley.

**Moriarty, P. J., & Hansen, A. C. (2005).** *AeroDyn theory manual*: National Renewable Energy Laboratory Colorado.

**Müller, G., Jentsch, M. F., & Stoddart, E. (2009).** Vertical axis resistance type wind turbines for use in buildings. *Renewable Energy, 34*(5), 1407-1412.

**Murakami, S., & Mochida, A. (1988).** 3-D numerical simulation of airflow around a cubic model by means of the k-ϵ model. *Journal of wind engineering and industrial aerodynamics, 31*(2), 283-303.

**Ohya, Y., Karasudani, T., Sakurai, A., Abe, K., & Inoue, M. (2008).** Development of a shrouded wind turbine with a flanged diffuser. *Journal of wind engineering and industrial aerodynamics, 96*(5), 524-539.

**Paraschivoiu, I. (2002).** *Wind turbine design: with emphasis on Darrieus concept*: Montreal: Polytechnic International Press.

**Parsons, D. R., Wiggs, G. F., Walker, I. J., Ferguson, R. I., & Garvey, B. G. (2004).** Numerical modelling of airflow over an idealised transverse dune. *Environmental Modelling & Software, 19*(2), 153-162.

**Patel, M. R. (2005).** *Wind and solar power systems: design, analysis, and operation*: CRC.

**Phillips, R., & Trust, B. (2007).** *Micro-wind turbines in urban environments: an assessment*: IHS BRE Press.

**Pope, A. (1954).** *Wind-tunnel testing*: Wiley.

**Pope, K., Rodrigues, V., Doyle, R., Tsopelas, A., Gravelsins, R., Naterer, G., & Tsang, E. (2010).** Effects of stator vanes on power coefficients of a zephyr vertical axis wind turbine. *Renewable Energy, 35*(5), 1043-1051.

**Prandti, L. (1925).** Magnuseffekt und Windkraftschiff. *Naturwissenschaften, 13*(6), 93-108.

**Ruppert, J. (1995).** A Delaunay refinement algorithm for quality 2-dimensional mesh generation. *J. Algorithms, 18*(3), 548-585.

**Setoguchi, T., Kaneko, K., Maeda, H., Kim, T., & Inoue, M. (1993).** Impulse turbine with self-pitch-controlled guide vanes for wave power conversion: performance of mono-vane type. *International Journal of Offshore and Polar Engineering, 3*(1).

**Setoguchi, T., Kaneko, K., Taniyama, H., Maeda, H., & Inoue, M. (1996).** Impulse Thrbine With Self-Pitch-Controlled Guide Vanes For Wave Power Conversion: Guide Vanes Connected By Links. *International Journal of Offshore and Polar Engineering, 6*(1).

**Setoguchi, T., Santhakumar, S., Maeda, H., Takao, M., & Kaneko, K. (2001).** A review of impulse turbines for wave energy conversion. *Renewable Energy, 23*(2), 261-292.

**Sharpe, T., & Proven, G. (2010).** Crossflex: Concept and early development of a true building integrated wind turbine. *Energy and Buildings, 42*(12), 2365-2375.

**Spera, D. A. (1994).** *Wind turbine technology: fundamental concepts of wind turbine engineering* (Vol. 3): ASME press New York.

**Stern, F., Wilson, R., & Shao, J. (2006).** Quantitative V&V of CFD simulations and certification of CFD codes. *International journal for numerical methods in fluids, 50*(11), 1335-1355.

**SURESHAN, V. (2008).** OMNI-DIRECTIONAL WIND POWER STATION: WO Patent WO/2008/017,106.

**Syngellakis, K., Carroll, S., & Robinson, P. (2006).** Small wind power: Introduction to urban small scale wind in the UK. *Refocus, 7*(2), 40-45.

**Tangler, J. L. (2000).** *The evolution of rotor and blade design*: National Renewable Energy Laboratory.

**Thakker, A., Sheahan, C., Frawley, P., & Khaleeq, H. (2002).** Innovative manufacture of impulse turbine blades for wave energy power conversion. *Proceedings of the Institution of Mechanical Engineers, Part B: Journal of Engineering Manufacture, 216*(7), 1053-1059.

**Thomas, R. L., & Robbins, W. H. (1980).** Large wind-turbine projects in the United States wind energy program. *Journal of wind engineering and industrial aerodynamics, 5*(3), 323-335.

**Van Bussel, G., & Mertens, S. (2005).** *Small wind turbines for the built environment*.

**Van Doormaal, J., & Raithby, G. (1984).** Enhancements of the SIMPLE method for predicting incompressible fluid flows. *Numerical heat transfer, 7*(2), 147-163.

**Versteeg, H. K., & Malalasekera, W. (2007).** *An introduction to computational fluid dynamics: the finite volume method*: Prentice Hall.

**Vries, O. (1979).** Fluid dynamic aspects of wind energy conversion: DTIC Document.

**Vries, O. (1983).** On the theory of the horizontal-axis wind turbine. *Annual review of fluid mechanics, 15*(1), 77-96.

**Walker, S. L. (2011).** Building mounted wind turbines and their suitability for the urban scale—A review of methods of estimating urban wind resource. *Energy and Buildings, 43*(8), 1852-1862.

**Webster, G. W. (1979).** Devices for utilizing the power of the wind: Google Patents.

**Wilcox, D. C. (1998).** *Turbulence Modelin for CFD*: DCW Industries, Inc.

**Williams, M. C., Strakey, J. P., & Surdoval, W. A. (2005).** The US department of energy, office of fossil energy stationary fuel cell program. *Journal of power sources, 143*(1), 191-196.

**Wilson, R. E., & Lissaman, P. B. S. (1974).** Applied aerodynamics of wind power machines: Oregon State Univ., Corvallis (USA).

**Wilson, R. E., Lissaman, P. B. S., & Walker, S. N. (1976).** Aerodynamic performance of wind turbines: Oregon State Univ., Corvallis (USA).

**Wood, D. (2004).** Dual purpose design of small wind turbine blades. *Wind Engineering, 28*(5), 511-527.

**Wright, A., & Wood, D. (2004).** The starting and low wind speed behaviour of a small horizontal axis wind turbine. *Journal of wind engineering and industrial aerodynamics, 92*(14), 1265-1279.

**Ying, P., Chen, Y., & Xu, Y. (2012).** *Computational modelling of blades for a novel wind turbine system.* Paper presented at the Modelling, Identification & Control (ICMIC), 2012 Proceedings of International Conference on.

# Appendix A – List of Publications

1. **X. Zhang, Y. Chen, et al. (2012).** *A study of a novel wind turbine structure for urban skyscrapers using CFD simulation. Modelling*, Identification & Control (ICMIC), 2012 Proceedings of International Conference on, IEEE.
2. **X. Zhang, Y. Chen and R. Calay (2013).** Modelling and analysis of a novel wind turbine structure. *International Journal of Modelling, Identification and Control.*Vol.19, No.2, p.142.
3. **X.Zhang, Y. Chen, V.Voloshin and R.Calay.** Urban wind energy conversion : The potential of novel shrouded wind turbine. *Journal of Wind Engineering and Industrial Aerodynamics*. Submitted

# Appendix B – Coordinates of Points for Four Chambers Model

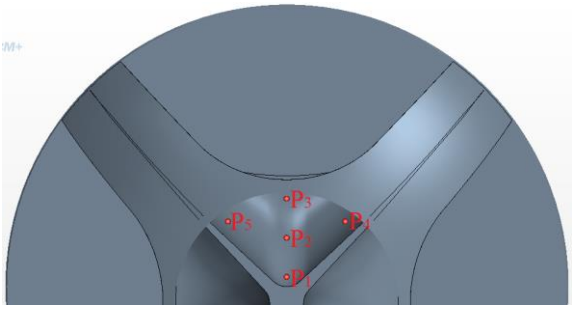


0° of approaching flow

| | x | y | z |
|---|---|---|---|
| $P_1$ | 0 | 0.04 | 0.195 |
| $P_2$ | 0 | 0.1 | 0.195 |
| $P_3$ | 0 | 0.16 | 0.195 |
| $P_4$ | 0.09 | 0.125 | 0.195 |
| $P_5$ | -0.09 | 0.125 | 0.195 |

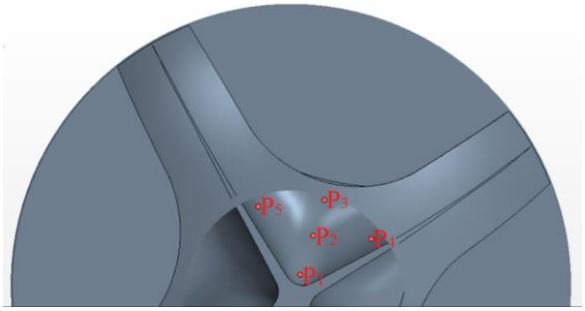


15° of approaching flow

| | x | y | z |
|---|---|---|---|
| $P_1$ | 0.01 | 0.04 | 0.195 |
| $P_2$ | 0.03 | 0.1 | 0.195 |
| $P_3$ | 0.0475 | 0.155 | 0.195 |
| $P_4$ | 0.12 | 0.095 | 0.195 |
| $P_5$ | -0.055 | 0.145 | 0.195 |

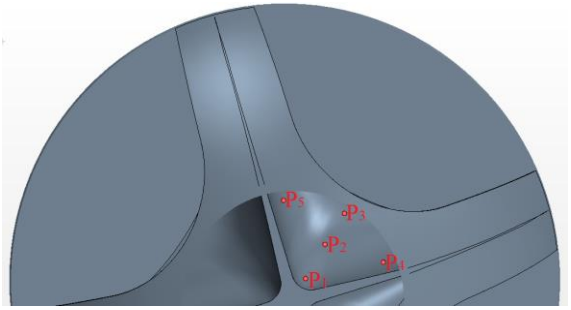


30° of approaching flow

| | x | y | z |
|---|---|---|---|
| $P_1$ | 0.02 | 0.035 | 0.195 |
| $P_2$ | 0.05 | 0.0875 | 0.195 |
| $P_3$ | 0.08 | 0.135 | 0.195 |
| $P_4$ | 0.14 | 0.06 | 0.195 |
| $P_5$ | -0.014 | 0.155 | 0.195 |

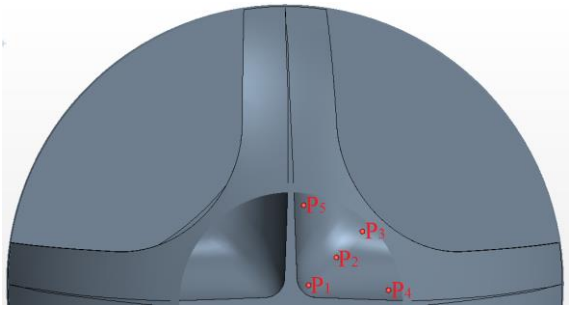


45° of approaching flow

| | x | y | z |
|---|---|---|---|
| $P_1$ | 0.0275 | 0.0275 | 0.195 |
| $P_2$ | 0.7 | 0.7 | 0.195 |
| $P_3$ | 0.11 | 0.11 | 0.195 |
| $P_4$ | 0.15 | 0.02 | 0.195 |
| $P_5$ | 0.02 | 0.15 | 0.195 |

# Appendix C – Coordinates of Points for Three Curves inside Chamber

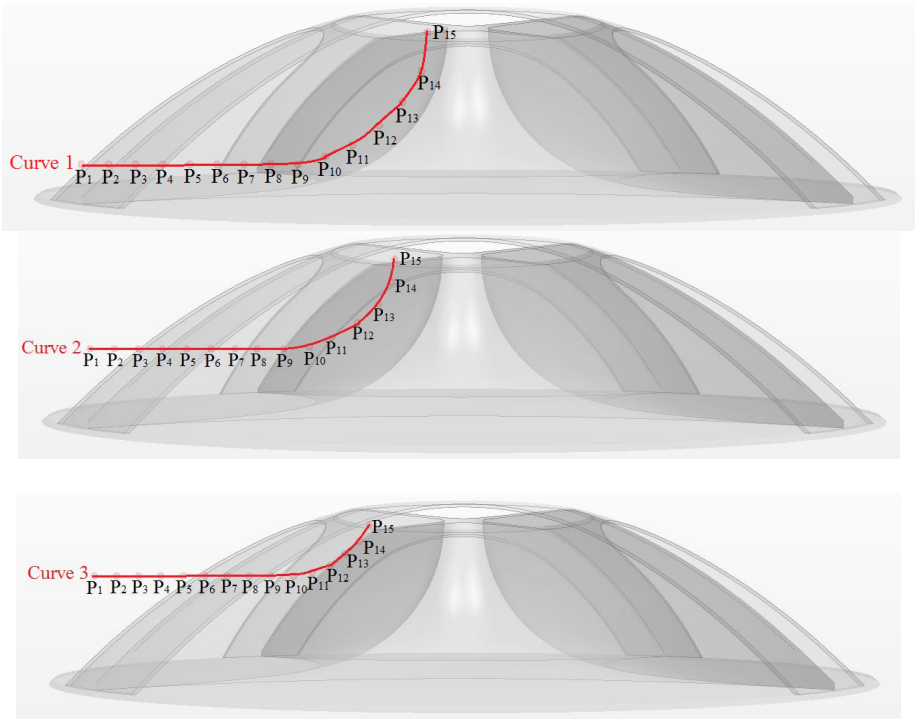


Fig.1. Locations of points on three curves

| | Curve 1 | Curve 2 | Curve 3 |
|---|---|---|---|
| Point 1 | (0.5,0,0.025) | (0.5,0,0.075) | (0.5,0,0.125) |
| Point 2 | (0.465,0,0.025) | (0.4675,0,0.075) | (0.47,0,0.125) |
| Point 3 | (0.43,0,0.025) | (0.435,0,0.075) | (0.44,0,0.125) |
| Point 4 | (0.395,0,0.025) | (0.4025,0,0.075) | (0.41,0,0.125) |
| Point 5 | (0.36,0,0.025) | (0.37,0,0.075) | (0.38,0,0.125) |
| Point 6 | (0.325,0,0.025) | (0.3375,0,0.075) | (0.35,0,0.125) |
| Point 7 | (0.29,0,0.025) | (0.305,0,0.075) | (0.32,0,0.125) |
| Point 8 | (0.255,0,0.025) | (0.275,0,0.075) | (0.29,0,0.125) |
| Point 9 | (0.22,0,0.025) | (0.24,0,0.075) | (0.26,0,0.125) |
| Point 10 | (0.185,0,0.035) | (0.205,0,0.078) | (0.23,0,0.125) |
| Point 11 | (0.15,0,0.05) | (0.175,0,0.09) | (0.205,0,0.13) |
| Point 12 | (0.115,0,0.075) | (0.14,0,0.11) | (0.18,0,0.14) |
| Point 13 | (0.085,0,0.105) | (0.112,0,0.135) | (0.16,0,0.155) |
| Point 14 | (0.06,0,0.145) | (0.095,0,0.165) | (0.141,0,0.1725) |
| Point 15 | (0.0525,0,0.195) | (0.09,0,0.195) | (0.1275,0,0.195) |

Table 1. Coordinates of points on three curves

# Appendix D – Coordinates of Points for Comparing CFD Results

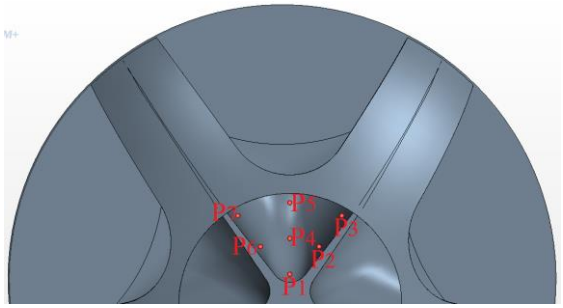


0° of approaching flow

| | x | y | z |
|---|---|---|---|
| $P_1$ | 0 | -0.045 | 0.195 |
| $P_2$ | -0.045 | -0.0875 | 0.195 |
| $P_3$ | -0.08 | -0.135 | 0.195 |
| $P_4$ | 0 | -0.1 | 0.195 |
| $P_5$ | 0 | -0.155 | 0.195 |
| $P_6$ | 0.045 | -0.875 | 0.195 |
| $P_7$ | 0.08 | -0.135 | 0.195 |

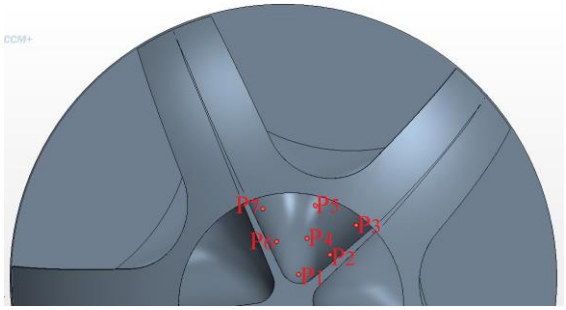


12° of approaching flow

| | x | y | z |
|---|---|---|---|
| $P_1$ | -0.0085 | -0.0475 | 0.195 |
| $P_2$ | -0.057 | -0.07 | 0.195 |
| $P_3$ | -0.1 | -0.1125 | 0.195 |
| $P_4$ | -0.0225 | -0.1 | 0.195 |
| $P_5$ | -0.036 | -0.15 | 0.195 |
| $P_6$ | 0.0225 | -0.09 | 0.195 |
| $P_7$ | 0.045 | -0.145 | 0.195 |

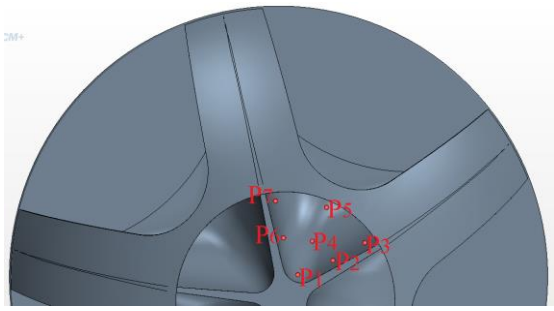


24° of approaching flow

| | x | y | z |
|---|---|---|---|
| $P_1$ | -0.02 | -0.04 | 0.195 |
| $P_2$ | -0.075 | -0.0625 | 0.195 |
| $P_3$ | -0.125 | -0.09 | 0.195 |
| $P_4$ | -0.0425 | -0.0925 | 0.195 |
| $P_5$ | -0.065 | -0.145 | 0.195 |
| $P_6$ | 0.0025 | -0.0975 | 0.195 |
| $P_7$ | 0.015 | -0.155 | 0.195 |

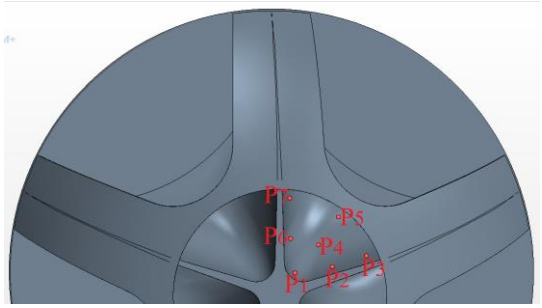


36° of approaching flow

| | x | y | z |
|---|---|---|---|
| $P_1$ | -0.025 | -0.035 | 0.195 |
| $P_2$ | -0.085 | -0.045 | 0.195 |
| $P_3$ | -0.14 | -0.0625 | 0.195 |
| $P_4$ | -0.0625 | -0.08 | 0.195 |
| $P_5$ | -0.095 | -0.125 | 0.195 |
| $P_6$ | -0.018 | -0.09 | 0.195 |
| $P_7$ | -0.0165 | -0.155 | 0.195 |

# Appendix E – Wind Tunnel Data for Four Chamber Model

| Flow Velocity(m/s) / Flow Direction | | 2 | 3 | 4 | 5 | 6 | 7 | 8 | 9 | 10 |
|---|---|---|---|---|---|---|---|---|---|---|
| 0° | Point 1 | 2.22 | 3.46 | 4.76 | 5.94 | 7.24 | 8.42 | 9.9 | 11 | 12.14 |
| | Point 2 | 2.02 | 3.2 | 4.38 | 5.5 | 6.48 | 7.56 | 8.86 | 9.82 | 10.92 |
| | Point 3 | 2.1 | 3.3 | 4.56 | 5.72 | 7.1 | 8.64 | 9.64 | 10.84 | 12.24 |
| | Point 4 | 2.22 | 3.54 | 4.84 | 5.98 | 7.02 | 8.2 | 9.72 | 10.96 | 12.06 |
| | Point 5 | 2.2 | 3.54 | 4.88 | 5.92 | 7.1 | 8.18 | 9.62 | 11 | 12.08 |
| 15° | Point 1 | 2.28 | 3.42 | 4.68 | 5.96 | 6.96 | 8.06 | 9.12 | 10.24 | 11.34 |
| | Point 2 | 1.74 | 2.62 | 3.5 | 4.34 | 5.3 | 6.56 | 7.42 | 8.6 | 9.86 |
| | Point 3 | 2.2 | 3.34 | 4.5 | 5.8 | 7.14 | 8.38 | 9.64 | 10.76 | 12.38 |
| | Point 4 | 2.06 | 3.1 | 4.16 | 5.42 | 6.48 | 7.52 | 8.7 | 9.74 | 10.9 |
| | Point 5 | 1.92 | 2.92 | 4.06 | 5.18 | 6.18 | 7.1 | 8.18 | 9.2 | 10.06 |
| 30° | Point 1 | 2.18 | 3.28 | 4.3 | 5.48 | 6.4 | 7.34 | 8.36 | 9.28 | 9.78 |
| | Point 2 | 1.92 | 2.94 | 4.04 | 5.02 | 6.04 | 7.02 | 7.9 | 9.06 | 9.98 |
| | Point 3 | 2.22 | 3.54 | 4.82 | 6.1 | 7.22 | 8.6 | 9.74 | 11.14 | 12.44 |
| | Point 4 | 1.92 | 2.98 | 3.96 | 5.28 | 6.18 | 7.06 | 8.2 | 9.32 | 10.16 |
| | Point 5 | 1.42 | 1.98 | 2.42 | 3.38 | 4.02 | 4.52 | 5.42 | 5.78 | 6.4 |
| 45° | Point 1 | 1.76 | 2.68 | 3.62 | 4.5 | 5.24 | 6.18 | 6.68 | 7.48 | 8.4 |
| | Point 2 | 1.98 | 3.1 | 4.12 | 5.3 | 5.38 | 7.36 | 8.28 | 9.54 | 10.62 |
| | Point 3 | 2.38 | 3.68 | 5.02 | 6.32 | 7.68 | 8.92 | 10.3 | 11.34 | 12.94 |
| | Point 4 | 1.72 | 2.54 | 3.42 | 4.4 | 5.2 | 6.04 | 7.04 | 7.84 | 9.04 |
| | Point 5 | 1.48 | 2.02 | 2.78 | 3.14 | 3.94 | 4.54 | 5.26 | 5.98 | |

Table 2. Wind tunnel data for four chamber model

# Appendix F – Wind Tunnel Data for Five Chamber Model

| Flow Velocity (m/s) / Flow Direction | | 2 | 3 | 4 | 5 | 6 | 7 | 8 | 9 | 10 | 12 |
|---|---|---|---|---|---|---|---|---|---|---|---|
| 0° | Point1 | 2 | 2.9 | 3.9 | 5.2 | 6.2 | 7.1 | 8.3 | 9.5 | 10.6 | 12.7 |
| | Point 2 | 1.8 | 2.6 | 3.4 | 4.6 | 5.7 | 6.6 | 7.7 | 8.6 | 9.7 | 11.6 |
| | Point 3 | 2.1 | 3.1 | 4.2 | 5.4 | 6.5 | 7.2 | 8.3 | 9.3 | 10.2 | 12.7 |
| | Point 4 | 1.7 | 2.1 | 3.1 | 4 | 5 | 5.7 | 6.7 | 7.7 | 8.5 | 10.2 |
| | Point 5 | 1.8 | 2 | 2.9 | 3.8 | 4.6 | 5.4 | 6.1 | 7 | 7.6 | 9.5 |
| | Point 6 | 2 | 2.8 | 3.8 | 5.1 | 5.8 | 6.9 | 7.9 | 8.9 | 9.7 | 12.1 |
| | Point 7 | 2 | 3 | 3.9 | 5 | 5.9 | 7.1 | 8 | 8.9 | 9.9 | 12 |
| 12° | Point 1 | 2.2 | 3.3 | 4.5 | 5.7 | 6.5 | 7.7 | 8.8 | 9.1 | 10.6 | 12 |
| | Point 2 | 1.9 | 3 | 3.9 | 5.2 | 6.3 | 7.2 | 8 | 9.1 | 9.8 | 11.3 |
| | Point 3 | 2 | 3.1 | 4.2 | 5.3 | 6.3 | 7.3 | 8.6 | 9.7 | 10.6 | 12 |
| | Point 4 | 1.6 | 2.4 | 3 | 4 | 4.5 | 5.5 | 6 | 7.3 | 7.8 | 9.4 |
| | Point 5 | 1.6 | 2.4 | 3.1 | 3.9 | 4.4 | 5.4 | 5.7 | 6.7 | 7.5 | 8.9 |
| | Point 6 | 1.8 | 2.7 | 3.5 | 4.5 | 5.2 | 6.3 | 6.9 | 7.8 | 8.6 | 10.7 |
| | Point 7 | 1.5 | 2.3 | 3 | 3.7 | 4.3 | 4.9 | 5.6 | 6.4 | 7.2 | 8.4 |
| 24° | Point 1 | 2.1 | 3.2 | 4.4 | 5.7 | 6.6 | 8.5 | 9.3 | 10.4 | 11.5 | 13.4 |
| | Point 2 | 2 | 3.1 | 4.3 | 5.5 | 6.5 | 8.3 | 9.1 | 10.2 | 11.2 | 13.6 |
| | Point 3 | 2.2 | 3.3 | 4.6 | 5.9 | 7.2 | 8.6 | 9.8 | 11.1 | 12.3 | 14.1 |
| | Point 4 | 1.8 | 2.4 | 3 | 4 | 4.8 | 5.5 | 6.5 | 7 | 8 | 9.8 |
| | Point 5 | 1.7 | 2.5 | 3.2 | 4.1 | 5 | 6.2 | 6.9 | 7.5 | 8.5 | 10.7 |
| | Point 6 | 1.8 | 2.4 | 3 | 4.2 | 5.3 | 6.6 | 7 | 7.6 | 8.6 | 10.6 |
| | Point 7 | 1.5 | 1.9 | 2.6 | 3 | 4.1 | 4.8 | 5.3 | 6 | 6.1 | 7.2 |
| 36° | Point 1 | 2.2 | 3.1 | 4.3 | 5.7 | 7.1 | 8.2 | 9.1 | 10.7 | 12 | 13.5 |
| | Point 2 | 2.2 | 2.9 | 4.2 | 5.6 | 7 | 8 | 9.2 | 10.1 | 10.9 | 13.3 |
| | Point 3 | 2.4 | 3.6 | 5 | 6.3 | 7.4 | 8.5 | 9.8 | 11 | 12.4 | 15 |
| | Point 4 | 1.8 | 2.6 | 3.4 | 4.8 | 5.4 | 6.3 | 7 | 7.9 | 9.1 | 10.2 |
| | Point 5 | 1.6 | 2.4 | 3.3 | 4.4 | 5.3 | 6.1 | 7 | 8 | 8.6 | 10.1 |
| | Point 6 | 1.8 | 2.5 | 3.4 | 4.3 | 5.6 | 6.3 | 6.9 | 8.2 | 8.7 | 9.8 |
| | Point 7 | 1.5 | 2.1 | 2.5 | 3.4 | 4 | 4.5 | 5.1 | 5.4 | 6 | 7 |

Table 3. Wind tunnel data for five chamber model

# Appendix G – Flow Distribution at the Outlet of Shroud (Five Chamber Model)

This appendix shows the flow visualisation at the outlet of shroud in various directions (0°, 12°, 24° and 36°) and different flow velocities (2m/s and 10m/s)

U=2m/s

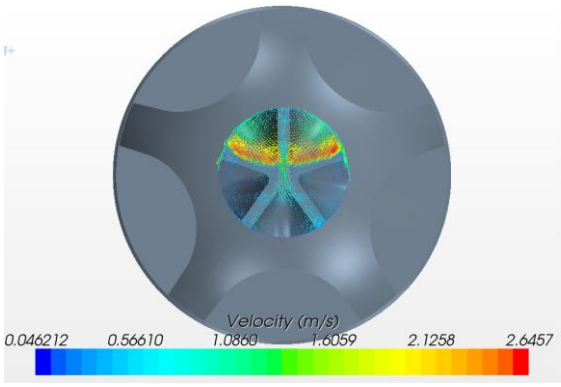


0°

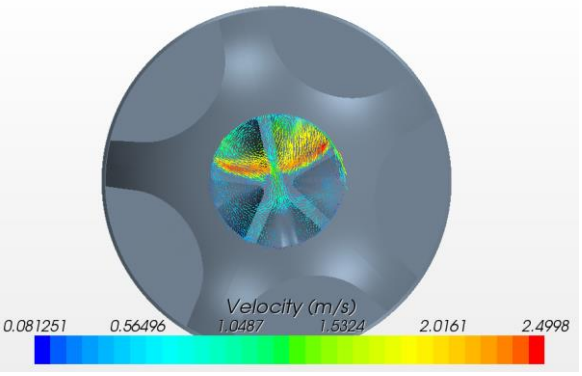


12°

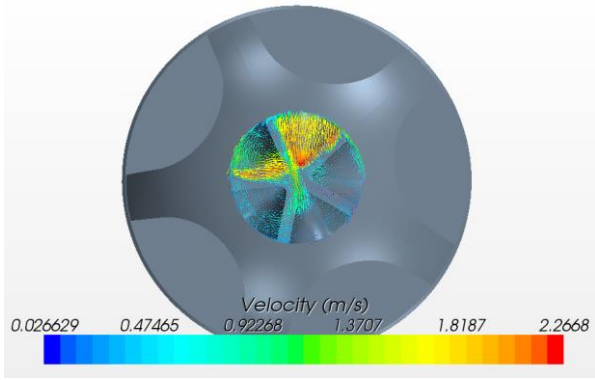


24°

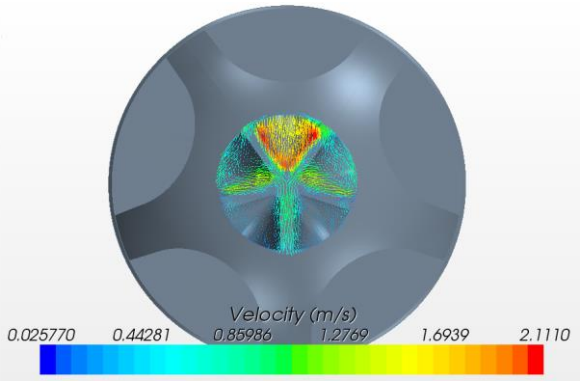


36°

U=10m/s

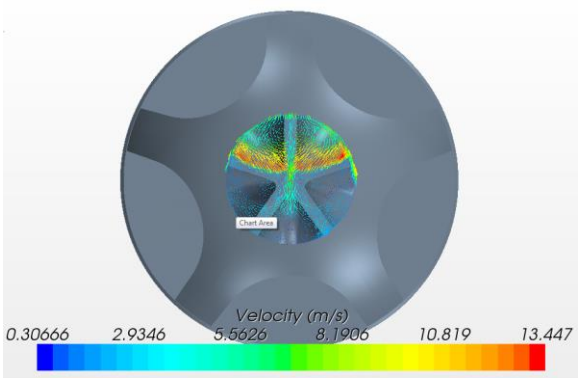


0°

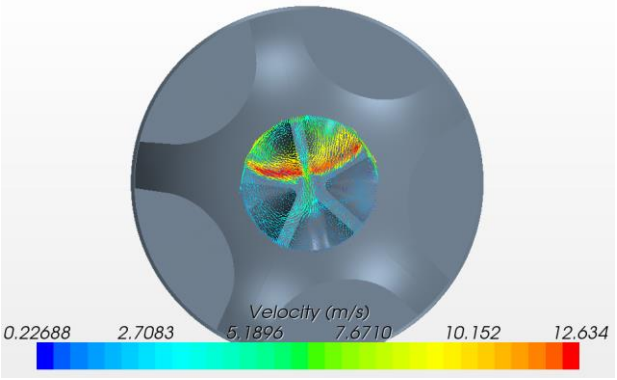


12°

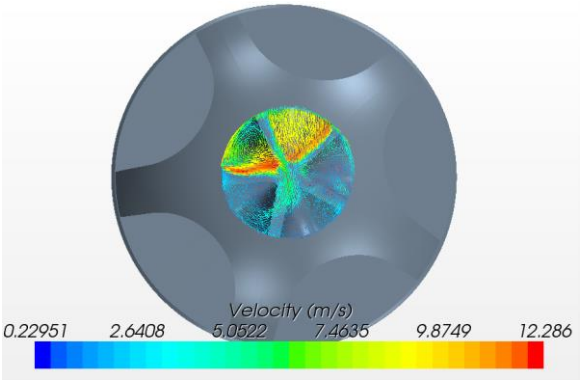


24°

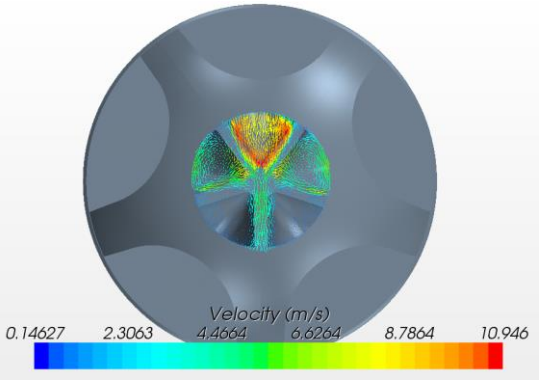


36°

# Appendix H – Coordinates of Points on the Pressure Line

| | x | y | z |
|---|---|---|---|
| Point 1 | 0 | -0.06 | 0.008 |
| Point 2 | 0 | -0.06 | 0.025 |
| Point 3 | 0 | -0.06 | 0.042 |
| Point 4 | 0 | -0.06 | 0.059 |
| Point 5 | 0 | -0.06 | 0.076 |
| Point 6 | 0 | -0.06 | 0.093 |
| Point 7 | 0 | -0.06 | 0.11 |
| Point 8 | 0 | -0.06 | 0.127 |
| Point 9 | 0 | -0.06 | 0.144 |
| Point 10 | 0 | -0.06 | 0.161 |
| Point 11 | 0 | -0.06 | 0.178 |
| Point 12 | 0 | -0.06 | 0.195 |
| Point 13 | 0 | -0.06 | 0.212 |
| Point 14 | 0 | -0.06 | 0.229 |
| Point 15 | 0 | -0.06 | 0.246 |

Table 4. Coordinates of points on the pressure line for test model with different vertical length

| | x | y | z |
|---|---|---|---|
| Point 1 | 0 | -0.06 | 0.02 |
| Point 2 | 0 | -0.06 | 0.05 |
| Point 3 | 0 | -0.06 | 0.08 |
| Point 4 | 0 | -0.06 | 0.11 |
| Point 5 | 0 | -0.06 | 0.14 |
| Point 6 | 0 | -0.06 | 0.17 |
| Point 7 | 0 | -0.06 | 0.2 |
| Point 8 | 0 | -0.06 | 0.23 |
| Point 9 | 0 | -0.06 | 0.26 |
| Point 10 | 0 | -0.06 | 0.29 |
| Point 11 | 0 | -0.06 | 0.32 |
| Point 12 | 0 | -0.06 | 0.35 |
| Point 13 | 0 | -0.06 | 0.38 |
| Point 14 | 0 | -0.06 | 0.41 |
| Point 15 | 0 | -0.06 | 0.44 |
| Point 16 | 0 | -0.06 | 0.47 |
| Point 17 | 0 | -0.06 | 0.5 |

Table 5. Coordinates of points on the pressure line for improved models

# Appendix I – Engineering Drawing of Four Chambers Model

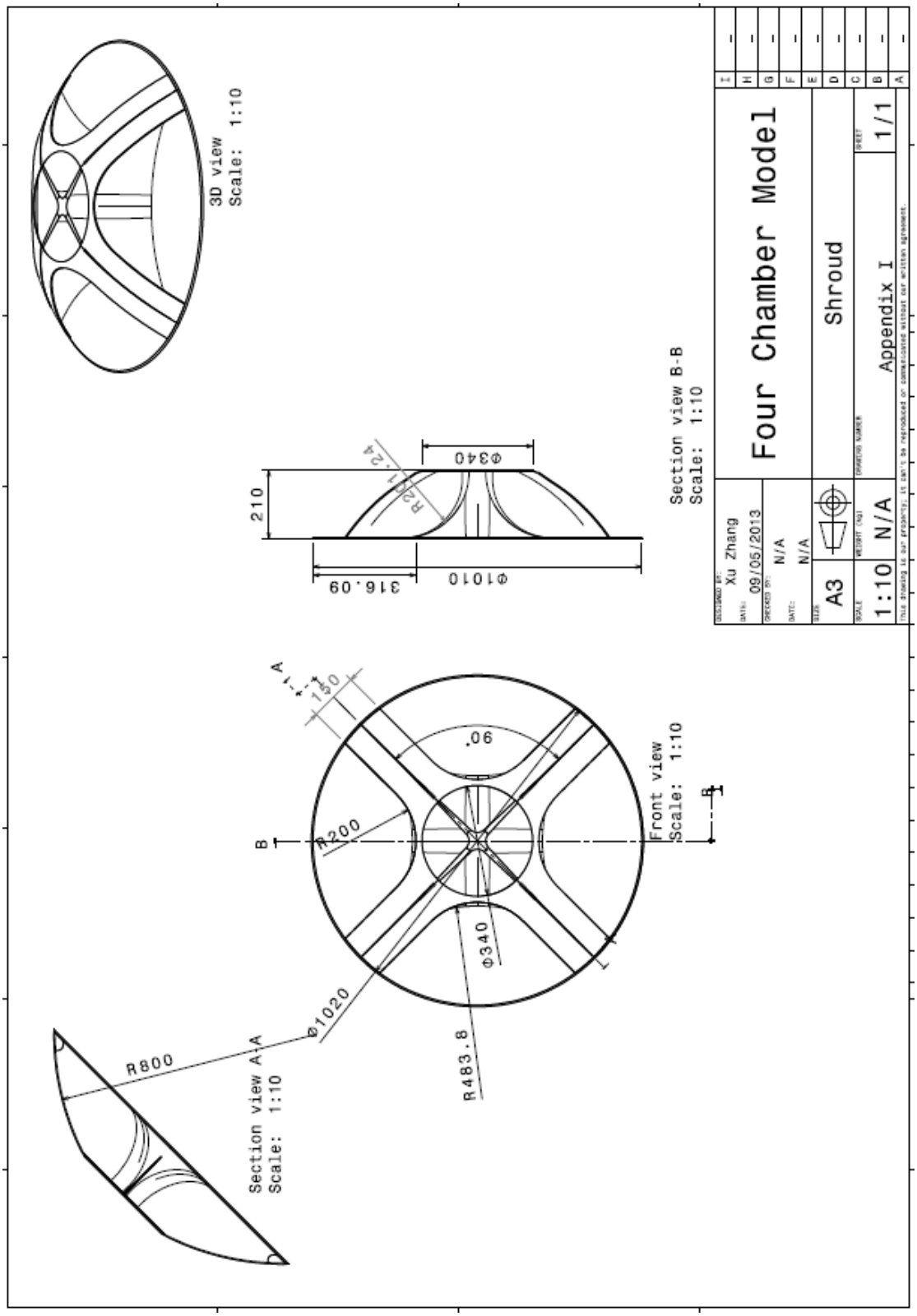

# Appendix J – Engineering Drawing of Three Chambers Model

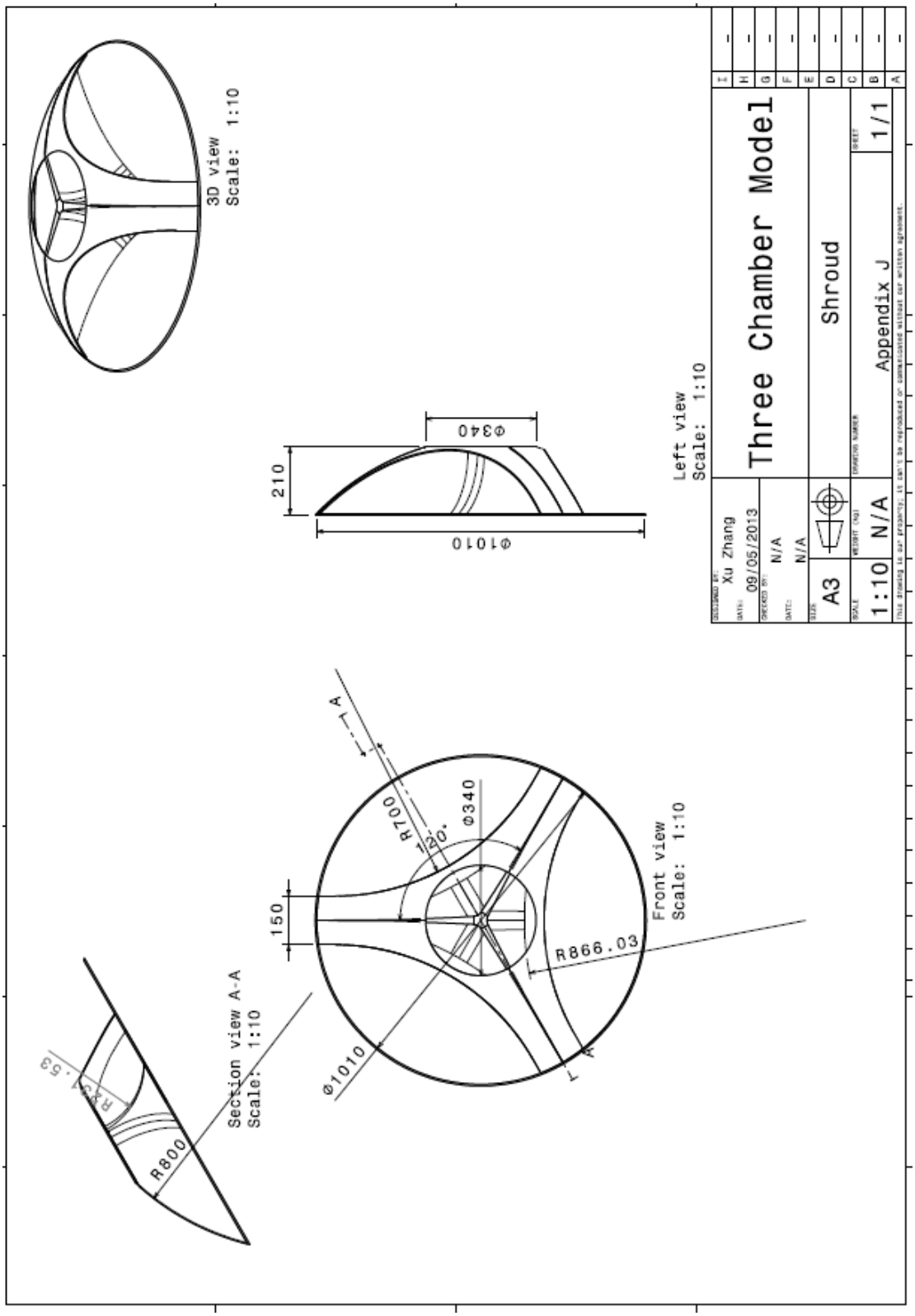

# Appendix K – Engineering Drawing of Five Chamber Model

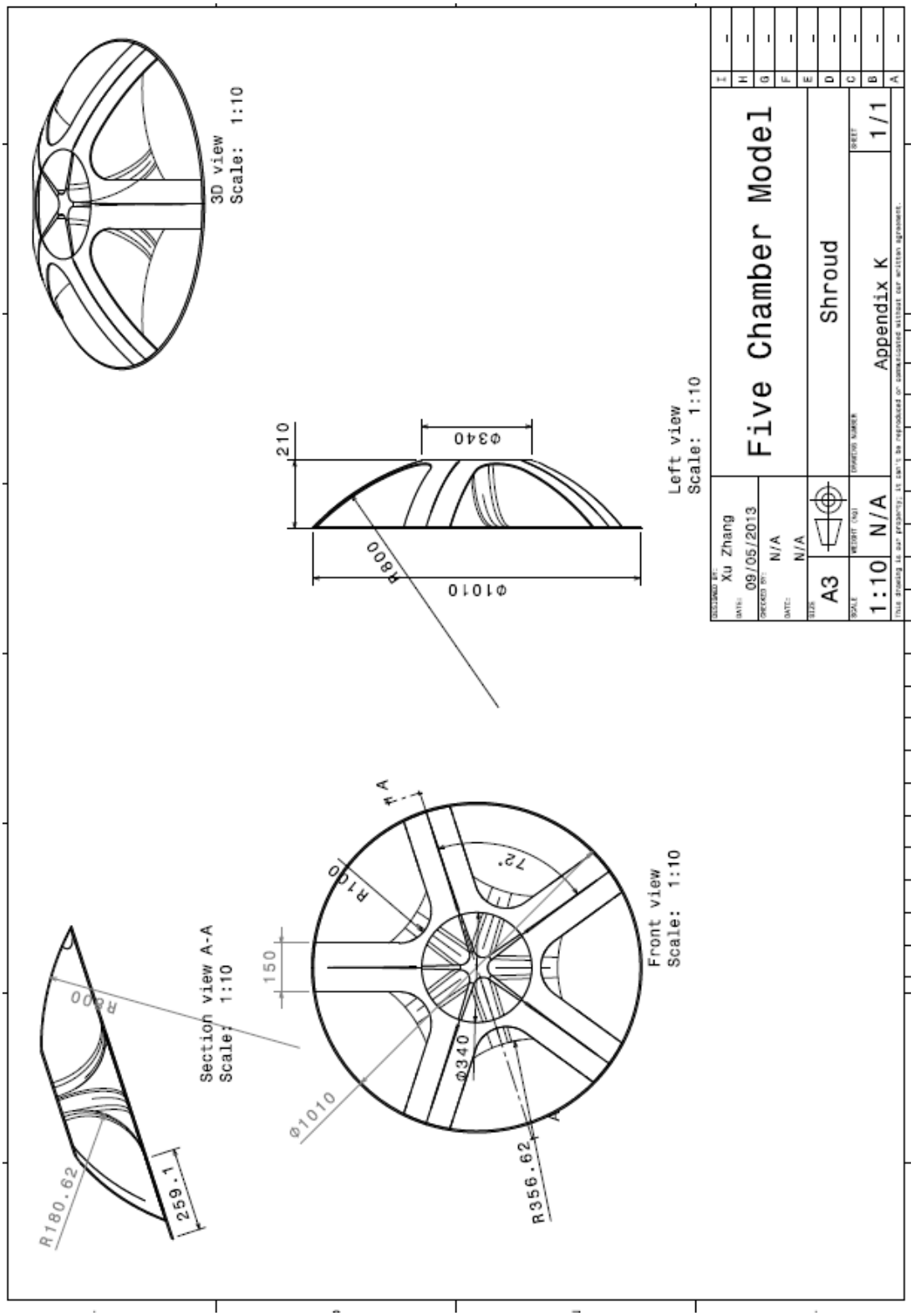

# Appendix L – Engineering Drawing of Final Model